INVESTIGATIONS ON FAULT DIAGNOSIS IN DC SIDE OF SOLAR PHOTOVOLTAIC (PV) SYSTEMS

Thesis

Submitted in partial fulfillment of the requirements for the degree of

DOCTOR OF PHILOSOPHY

by

DONGARA RAMESH

DEPARTMENT OF ELECTRICAL AND ELECTRONICS ENGINEERING,
NATIONAL INSTITUTE OF TECHNOLOGY KARNATAKA,
SURATHKAL, MANGALORE -575025

September, 2024

DEDICATED

TO

MY PARENTS

AND

FAMILY MEMBERS

DECLARATION

by the Ph.D. Research Scholar

I hereby *declare* that the Research Thesis entitled "**INVESTIGATIONS ON FAULT DIAGNOSIS IN DC SIDE OF SOLAR PHOTOVOLTAIC (PV) SYSTEMS**" which is being submitted to the **National Institute of Technology Karnataka, Surathkal** in partial fulfillment of the requirement for the award of the Degree of **Doctor of Philosophy** in **Electrical and Electronics Engineering** is a *bonafide report of the research work carried out by me.* The material contained in this Research Thesis has not been submitted to any University or Institution for the award of any degree.

D. Ramesh

.....

DONGARA RAMESH, 197072

Department of Electrical and Electronics Engineering

Place: NITK Surathkal

Date: 30-09-2024.

CERTIFICATE

This is to *certify* that the Research Thesis entitled **"INVESTIGATIONS ON FAULT DIAGNOSIS IN DC SIDE OF SOLAR PHOTOVOLTAIC (PV) SYSTEMS"** submitted by **Dongara Ramesh** (Register Number: 197072) as the record of the research work carried out by him, is *accepted as the Research Thesis submission* in partial fulfillment of the requirements for the award of degree of **Doctor of Philosophy**.

Dr A. Karthikeyan
(Research Guide)

Prof. Debashisha Jena
(Chairman-DRPC, EEE dept.)

PROFESSOR AND HEAD
DEPARTMENT OF ELECTRICAL AND ELECTRONICS ENGINEERING
NATIONAL INSTITUTE OF TECHNOLOGY KARNATAKA
SRINIVASNAGAR, SURATHKAL, MANGALORE - 575 025, INDIA

Acknowledgements

It gives me immense pleasure and great sense of satisfaction to express my heartfelt gratitude to those who made this dissertation possible. I take this opportunity to sincerely thank my research supervisor Dr. A. Karthikeyan for all his invaluable guidance, patience, encouragement, timely advice and support. He has been a constant source of inspiration throughout this journey. I feel proud to have worked under his guidance.

I thank National Institute of Technology Karnataka for giving me an opportunity for doing research and Ministry of Human Resource Department(MHRD) Government of India for awarding research scholarship.

I wish to thank my research progress assessment committee (RPAC) members Prof.U. Shripathi Acharya and Prof. Vinatha. U, for their constructive feedback and guidance from research problem definition stage to thesis submission stage. Without their help the thesis would not have taken this shape.

I would like to thank Prof. Debashisha Jena, HOD-EEE for providing the necessary resources in the department to carry out my research.

I take this opportunity to thank all teaching and non-teaching staff of EEE Department, NITK Surathkal.

My stay at NITK Surathkal was a sweet and memorable in the company of my fellow researchers who never let me knew that I am away from home. Big thanks to all the research scholars. Finally, I would like to thank Family members for their patience, care and love which drew me with inspiration to carry out my research.

Dongara Ramesh

Abstract

The solar energy conversion into electricity is a very promising technique, knowing that the source is free, clean and abundant in several countries. Solar photovoltaic (PV) systems contribute 2% of the world's total energy consumption. India's solar installed capacity has reached 37.62 GW as of 31st march 2020. In view of increasing grid connected solar PV plants and environmental conditions there are possibilities of faults (line-ground, line-line, open circuit and partial shading) occurring in solar PV arrays. The conventional protection devices are unable to detect the faults in PV array under lower module mismatch (one module), severe partial shading conditions and low irradiation levels because of PV's nonlinear characteristics, lower magnitudes of fault current and active Maximum Power Point Tracking (MPPT's). Once the fault is diagnosed, should be cleared in minimum time. The faults (line-ground, line-line, open circuit) can be cleared manually but partial shading cannot be cleared manually. So, to reduce the effect of partial shading the PV array can be reconfigured without changing the electrical connections. Therefore, fault analysis in solar photovoltaic (PV) arrays is a fundamental task to increase reliability, efficiency and safety in PV systems. Firstly, to identify and localize the faults in the PV array, a Diagonal Sensor Arrangement (DSA) method is proposed. This DSA method works on the principle of measurement of differential voltage across two different potential points in the solar PV array. The proposed DSA method is verified in simulation (4kW system) and hardware (0.16kW system) for a 4×4 PV array. The conditions of short circuit faults with one, two module mismatch within the string and between the strings are analyzed. Also, the characteristics of PV array under open circuit faults and partial shading faults are discussed. A comparative analysis is done between the proposed DSA method and various methods available in the literature which shown the efficacy of the proposed SDA method.

Partial shading in photovoltaic (PV) arrays is a common and challenging issue that significantly impacts the overall performance and efficiency of solar energy systems. Partial shading leads to formation of hot spots and

multiple peaks in characteristic curves. Several techniques are reported in the literature to mitigate the effects of partial shading. Configuration of the PV array plays an important role in increasing the output power. The conventional PV array configurations are Series-Parallel (SP), Bridge Link (BL), Honey Comb (HC) and Total Cross Tied (TCT) configurations. Among which TCT configuration is able to generate more output under partial shading conditions. However, TCT configuration has more number of cross ties which increases the cost of wire required for connecting the modules. Hence, a novel Reduced Cross Tied (RCT) PV array configuration with reduced cross ties which is capable of generating output power closer to TCT configuration is proposed. It is implemented on 8×8 and 7×7 PV arrays and verified in simulation and experimental environments. The PV array output power can be further increased by re configuring the PV modules without changing the electrical connections. This report presents a new static reconfiguration technique -Cyclic Back Shift (CBS) method to mitigate the effects of partial shading.The proposed CBS method is implemented on 9×9 PV array and verified in simulation (20.25kW system) and experimental (0.81kW system) environments. From the results obtained, it is observed that proposed CBS method is able to enhance the output power and improves efficiency of PV systems under partial shading conditions. Further, a new static reconfiguration technique Modified Odd Even Prime (MOEP) is proposed to mitigate the effects of partial shading. The proposed MOEP method is implemented on 9×9 and 8×8 PV arrays and verified in simulation (20.25kW system and 16kW system) and hardware (0.81kW system and 0.64kW system) environments. A detailed qualitative and quantitative comparative analysis is made between the proposed MOEP method and various other techniques in the literature. From the results obtained, it is observed that proposed MOEP method is able to enhance the output power and improves efficiency of PV systems under partial shading conditions. All the developed algorithms are simulated in MATLAB/Simulink.

Contents

List of Figures

List of Tables

Nomenclature

AAR	Adaptive Array Reconfiguration
AC	Alternating Current
ACM	Arnold's Cat Map
ACMS	Ancient Chinese Magic Square
AFCI	Arc Fault Circuit Interrupter
APS	Addition Progression Structure
BL	Bridge Link
CAT	Circular Array Transformation
CBMT	Chaotic Baker Map Technique
CBS	Cyclic Back Shift
CCC	Current Carrying Conductor
CK	Cross Kit
CST	Competence Square Technique
DAQ	Data Acquisition System
DC	Direct Current
DSP	Digital Signal Processing
DTCL	Double Tied Cross Linked
ECM	Earth Capacitance Measurement
EGC	Earth Ground Conductors
FLC	Fuzzy Logic Controller
FPGA	Field Programmable Gate Array
GFDI	Ground Fault Detector and Interrupter
GMPP	Global Maximum Power Point
HC	Honey Comb
IE	Image Encryption
IEC	International Electrotechnical Commission
IMD	Insulation Monitoring Devices
IMI	Irradiance Mismatch Index
KKS	Ken-Ken Square
LMPP	Local Maximum Peak Points
LS	Latin Square
MOEP	Modified Odd Even Prime

MPPT	Maximum Power Point Tracking
MS	Magic Square
MSEC	Magic Square Enhanced Configuration
MTT	Modified Triple Tied
OCPD	Over Current Protection Device
OS	Optimal Sudoku
PV	Photovoltaic
RAA	Recursive Addition Approach
RCD	Residual Current Monitoring Device
RCT	Reduced Cross Tied
SDF	Shade Dispersion Effect
SP	Series Parallel
SRA	Successive Rotation Approach
TCT	Total Cross Tied
TT	Triple Tied
TTCL	Triple Tied Cross Link
P_{mp}	Fundamental reference frequency
V_{oc}	Fundamental reference frequency
V_{mp}	Switching frequency
I_{sc}	Collector current
I_{mp}	Forward current of the diode

Chapter 1

INTRODUCTION

1.1 Background

Electricity is the most convenient form of energy for industrial, agricultural, commercial and domestic activities. It is the key input for the economic and industrial development of country. In recent years, countries all over the world have taken up industrialization, transport, communication as well as automation projects on large scale and to maintain reasonable growth they must have a sustainable electricity supply to achieve their developmental goals Manju and Sagar (2017). However, the current state of affairs is quite dismal due to the following challenges

1. Gap in Supply and Demand
2. Fuel Security Concerns
3. Environmental Concerns
4. Rising Prices

In view of above challenges, non-conventional methods of power generations have received steadily increasing attention around the world to control the dependence on fuels with escalating costs and pollution resulting from the use of nuclear and fossil fuels. Non-conventional methods of power generation include solar photovoltaic, bio conversion, small hydro, wind and ocean temperature gradients and currents, which are also known as renewable resources of energy Sahoo (2016). These resources are replenished almost as fast as they are used and they do not lead to environmental

pollution. Renewable energy sources have lately acquired a prominent place in energy policy decisions of countries all over the world, prompted by the increased prices of petroleum products. It is widely perceived that the conventional energy sources by and large are likely to dwindle very fast in the near future. So to replace these fast depleting conventional sources with renewable counterparts have become a challenging task. Among various renewable technologies, the wind and solar PV energy are the most commercially implemented and widely adopted in today's energy paradigms across the globe Lal SR et al. (2022).

1.2 Motivation

India along with the world is facing energy crisis. There is a significant gap in the demand and supply for electricity. In order to meet this situation, number of alternate options to generate electricity is being considered with wide focus on renewable energy generation. Solar power generation is one of the most promising options. Several factors have promoted the development of solar photovoltaic systems such as environmental concerns, incentives, more performing and less expensive technology and the need to replace carbon fossil energy systems. However, the major concern in solar power generation is to make them energy efficient. Under adverse operating conditions the output power from the solar photovoltaic(PV) systems decrease and are unable to meet the required load Markvart and Castañer (2003). There are many factors responsible for decrease in efficiency of solar photovoltaic(PV) systems. They are solar cell characteristics, environmental conditions, shading of the panels, faults in solar photovoltaic(PV) systems, inverter efficiency and battery efficiency. These days the solar panels are coming with new technology with increased efficiency. And also the inverters and batteries are designed to have high efficiencies. The shading and environmental impacts are temporary in nature.

Coming to faults in solar photovoltaic systems, they are categorized into ac side and dc side faults. AC side faults deals with faults in the inverter and ac transmission lines. These faults are able to clear by conventional protection devices. OCPD's, GFDI fuses and AFCI's are employed for protection on the DC side of PV systems Strobl and Meckler (2010). Because of lower fault current magnitudes, presence of MPPT, non-linear PV characteristics and dependency on irradiation levels, these protection devices have failed to detect the PV array faults. Further faults occurring in low

irradiation levels may remain undetected in the PV system and leads to significant energy loss and degradation of PV panels. Hence early detection of faults is necessary to improve the efficiency and reliability of the solar PV system.

1.3 Solar Photovoltaic Systems

The sun delivers its energy in two main forms heat and light. There are two main types of solar power systems, namely solar thermal systems that trap heat to warm up water, and solar PV systems that convert sunlight directly into electricity. Photovoltaic (PV) power generation is reliable, involves no moving parts, operation and maintenance costs are very low. The PV cells form the core part of solar photovoltaic (PV) power generation unit. The basic element of a solar photovoltaic (PV) System is the PV cell shown in Fig.1.1.

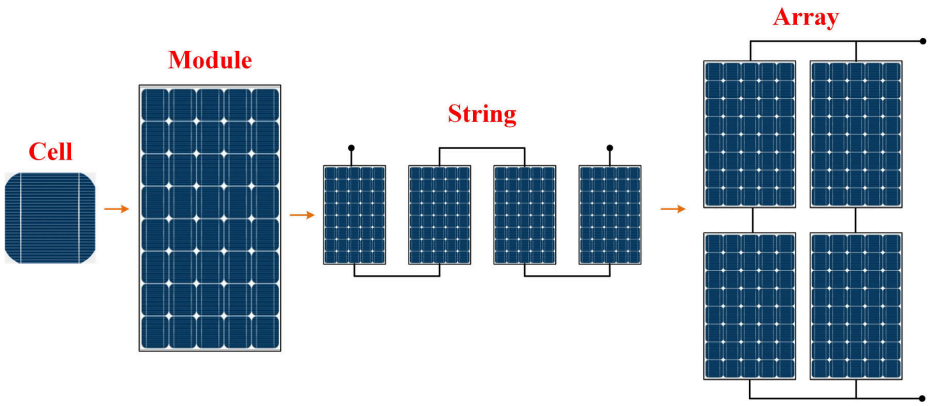

Figure 1.1: Illustration of PV cell, Module, String, and Array

A PV cell is a semiconductor device that can convert solar energy into DC electricity through photovoltaic effect. The photovoltaic effect is a process that generates voltage or electric current in a PV cell when it is exposed to sunlight. When light falls on a PV cell it may be reflected, absorbed, or passes right through. But only the absorbed light generates electricity. A number of individual PV cells are interconnected together in a sealed, weather proof package called a Module. To get the desired voltage the PV modules are connected in series to form a string. To achieve the desired voltage and current, modules are wired in series and parallel, which is called a PV Array. The flexibility of the modular PV system allows designers to create solar power systems that can meet a wide variety of electrical needs. The

PV array converts the solar energy to DC power, which is directly dependent on the incident solar radiation Brenna et al. (2012). This is followed by a power conditioner which contains a maximum power point tracker (MPPT) and a battery charge and discharge controller. The MPPT ensures that at all times the maximum power generated by the PV array is extracted. The charge/discharge controller is responsible for preventing overcharging or over discharging the battery bank, required to store the electricity generated by the PV array for use during sunless times. The DC output power thus stored or generated is then fed to DC loads. An inverter is used to convert the DC power output into AC output power. This AC output power from the inverter can be fed to AC loads and grid. The PV array combined with a set of additional components form a complete solar photovoltaic (PV) system as shown below in Fig. 1.2. Solar photovoltaic (PV) systems can be broadly classified into two major groups.

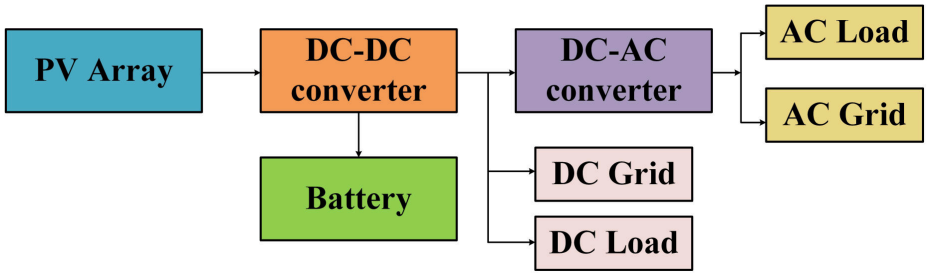

Figure 1.2: Solar Photovoltaic System

Stand-Alone system: Stand-Alone PV systems are designed to operate independent of the electric utility grid, and are generally designed and sized to supply certain DC or AC loads Capparella and Falvo (2014). The number of components in the system will depend on the type of load that is being served. The simplest type of stand-alone PV system is a direct-coupled system, where the DC output of a PV module or array is directly connected to a DC load. Since there is no electrical energy storage element in direct-coupled systems, the load only operates during sunlight hours, making these designs suitable for common applications such as ventilation fans, water pumps, and small circulation pumps for solar thermal water heating systems. A typical block diagram of Stand-Alone Solar Photovoltaic (PV) system is shown in Fig. 1.3.

Grid connected systems: Grid-connected or utility-interactive PV systems are designed to operate in parallel with the electric utility grid Albers and Ball (2015). The primary component in grid-connected PV systems is the inverter. The inverter

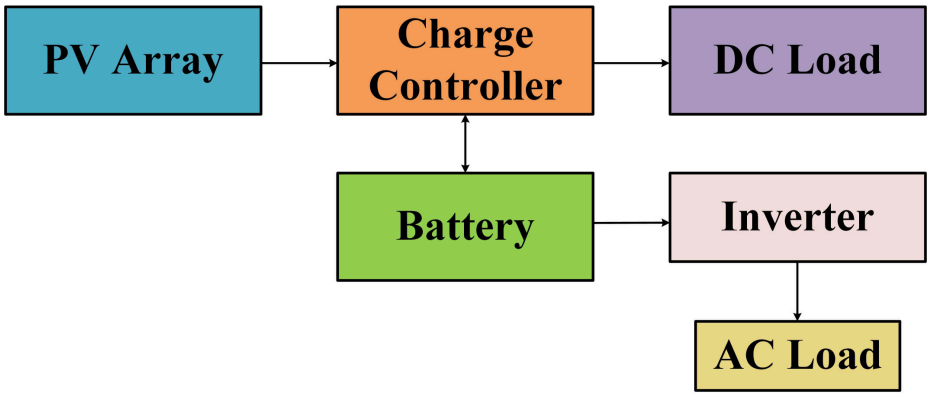

Figure 1.3: Stand Alone system

converts the DC power produced by the PV array into AC power with the voltage and power quality requirements of the utility grid, and automatically stops supplying power to the grid when the utility grid is not energized. The block diagram of Grid Connected Solar Photovoltaic (PV) system is shown in Fig.1.4. A bi-directional interface is made between the PV system AC output circuits and the electric utility network, typically at an on-site distribution panel or service entrance. This allows the AC power produced by the PV system to either supply on-site electrical loads or to back-feed the grid when the PV system output is greater than the on-site load demand. At night and during other periods when the electrical loads are greater than the PV system output, the balance of power required by the loads is received from the electric utility Triki-Lahiani et al. (2018). This safety feature is required in all grid connected PV systems, and ensures that the PV system will not continue to operate and feed back into the utility grid when the grid is down for service or repair.

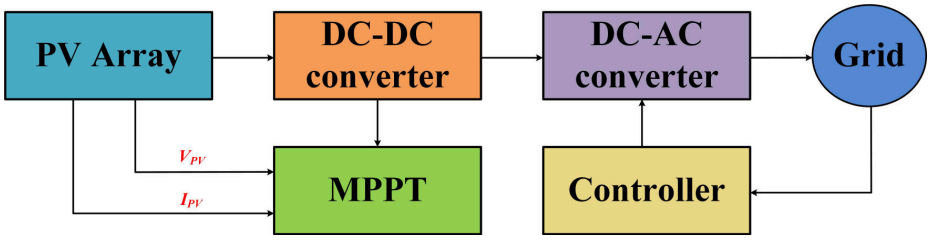

Figure 1.4: Grid connected system

1.4 Objectives

1. Development of novel fault finding algorithm to diagnose the faults in solar photovoltaic (PV) array for enhancing the reliability of solar photovoltaic (PV) systems.
2. Development of new reconfiguration scheme to enhance the maximum output power from the PV array under various partial shading conditions.
3. Verification of the proposed fault finding algorithm with simulation and experimental studies.
4. Verification of the proposed reconfiguration scheme with simulation and experimental studies.

1.5 Thesis organization

The thesis is organized as follows

Chapter 1: This presents an introduction which consists of a brief overview of the thesis and the reasons for its motivation followed by the research objectives and a concise description of the flow in which the thesis is organized.

Chapter 2: In this chapter literature survey of faults in the DC side of the solar photovoltaic systems is presented. Further the chapter also presents various techniques to identify the faults and mitigating techniques of partial shading.

Chapter 3: In this chapter an algorithm is proposed to detect the faults (Line-Line, Line-Ground, and Open Circuit) occurring in the solar PV array. The proposed algorithm is verified in simulation and hardware environments.

Chapter:4 In this chapter the proposed reduced cross tied PV array configuration is evaluated extensively through simulation and experimental studies.

Chapter 5: This chapter presents a novel static reconfiguration technique Cyclic Back Shift (CBS) to enhance the GMPP from the PV array under partial shading conditions. The systems description is presented and validated the technique in simulation and hardware environments.

Chapter 6: This chapter presents a novel static reconfiguration technique Modified Odd Even Prime (MOEP) to mitigate the effects of partial shading of the PV array. The systems description is presented and validated the technique in simulation and hardware environments.

Chapter 7: Summarizes the thesis major contributions and includes some discussions on possible future research.

1.6 Literature Survey

The last few decades have seen an exponential increase in the world's photovoltaic (PV) power capacity, making PV system protection extremely important. Despite this, PV systems are susceptible to malfunctions that seriously impair the system's dependability, efficiency, and safety. Faults in a PV array may go unnoticed even when typical protective devices are used in a system Madeti and Singh (2017). PV generating systems are extremely susceptible to fault incidence, much like any other type of power system. The DC stage and the AC stage are the two primary phases of power flow in a conventional grid-connected photovoltaic system. Temperature and insolation level affect a PV module's voltage and current during the DC stage. Due to active Maximum Power Point Tracking (MPPTs), all the PV modules operate at a point which is very near to its I_{sc} and 80% of its V_{oc}. Because of this, faults that arise in the DC side of solar photovoltaic (PV) systems have a variety of features, particularly low fault current magnitudes, which make it extremely challenging to identify and classify the many types of PV system defects. As a result, enhancing the efficiency and dependability of solar photovoltaic (PV) systems requires effective problem detection in PV arrays. A summary of the fundamental approaches to fault analysis is provided by Hare et al. (2016), which draws on MPPT algorithms, electric circuit analysis, numerical computations, and I-V characteristic analysis. In a solar photovoltaic (PV) system, faults can arise for a variety of causes. To identify each fault occurrence, comprehend the need for fault detection, and assess the protection problems, a thorough understanding is required. The faults that can occur in a photovoltaic (PV) array can be classified using a tree diagram as shown in Fig. 1.5.

The faults in the PV array are classified into three categories, Physical, Environmental, and Electrical faults. The physical faults are cracks in the PV modules,

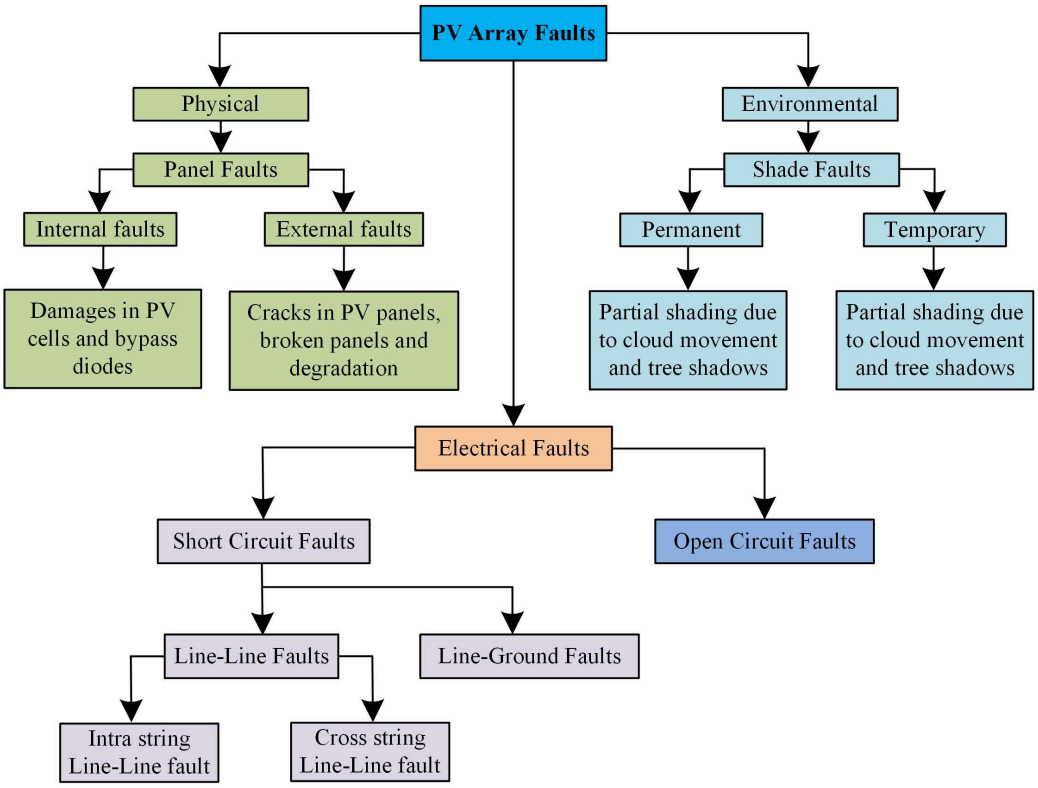

Figure 1.5: Various Faults Occurring in PV Array

broken modules and degradation of the module. The environmental faults are shading faults which occur due to shadows of tall buildings, trees, clouds, and dust on the PV modules. The electrical faults constitute line-line and line-ground faults. The common faults faults among these are electrical and shade faults Alam et al. (2015).

1.7 Electrical Faults

1.7.1 Short Circuit Faults

1.7.1.1 Line-Line Faults

An accidental short circuit between two points in a PV array which are at different potentials is termed as a line-line fault as shown in Fig. 1.6. This happens due to physical damage, environmental factors, manufacturing defects, aging, and wear. Compared to other defects, these faults are severe and difficult to identify Bower and Wiles (1994). Simply put, because the fault current is dependent on the potential dif-

ference or degree of mismatch between two fault spots, line-line faults are understood as short circuit faults in a grounded PV system.

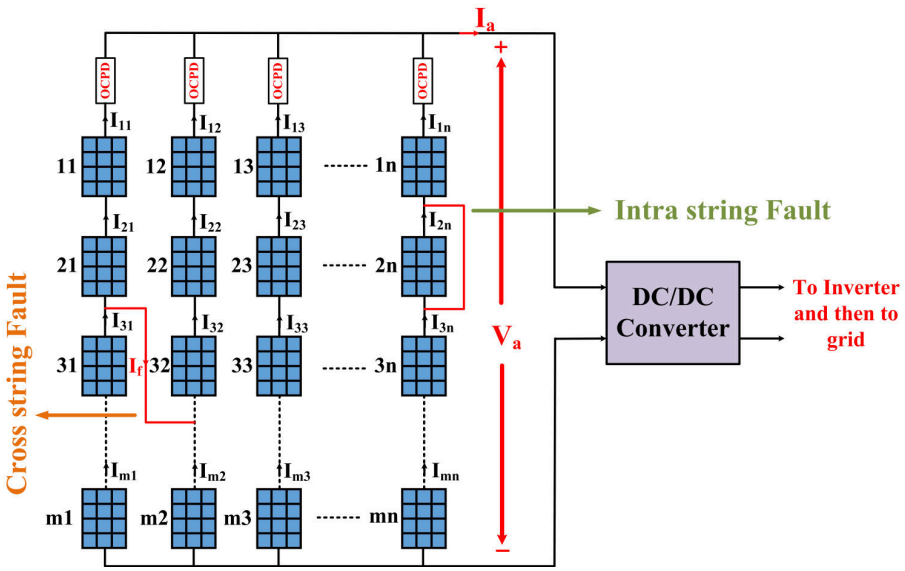

Figure 1.6: Line-Line Faults Occurring in PV Array

In a PV system, intra string faults and cross string faults are the two most frequent types of line-line faults. A cross string fault is a short circuit between two places on different strings, whereas an intra string fault is a short circuit between two points within the same string. Over Current Protection Devices (OCPDs) are typically used to protect line-line faults and are connected in series with each string. It is quite likely that line-line defects in a PV array will go unnoticed, even in the absence of OCPDs. The PV array's I-V characteristics undergo a catastrophic change due to an undiscovered line-line fault Zhao and Lyons Jr (2011). The presence of MPPT reduces the effect of line-line fault by optimizing the operating point of PV array after the fault with a significant reduction in PV array output power and operating voltage.

The severity of a fault depends on the level of mismatch between the PV modules. For example consider a 5×5 PV array as shown in Fig. 1.7.

A mismatch of three modules, or 60%, is represented by fault (f1), and a mismatch of two modules, or 40%, is represented by fault (f2). If all PVs are at the same irradiation level, the fault current magnitude is greater in the event of a three module mismatch than in a two module mismatch. OCPDs connected in series with each

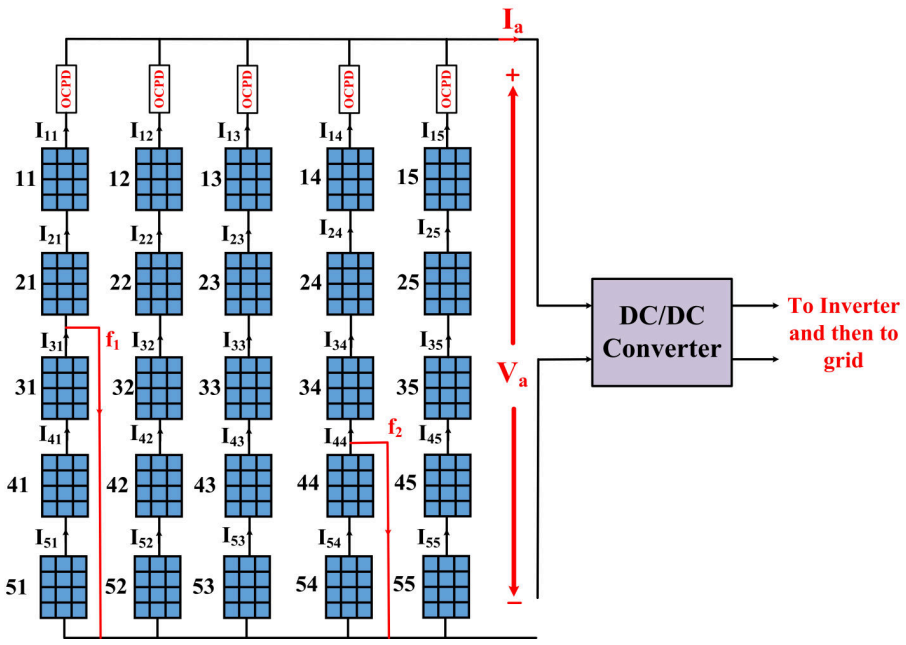

Figure 1.7: Line-Line faults in the PV array

string are typically used to prevent against line-line faults Zhao and Lyons Jr (2011). The fuse rating of an OCPD in accordance with IEC specifications is given in eqn.1.1.

$$I_0 = 1.56 \times I_{SC} \tag{1.1}$$

However, the minimum breaking capacity of fuses is given by equation 1.2.

$$I_{min} = 1.35 \times I_0 \tag{1.2}$$

Combining equations 1.1 and 1.2, installed fuse rating of any OCPD is expressed as

$$I_{min} = 2.1 \times I_{SC} \tag{1.3}$$

1.7.1.2 Protection challenges for line-line Faults

Line-Line fault brings about a catastrophic change in the current-voltage (I-V) characteristics of the PV array as illustrated in Fig. 1.8. It is seen that, the presence of MPPT reduces the effect of line-line fault by optimizing the post fault operating point of the PV array to point with a significant reduction in power and operating voltage Sabbaghpur Arani et al. (2016).

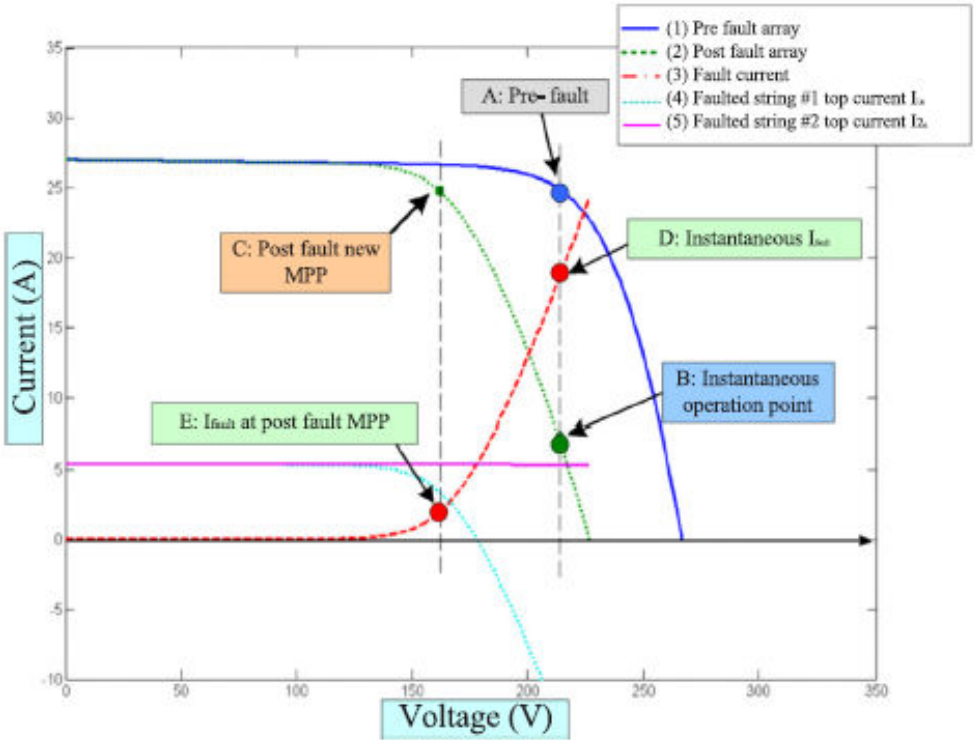

Figure 1.8: I-V characteristics under Line-Line faults in the PV array

1.7.1.3 Line-Ground Faults

In order to protect the users from potential electric shock, the non current carrying parts of a PV array i.e. the metallic parts are usually grounded using Earth Ground Conductors (EGC) Ball et al. (2013). Any accidental connection between EGC and Current Carrying Conductors (CCC) in a PV array leads to rapid and continuous current ow into the ground, which is often termed as a "Ground fault" as shown in Fig. 1.9.

To provide adequate safety and to avoid permanent failure of the PV systems, ground faults must be detected and isolated. For an un grounded PV array, a Residual Current Monitoring Device (RCD) is connected between the positive and negative terminal of each string to detect ground faults. Alternative to RCD, offline measurement of dc insulation resistance using Insulation Monitoring Devices (IMDs) can also be employed to detect ground faults. On the other hand, in grounded PV systems, continuous flow of current to the ground melts the Ground Fault detection and Interruption(GFDI) fuse, which is connected in series to the ground conductor to isolate

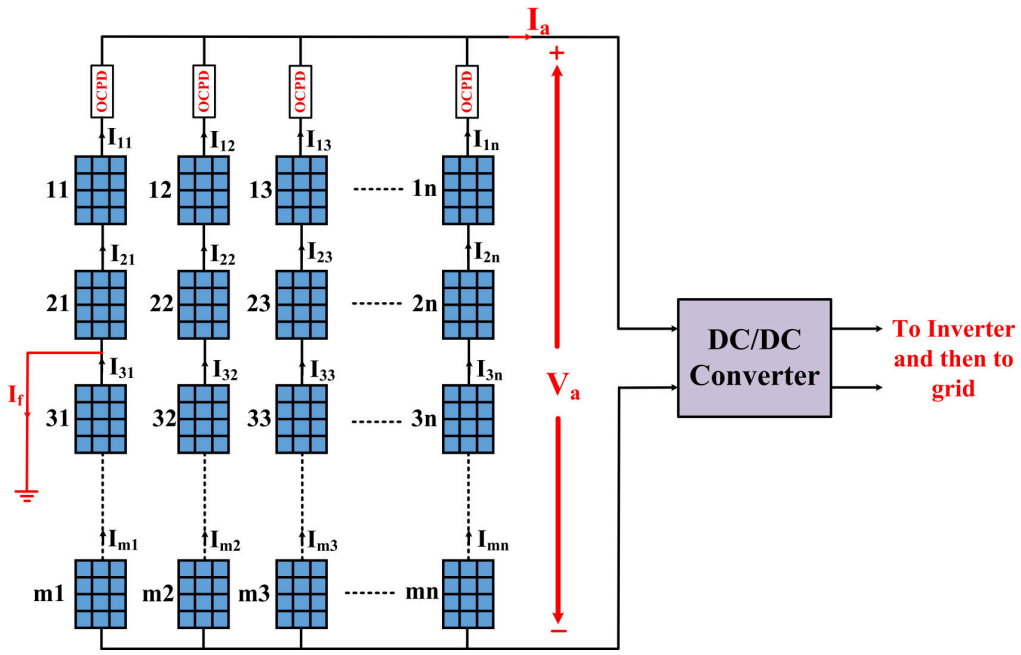

Figure 1.9: Line-Ground Faults Occurring in PV Array

the PV array in the presence of a fault. Hence, grounded PV systems are globally preferred over un grounded systems Ball et al. (2013).

1.7.1.4 Protection challenges for Line-Ground Faults

The severity of Line-Ground faults depends upon the location of the fault point and may even remain undetected. Anomalies present in the I-V curve as a result of ground fault are extensively studied in Flicker and Johnson (2013a) Flicker and Johnson (2013b) Wiles and King (1997) and is shown in Fig. 6, where seven distinctive operating points, 'A-F' are depicted. At the instant of fault, the operating point of both the array and the faulty string changes instantaneously to point B and point E respectively, where the array current is zero and string current is negative due to heavy back fed current. Whenever there is a drop in power, MPPT tries to optimize the operating point such that maximum power can be delivered. As a result, MPPT reduces the operating voltage of the PV array to operate at post fault MPP point, C. At the same time, the operating point of the faulty string is also optimized to work at point, F such that the string current remains positive. It is also evident that the change in operating point leads to a huge reduction in power. Therefore, reduced power with simultaneous reduction in operating voltage is an indicator of

ground faults.

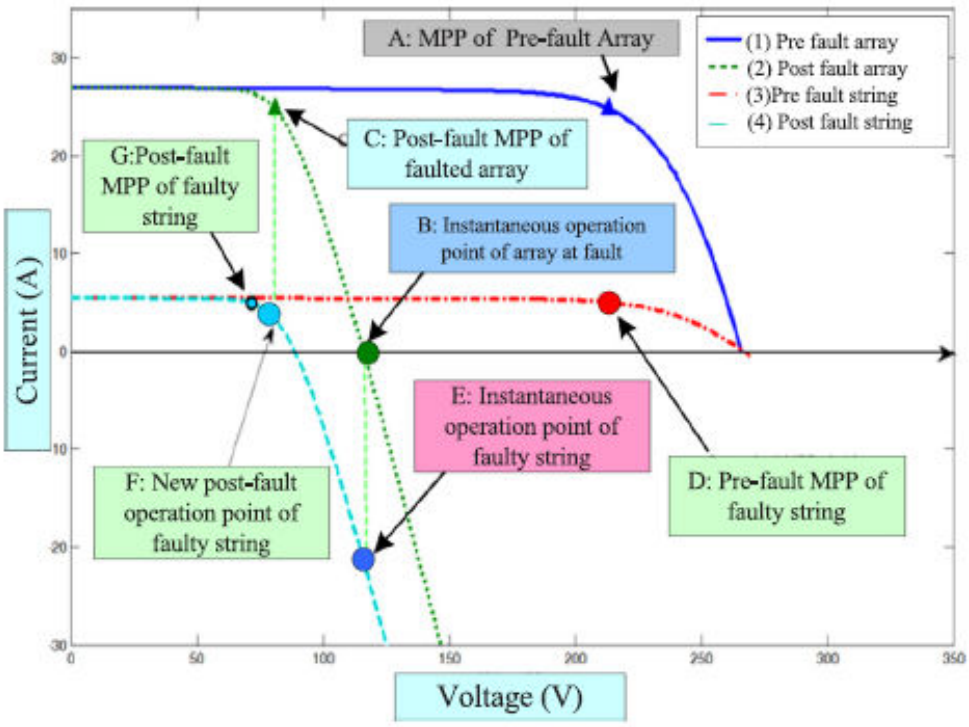

Figure 1.10: I-V characteristics under Line-Ground Faults Occurring in PV Array

Irrespective of the number of protection devices used, protecting ground faults may sometimes become a challenging task Bower and Wiles (2000)EDITION (2016) due to the following reasons: 1) The response of MPPT to ground faults diminishes the magnitude of fault current that in turn deceives GFDI fuses and OCPDs, 2) GFDI fuses are not sensitive enough to detect high impedance ground faults and hence, double ground faults can potentially harm the entire PV system, 3) RCDs are affected by the presence of external noise and sometimes may miss-trigger the protection circuits and 4) Any leakage current flowing in the opposite direction limits the magnitude of fault current and hence may deceive the operation of GFDI fuse and IMDs.

1.7.2 Open Circuit Faults

An open circuit fault in a photovoltaic (PV) string occurs when there is an interruption or break in the electrical continuity of the circuit as shown in Fig.1.11. Open

circuit faults occur as an after effect of line-line faults and can be detected manually using Earth Capacitance Measurement (ECM).

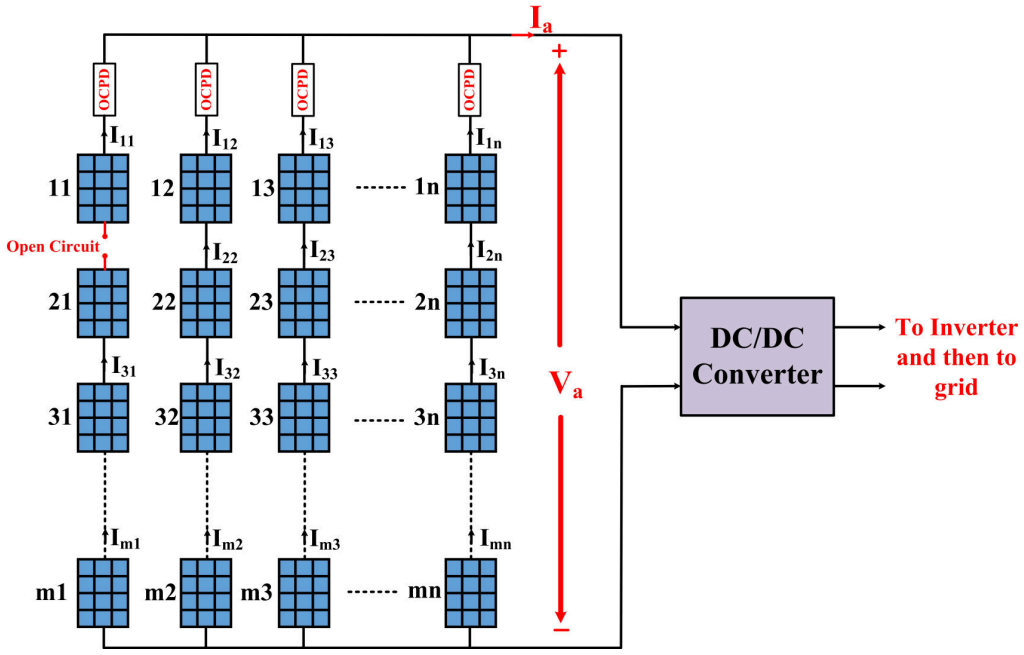

Figure 1.11: Open circuit faults in the PV array

Among advanced fault detection techniques, multi resolution analysis and artificial intelligence (AI)-based techniques such as wavelets and fuzzy inference system in Yi and Etemadi (2016), and random forest-based approach Chen et al. (2018) are used to identify the faults. However, these methods require voluminous training data sets for efficient operation. Besides, some techniques apply statistical difference measurement between simulated and field electrical quantities of PV system such as array losses in Hariharan et al. (2016), instantaneous dissimilarities in ac output power Murtaza et al. (2019), and Thevenin resistance Karmakar and Pradhan (2020). However, these methods require weather data, and requires module level converters, which limits its suitability for large PV systems. Recently, an MPPT-based fault detection is proposed in Pillai and Rajasekar (2018), though it is not suitable for PV systems with blocking diodes. Apart from the above, faults are also identified and localized using module voltages and their voltage-changing pattern in Miao et al. (2020), with optimal placement of voltage sensors alone in Kumar et al. (2020), based on sequential change detection framework and string current sensors Mehmood et al. (2021). In Miao et al. (2023) a new fault detection and identification method based on voltage

characteristics id proposed. In Ganesan et al. (2023) a new based with minimum number of sensors is proposed to detect the faults in the PV array. It fails to identify the module which is fault. However, these methods require substantial number of voltage and current sensors for its realization, which subsequently aggravates the system complexity as well as the overall cost.

1.7.2.1 Shade Faults

For optimum performance and energy yield, PV modules are suitably interconnected to form a PV array. However, the performance of PV systems varies as the irradiation profile varies. PV arrays can be subjected to partial shading as shown in Fig. 1.12, which is uniform or non uniform.

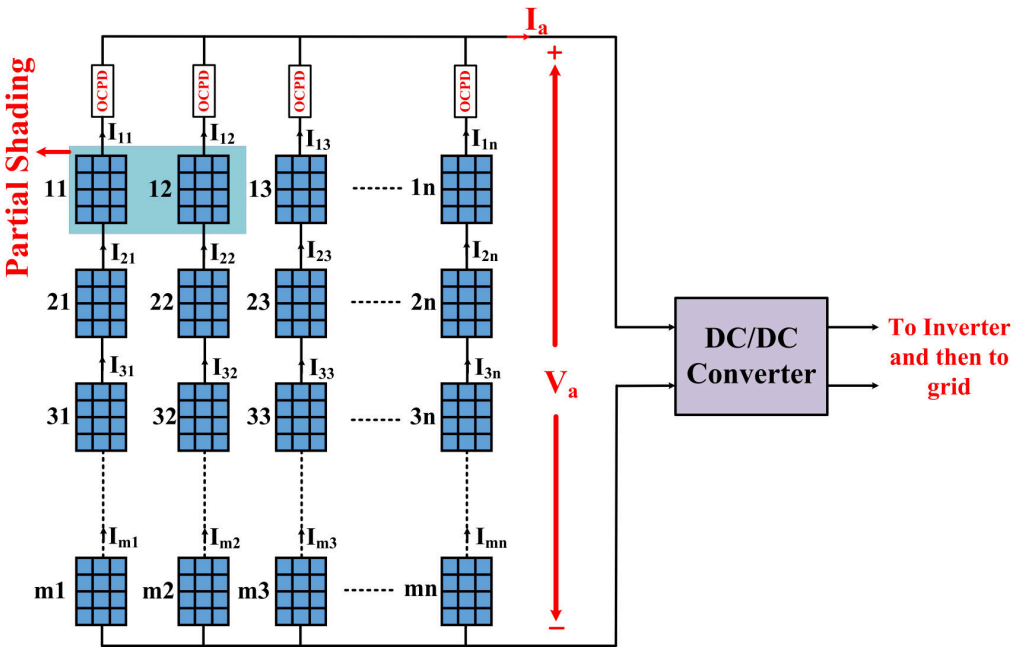

Figure 1.12: Partial shading on a PV Array

The factors affecting the PV array's output are temperature and incident irradiance. However, due to partial shading, the incident irradiance on the PV array is not uniform. Moving clouds, the shadows of trees and tall buildings contribute to partial shading on the PV array Yang et al. (2021) Belhachat and Larbes (2021) Krishna and Moger (2019b). Under partial shading, the power voltage (P-V) characteristic curve has numerous peaks, making it challenging for the maximum power point tracking

(MPPT) algorithm to track the global maximum power point (GMPP). This makes it a challenging task for the MPPT to catch the global peak La Manna et al. (2014) Rezazadeh et al. (2022) Jalil et al. (2022).

1.7.2.2 Protection challenges for shade faults

In addition to the reduction in output power, partial shading also leads to the formation of hot spots in the shaded panel, there by accelerating its aging process. Hence, to diminish the effects of partial shading and to improve the power flow, bypass diodes have been proposed Malathy and Ramaprabha (2018a) Pachauri (2022). Even though bypass diodes improve the power flow, bypassing of panels will introduce multiple peaks in the I-V and P-V curves; making it a challenging task for the MPPT to catch the global peek. For the PV configuration illustrated in Fig.1.13, the effect of shading on the PV characteristics shown in Fig. 1.13 that indicates the presence of multiple peaks due to bypassing of panels. Permanent partial shading due to dust accumulation and bird droppings can cause degradation of the panels, if it remains undetected for a long time.

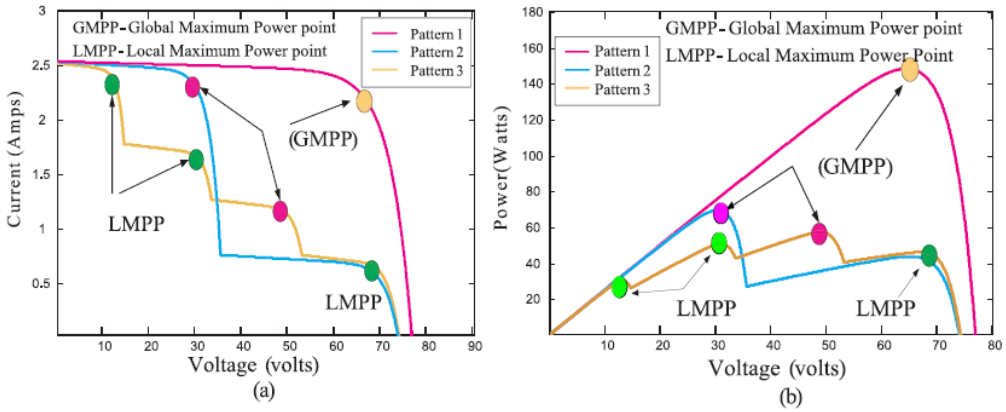

Figure 1.13: I-V characteristics under partial shading of the PV array

Till date, no protection devices are available which can detect shading faults in a PV system. Even though shading faults are common and is usually temporary, detecting shading faults is extremely important in the context of protection of PV systems due to the following facts: 1) Rapid detection of permanent shades increases the life span of a PV system, 2) Detecting shading faults reduces the complexity in the selection of MPPTs Amar Raj and Anil Naik (2023) Pachauri et al. (2020) and 3) More

importantly, since shading faults have similar signatures to that of other electrical faults, temporary shading faults must be detected and discriminated to avoid false tripping of PV systems.
After conducting an in-depth analysis of various faults occurrences in a PV system, the following key points are likely to be summarized.

- The magnitude of fault current depends upon the level of mismatch between the PV modules.
- Conventional protection devices are not sensitive enough to protect the PV array from all fault occurrences and hence, new fault detection tools are mandatory.
- Apart from detection, distinguishing faults is also important for proper isolation and maintenance of the system.

1.8 Partial shading reduction techniques

The major component of solar PV generation systems is photovoltaic (PV) cells.A PV module is formed by a series combination of PV cells. The PV modules are joined in various patterns to attain the desired voltage and current. However, various factors are considered to ensure the best possible usage of PV modules. In general, power output from the PV array relies on temperature and solar insolation. Most importantly, under Partial Shading Conditions (PSCs) power attainment decreases drastically, where the modules in the array receive variable irradiance. It occurs due to passing clouds, bird droppings, and shadows of tall buildings. Under PSCs, there occurs a decrease in GMPP and the formation of hot spots. To reduce the effect of hot spot formation, every module is accompanied by an anti-parallel connected by-pass diode. However, the use of bypass diodes under PSCs introduces multiple peaks in the characteristic curve of Power versus Voltage (P–V). The highest peak is the Global Maximum Peak Point (GMPP) and the remaining are Local Maximum Peak Points (LMPP). So, the tracking of GMPP under PSCs is becoming difficult. The power output due to PSCs from the PV array decreases and mismatch loss increases. Addressing the issue of PSCs, several techniques are proposed in the literature like MPPT techniques, PV array configuration schemes Ramaprabha et al. (2011) Satpathy et al. (2017), and reconfiguration methods which is shown in Fig. 1.14.

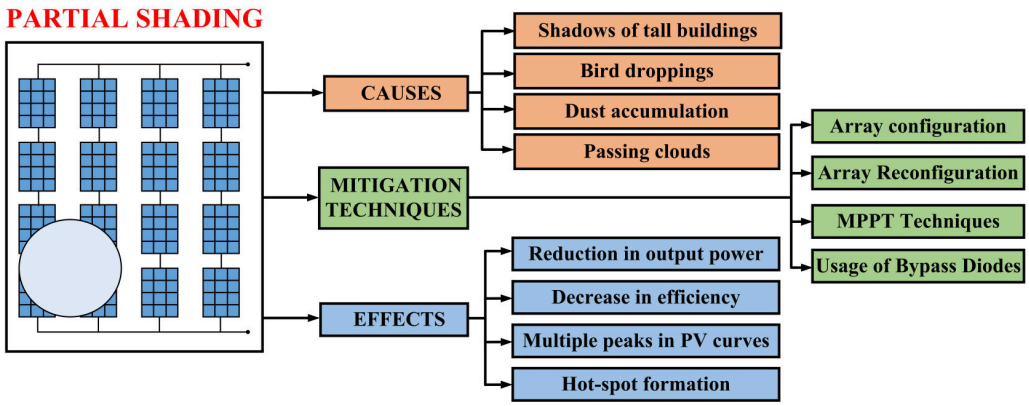

Figure 1.14: Partial shading causes, mitigation techniques and effects

1.8.1 PV Array Configuration

A PV array configuration defines the way in which the PV modules are interconnected. The main topologies are Series-Parallel (SP), Bridge-Linked (BL) and Honey-Comb (HC), and Total- Cross-Tied (TCT) Bonthagorla and Mikkili (2020c) Pendem and Mikkili (2018).

1.8.1.1 Series- parallel (SP) connection

In this method, a set of PV modules are joined in series forming a string, and set of these strings are connected in parallel to form the array. Fig. 1.15(a) shows the arrangement of the series-parallel connection of PV modules Winston et al. (2020). Blocking diodes are inserted in series with each string to ensure no reverse current under short circuit conditions and PSCs. Every module in the PV array is provided with a bypass diode to prevent local hot spots during PSCs.

1.8.1.2 Bridge Link (BL) connection

In the case of SP configuration, the mismatch loss is more due to series-connected modules. To address this issue, the PV modules are organized into a unique setup called a bridge rectifier structure which is termed a Bridge Link (BL) arrangement as shown in 1.15(b). Here all the bridges are connected with the help of cross ties Winston et al. (2020). Here two modules are connected in series within each bridge, and then these bridge connections are made in parallel with the other two series-connected modules.

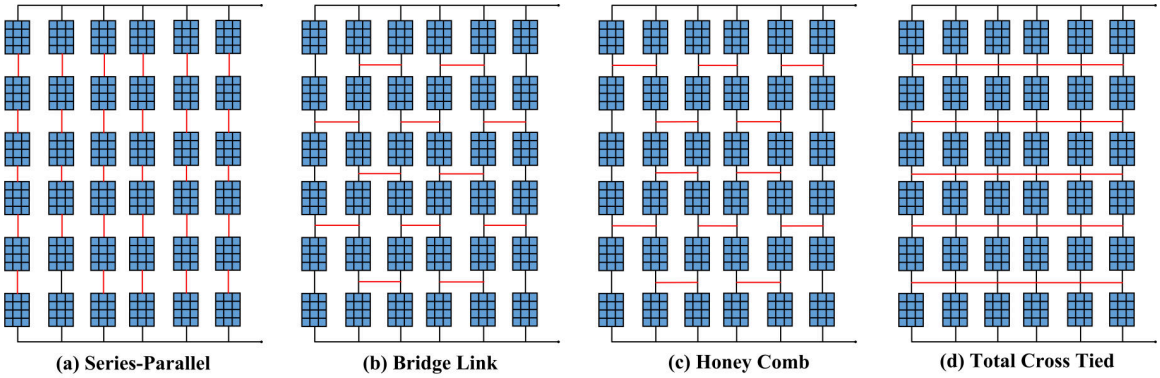

Figure 1.15: Conventional PV array configurations (a) Series Parallel (b) Bridge Link (c) Honey Comb (d) Total Cross Tied

1.8.1.3 Honey Comb (HC) connection

The hexagonal shape of honey bee houses is the basis for the connection of PV modules in Honey Comb (HC) configuration. In this arrangement, a hexagonal shape of a honey bee house is formed with every six modules and is joined using cross ties Chandra Sekhar and Ramesh (2023a). Here, three series-connected modules are joined in parallel to another three sets of series-connected modules. For a symmetrically connected PV array, the performance of the HC arrangement is moderate compared to the BL arrangement. The array connection of the HC arrangement is depicted in Fig. 1.15(c).

1.8.1.4 Total Cross Tied (TCT) connection

To overcome the drawbacks of SP, BL, and HC configurations, the Total Cross Tied arrangement of the PV array is formed. Here cross ties are connected at every row of the junction of the Series–Parallel (SP) array Chandra Sekhar and Ramesh (2023a). In this arrangement row and module voltages are equal. TCT configuration has more wiring loss compared to other configurations. The voltage across each row is the same as each module voltage and the voltage of the array is equal to the sum of row voltages. The PV array output current is equal to the sum of module currents in a row. The TCT arrangement of PV array is depicted in Fig. 1.15(d). A comparative analysis of various PV array configuration is presented in Table.1.1.

Table 1.1: Comparison between different PV configuration techniques

Authors	Year	Array Size	Configuration	Analysis Parameter	Observations
Praveen Kumar *et.al*	2020	7×7	SP, BL, HC, TCT	GMPP, FF, Mismatch Loss, Efficiency	TCT generates highest GMPP compared to SP and BL configurations
Okan *et.al*	2018	6×6	SP, BL, HC, TCT	GMPP, FF, Mismatch Loss, Efficiency	TCT scheme gives highest FF, lowest MPL, and highest GMPP.
Suneel *et.al*	2018	5×5	SP, BL, HC, TCT	GMPP, FF, Mismatch Loss, Efficiency	TCT generates highest GMPP compared to SP, BL, and HC configurations
Sasmita Jena *et.al*	2017	3×3	SP, BL, HC, TCT	GMPP, FF, Mismatch Loss, Efficiency	TCT has lower power loss and better efficiency than SP and BL configurations.
R.Ramaprabha *et.al*	2011	2×4, 6×3, 7×4, 8×6	SP, BL, HC, TCT	GMPP, FF, Mismatch Loss, Efficiency	TCT is the best configuration for symmetrical array and HC for asymmetrical array

Table 1.2: Comparison between Hybrid PV configuration techniques

Authors	Year	Array Size	Configuration	Analysis Parameter	Observations
Praveen Kumar *et.al*	2021	7×7	SP, BL, HC, TCT	GMPP, FF, Mismatch Loss, Efficiency	Superior to SP, BL, HC. Preferred for standalone and grid connected systems
T.Ramesh *et.al*	2021	9×9	SP, BL, HC, TCT	GMPP, FF, Mismatch Loss, Efficiency	Better compared to TCT configuration. Able to generate GMPP onpar to TCT scheme.
Debyan Sarkar *et.al*	2023	7×6	SP, BL, HC, TCT	GMPP, FF, Mismatch Loss, Efficiency	Requires fewer cables and economical compared to TCT connection.
T.Ramesh *et.al*	2023	9×9	SP, BL, HC, TCT, TTCL	GMPP, FF, Mismatch Loss, Efficiency	Generates more GMPP compared to TTCL and HC configurations.

1.8.1.5 Hybrid PV array configurations

Among the conventional PV array configurations (SP, BL, HC, and TCT), TCT configuration has shown better performance in terms of increase in GMPP, Fill Factor, and Efficiency. Further to increase the GMPP from the PV array with reduced cross ties Hybrid PV array configurations are formed. They are formed by the combination of SP, BL, HC, and TCT connections. The Hybrid PV array configurations proposed in the literature are Triple Tied (TT) Bonthagorla and Mikkili (2020a), Triple Tied Cross Link (TTCL) Ramesh et al. (2020), Modified Triple Tied (M-TT) Sarkar and Sadhu (2023), and Novel Double Tied Cross Link (DTCL) Chandra Sekhar and Ramesh (2023b). The array connection diagrams are shown in Fig. 1.16. A comparison of cross ties required for TCT and above mentioned hybrid configurations are listed in Table.1.3. The hybrid PV array configurations are able to generate GMPP on par to the TCT configuration with reduced cross ties and can be considered as an alternative to the TCT configuration. A comparative analysis of the hybrid PV array configurations Bonthagorla and Mikkili (2020b) Bonthagorla and Mikkili (2020d) Nayak et al. (2017) Bana and Saini (2017) is shown in Table. 1.2.

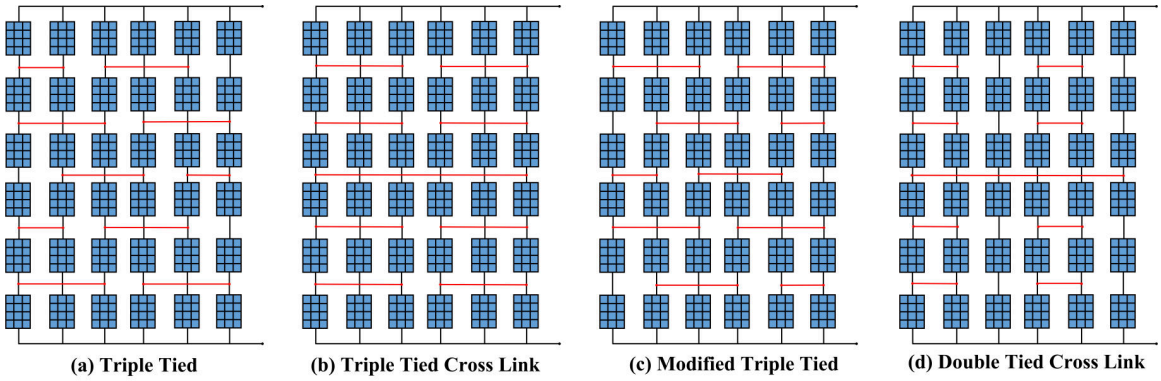

Figure 1.16: Hybrid PV array configurations (a) Triple Tied (b) Triple Tied Cross Link (c) Modified Triple Tied (d) Double Tied Cross Link

.

Table 1.3: Comparison of Cross Ties in TCT and other PV Array configurations

Array Size	TCT	TT	TTCL	M-TT	DTCL
6×6	25	17	21	17	13
9×9	64	43	52	52	40
12×12	121	81	91	81	81

1.8.2 Reconfiguration of PV Array

Reconfiguration strategies are most promising techniques for increasing the GMPP from the PV array under PSCs. These reconfiguration strategies are classified into types: (1) Dynamic PV array reconfiguration techniques (2) Static PV array reconfiguration techniques as shown in Fig. 1.17

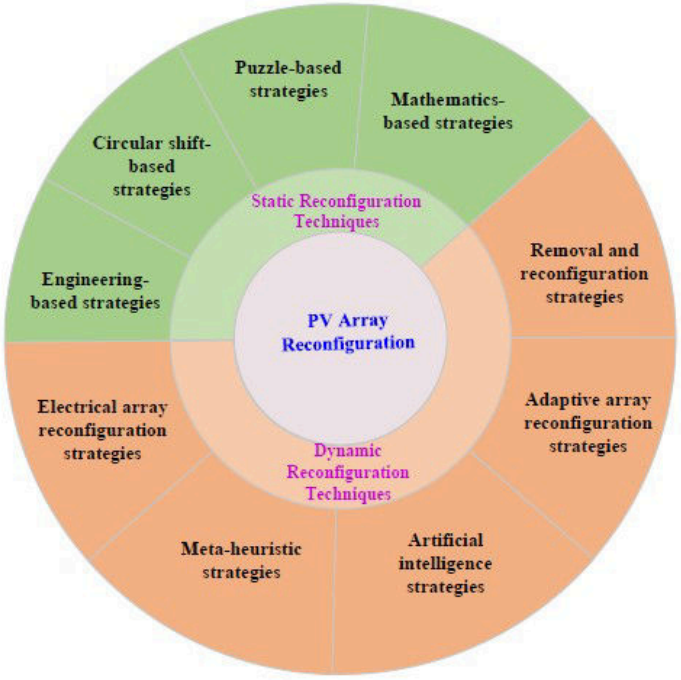

Figure 1.17: Summary reconfiguration techniques

1.8.2.1 Dynamic reconfiguration techniques

Dynamic reconfiguration is an adequate method to boost the generation of power from a PV during PSC. It involves altering the electrical connections between the PV modules without changing the position of the PV modules. This technique can be implemented in different ways, such as 1) Using switches between the interconnections of PV modules 2) Grouping the PV panels depending on shaded panels to avoid shading loss 3) Altering the series and parallel panels to equal the row current by using a switching matrix.

In Malathy and Ramaprabha (2018b), the PV array is reconfigured based on the irradiation levels and the row current. The switching matrix will generate switching

sequence between PV modules, based on the irradiation data received from a data acquisition system (DAQ). For configuring the switching matrix, field programmable gate array (FPGA) or digital signal processor (DSP) micro controllers have been widely used in Fig. 1.18(a) shows an switching sequence to reconfigure the series and parallel configuration of a PV array Deshkar et al. (2015). In El-Dein et al. (2012), the authors implemented a new dynamic reconfiguration technique for two parallel groups of PV modules. The switching matrix controller was developed using a fuzzy algorithm. In this method, reconfiguration of the PV array is takes place based on differences between maximum and minimum voltage of PV modules.

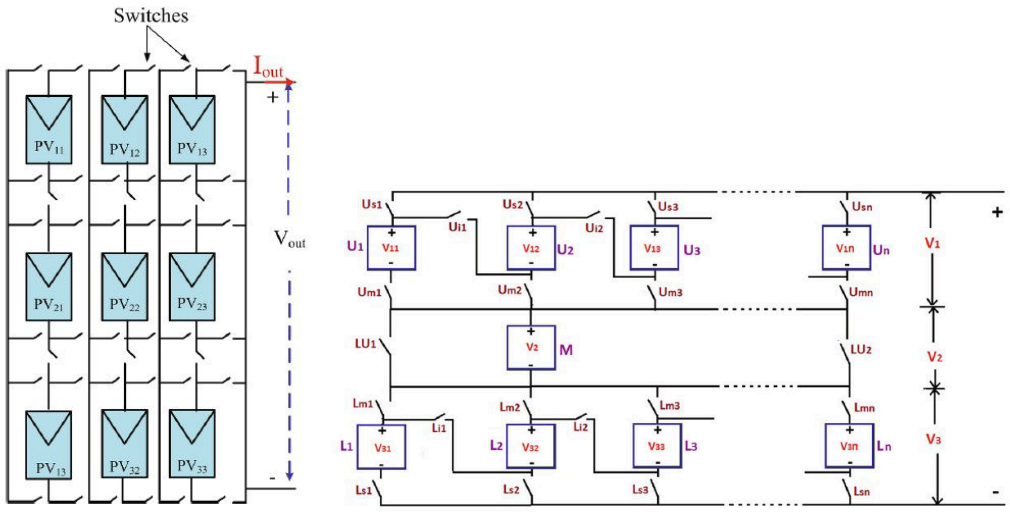

Figure 1.18: Summary reconfiguration techniques

A novel PV array reconfiguration method using dodging algorithm was proposed in Nguyen and Lehman (2008) that maintains a constant output current to the load which is shown in Fig. 1.18(b). The authors in Tabanjat et al. (2015) implemented reconfiguration using a fuzzy logic controller (FLC). In this method, the switching matrix is controlled by receiving the switching conditions from the FLC according to the degree of shading. The fuzzy method is not a reliable choice for reconfiguration because it is difficult to generate a switching matrix under shading conditions. In Ramasamy et al. (2016), Rough set theory was applied to a switching matrix controller to reconfigure the PV array for basic configuration schemes. The interconnections between the PV panels are changed dynamically by using mechanical switches. In this method, the authors measured the irradiation levels by considering the short circuit current (Isc) and open circuit voltage (Voc) of PV modules to describe the

favorable interconnection. The regular mechanical switches using in this approach increases the size of array. In addition, the use of driver circuits also increases the size and cost of the system because of the complexity in implementation. The authors in Babu et al. (2017)Ramaprabha (2014) implemented array reconfiguration for a 9×9 array. All these methods exhibit issues as they require multiple switches, driver circuits, sensors, time consuming and complex in controller Cheng et al. (2010). In Candela et al. (2007) author proposed an irradiation equalization (IE) technique that enhances the performance of the system and reduce the power losses during shading conditions. In this method, the IE controller reads the irradiation levels and re configures the PV modules. Half re configurable and full re configurable PV arrays were employed in Velasco-Quesada et al. (2009) to lessen the irradiance mismatch index (IMI) and develop the optimal reconfiguration structure of the PV array. An iterative and hierarchical sorting algorithm was developed in Rajan et al. (2017) to find the best reconfiguration that achieves maximum power generation. In Sanseverino et al. (2015), reconfiguration of a PV array based on IE method was developed using dynamic optimization algorithm for a switching matrix controller. Munkres optimization algorithm was proposed in Ngoc et al. (2017) to optimize the switching matrix based on the IE method. This method increases the processing speed to select the optimal reconfiguration of a PV array. A new dynamic reconfiguration for TCT connection was proposed in Jazayeri et al. (2017) that is based on capturing sky images that occur in real-time over the PV array to identify the shading positions. In this method, the switching matrix controller is developed based on IE to select the optimal interconnections of the PV array. Similarly in Matam and Barry (2018), a dynamic PV array technique was proposed to reconfigure the PV array during PSC. In this method, the PV array irradiance, voltage, and current are taken as input of the optimization process to choose the best reconfiguration of the PV array by a using switching matrix. This method reduces the initial calculations and computational time in-case of repeated shading conditions.

Adaptive array reconfiguration (AAR) is another type of reconfiguration technique in which the panels are categorized into two types: 1) fixed part and 2) adaptive part shows the AAR structure used in Nguyen et al. (2009) In this approach, the switching matrix is equipped amidst the fixed part and the adaptive part with a controller to equalize the irradiation of each row. The fixed part of the PV array in this method is configured as a TCT configuration, and the reconfiguration occurs on adaptive

part. This approach leads to reduction in the requirement of switching devices and sensors Parlak (2014). In Karakose et al. (2016), the authors used the bubble sort and model-based algorithm to control the switching matrix to find the optimal PV array reconfiguration that enhances power generation. In Mahmoud and El-Saadany (2017)Mostafaee and Ghandehari (2020), the temperature, irradiance level of the PV array, and the sun position are taken as inputs to control the switching matrix and to identify an optimal reconfiguration of PV array. A self-adaptive reconfiguration technique using fuzzy controller was proposed in Fathy (2018). In this method, the best reconfiguration of the PV array is achieved by connecting the adaptive part of the PV panels with the greatest irradiation to the fixed part. When the voltage of the top row V1 is below the output voltage , the shading degree and derivative of irradiation are calculated and send to the controller to reconfigure the shaded panels of PV array. In Yousri et al. (2020), a scanning technique was developed depending on the current variation index (CVI). In this method, the reconfiguration of the PV array is implemented by a connecting switching matrix between the fixed part and the adaptive part using current row algorithm.

1.8.2.2 Static reconfiguration techniques

Static reconfiguration of PV array involves altering the position of PV modules without changing the electrical connections. It is one time arrangement done at the installation. The position of PV modules is altered based on mathematical, puzzle-based, and meta heuristic-based approaches.

In Rao et al. (2014) a fixed array reconfiguration strategy is proposed to evenly distribute the partial shade across the full array. It is implemented on a 3×3 and 5×5 PV arrays and outperforms SP, TCT, and BL configurations in terms of output power generation. It is not applicable to rectangular and large size PV arrays. The authors in Sahu and Nayak (2016) Kumar (2020) proposed two techniques PRMFEC, PRFCPMFEC where the PV array modules are displaced on the basis array length. However, there exists repeated row positions across particular column and shade is not distributed more effectively. In Nasiruddin et al. (2019)Reddy and Yammani (2020b)] two methods Odd Even (OE) and Odd Even Prime (OEP) are presented and tested on a 9×9 PV array. Here the modules are displaced randomly to another position based on odd, even and prime patterns. Hence, it requires more wire and wiring loss increases. In Sahu et al. (2015)Tatabhatla et al. (2020) tw new puzzle

based schemes Futhoshiki and Tom-Tom are proposed and implemented on 5×5 PV array. The power generation from the PV array is the same as EAR scheme for different shading conditions. These are applicable to only square array. In Krishnan et al. (2022) Twisted Two Step array reconfiguration scheme is presented where the modules are displaced across different columns. The shade is not dispersed effectively over the array. In Tatabhatla et al. (2021) Chaotic baker map technique (CBMT) is proposed, where image analysis method used to encrypt communication by randomly changing pixel locations. The physical placements of panels are represented as pixel locations in the CBMT, and they are shifted to different points across the array. The Knight's tour is a chess-based approach Raj and Naik (2023) that re-configures photovoltaic (PV) arrays depending on the Knight's moves on the chessboard so that shadows are dispersed evenly across all rows and maximum power is harvested. In this instance, the tour begins in the field that is immediately next to the beginning spot. It is categorized as an open tour due to the fact that the Knight is unable to return straight to their starting location. In Raj and Naik (2022)Amar Raj and Naik (2022) the authors proposed two methods Image Encryption (IE) and Arnold's Cat Map (ACM). These are implemented on 9×9 PV array and are able to increase the GMPP, Efficiency, fill factor.

In Venkateswari and Rajasekar (2020) a different sort of puzzle-solver static reconfiguration design known as 'Lo Shu' is presented. Lo Shu re configures the first sub-array using the venation design and separates it into nine 3×3 sub-arrays from the 9×9 array 'Lo Shu.' Likewise, based on the initial sub array, the left sub-arrays are rearranged. The key benefit of the Lo Shu approach is that it achieves significant shade distribution with lesser physical rearrangements. In Pachauri et al. (2022) Ancient Chinese Magic Square (ACMS) technique is proposed and implemented on 9×9 PV array. It has minimum number of power maxima points with higher shade dispersion. The Dominance Square (DS) in Dhanalakshmi and Rajasekar (2018a) is a puzzle solver reconfiguration approach which maintains minimal row current variation such that effective shade dispersion occurs across the array. In Dhanalakshmi and Rajasekar (2018b), the authors proposed Competence square technique (CST) where the PV modules are relocated using particular logic. CST method is compared with TCT and DS configurations. The CST approach improves mismatch power loss elimination, power enhancement, and fill factor. The CST approach has the potential benefit of being easier to adopt in practice. The CST approach has difficulty with sig-

nificant wire losses. In Kumar and Raushan (2023) an Innovative Competence Square (ICS) algorithm is presented to overcome the limitations of CS technique. The Magic Square (MS) technique in Reddy and Yammani (2020a) can be implemented for any n×n PV array. MS matrix adheres to the mathematical principle that the sum of values in any column, row, or crosswise is equal. Furthermore, as compared to bridge BL, SP, and TCT, the proposed MS has lower power losses and an improved fill factor. The limitation of MS reconfiguration is that modules within the same row might still be dispersed in the next sub array. When such sub-arrays are darkened, the MS approach fails to disseminate the darkened panels throughout the complete array, resulting in higher mismatch losses.The MS puzzle is reformed with specific computational instructions to form the Latin Square (LS) Madhusudanan et al. (2018) and the Ken-Ken Square (KKS) Palpandian et al. (2021) methods. The LS and KKS reconfiguration provided better wire loss reduction, instantaneous maximum power, shade dispersion, and fill factor in prominent PSCs. An enhanced version of magic square method known as Magic Square Enhanced Configuration (MS-EC) is presented in Yadav et al. (2017). The proposed algorithm disperses the shading effects more evenly over the entire array surface, reducing the conduction losses due to the bypass diode operation.

In Pachauri and Singh (2023), a novel physical relocation technique Successive Rotation Approach (SRA) is presented, which illustrates high GMPP and better performance under PSCs. The SRA puzzle-based PV module restructuring methodology has a more significant shade dispersion factor (SDF) capability compared to traditional arrangements such as SP and TCT thus reducing mismatch power loss. An experimental system is developed to validate the MATLAB/Simulink-based results. In addition to this, the temperature effect due to shading is investigated and non-symmetrical 6×9 PV array configuration is considered for performance evaluation through experimental work. In Anjum et al. (2022a) the PV modules are relocated based on Addition Progression Structure (APS). The proposed APS topology provides a maximum reduction of 38.36% in mismatch power loss, and 1.62% more fill factor as compared to TCT configuration.

In Yadav et al. (2023b), a Recursive Addition Approach (RAA) is proposed such that the PV systems are immune to the negative effects of partial shading. This novel technique tries to achieve a constant row current by repositioning the panels while keeping the electrical connections intact. In contrast to conventional designs,

it ensures that no two panels in the same row are placed next to each other, thereby resulting in power augmentation. In Yadav et al. (2023a), a novel reconfiguration approach inspired by the circular array data structure a commonly utilized tool in the realm of computer science is proposed. The proposed circular array transformation (CAT) technique shows great potential in mitigating the impact of partial shading and maximizing the overall power generation across a wider range of PSCs. The effectiveness of the proposed technique is validated through simulations and experimental studies conducted on a 5×5 PV array. Furthermore, the scalability of the proposed reconfiguration technique is verified through extensive simulations on a 9×9 PV array.

Typically, most of the existing physical relocation methods have been conceptualized based on mathematical puzzles owing to its high shade dispersion capability. However, most of these methods are not compatible to both symmetrical and non-symmetrical PV arrays. In Nihanth et al. (2019) and Vijayalekshmy et al. (2016) two new physical relocation techniques Skyscraper puzzle and Zig-Zag method suitable for all PV arrays is designed, implemented and tested. It shows uniform characteristics and enhanced power output compared to the existing techniques in literature. Maintaining the uniform irradiance in an extensive photovoltaic (PV) system is almost impossible. The mismatch between panels of a PV array results in substantial power loss. In Jalil et al. (2023) the PV panels in an array are reconfigured by the proposed Cross-Kit (CK) technique to obtain optimal power output for different partial shading conditions (PSCs). The suggested approach allows the structure to balance the shade effect across the entire PV array with different physical places of panels.

The literature presented various Sudoku based reconfiguration techniques. In Rani et al. (2013) a random Sudoku puzzle based reconfiguration is proposed. The modules of the 9×9 PV array are physically displaced as per chosen Sudoku puzzle pattern. It has many sub arrays of sizes 2×2, 3×2, 2×3 and 3×3 where repeated digits occur. The shade on these sub arrays is not distributed to other rows, thereby system performance is not improved. To overcome the limitation of Sudoku techniques advanced versions of Sudoku puzzle patterns are presented in the literature. In Krishna and Moger (2019c) an Optimal SuDoKu arrangement is proposed. It is tested in SIMULINK under five shading patterns and is able to generate GMPP greater than Sudoku puzzle pattern. Where as this technique is not suitable for square array with prime numbers (5×5, 7×7, 11×11,..). Here, the complexity of arranging the modules is more as the array size increases. In Rajani and Ramesh (2020)Krishna and Moger

(2019a) two new puzzle patterns named Modified Sudoku and Improved Sudoku are presented. These methods are tested in simulation and proven better than Sudoku in mitigating the effects of partial shading. In Anjum et al. (2022b)Anjum et al. (2021)Anjum et al. (2022c) three Sudoku puzzle based techniques Hyper Sudoku, Advanced Sudoku, and AdDoKu are presented. The Sudoku puzzle based reconfiguration techniques are better to disperse the shade at the corners of the array. But these techniques are applicable only to square array. Further in Fathy et al. (2023)Yousri et al. (2022)Aljafari et al. (2023)Ye et al. (2021)Rezazadeh et al. (2021) different sudoku based techniques are proposed. These are applied on 9×9 PV array and are applicable to only square arrays.

1.9 Summary

In this chapter a brief introduction to solar photovoltaic systems, faults occurring in PV arrays, challenges in detecting the faults are presented. Further a detailed literature survey on faults in PV array, static and dynamic reconfiguration techniques is carried out.

Chapter 2

Faults in Solar PV Array

This chapter proposed A Diagonal Sensor Arrangement(DSA) scheme to identify and localize the faults occurring in the solar PV array. The proposed method is implemented on 4×4 PV array in both simulation and hardware environments. It is able to identify and localize the faults with greater accuracy. The proposed method utilizes minimal number of voltage sensors to detect the faults. The proposed method is applicable for square and non-square arrays of any desired size.

2.1 Introduction

Solar Photovoltaic (PV) arrays are subjected to faults that damage the PV modules. The common faults occurring in the PV arrays are Line to Line (LL), Line-Ground (LG), Open Circuit (OC) and partial shading faults. The PV arrays are equipped with conventional protection devices to detect the faults when the fault current magnitude exceeds the threshold value. But the fault current magnitudes depends upon level of irradiance, maximum power point tracking (MPPT) control, type of mismatch and presence of blocking diodes. So, faults in these situations remains undetected and leads to reliability issues. Therefore, timely detection of the faults in the PV array is essential. The contributions made in this chapter are listed as follows:

- An efficient fault detection algorithm is proposed by employing minimal number of voltage sensors.
- The characteristics of various faults is analyzed.

- The proposed method is implemented on 4×4 PV array and validated in software (4kW system) and hardware (0.16kW system) considering various fault conditions.
- Further, a comparative analysis in terms of sensor requirement between the proposed method and various other techniques in the literature is presented.
- Further, a comparative analysis in terms of sensor requirement between the proposed method and various other techniques in the literature is presented.

2.2 System Description

2.2.1 Analysis of various voltage sensor placement strategies

In the literature, there are various sensor placement schemes proposed to identify the faults in a PV array. To analyze various sensor placement strategies, a 4×4 PV array is considered.

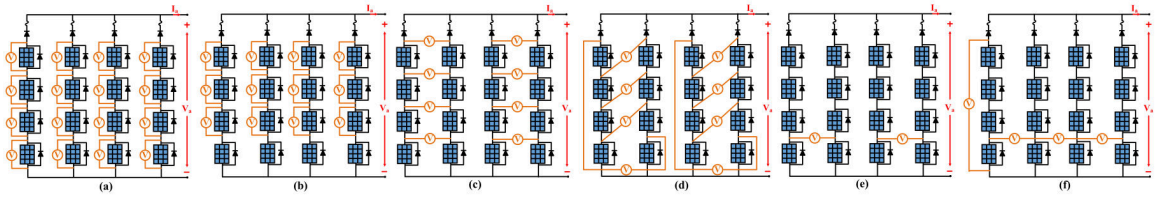

Figure 2.1: Sensor placement strategies for 4×4 PV Array (a) Method-I (b) Method-II (c) Method-III (d) Method-IV (e) Method-V (f) Method-VI

The voltage sensor placement schemes proposed by the authors in the literature are shown in Fig.2.1. In method I, each module of the PV array is provided with a voltage sensor as shown in Fig.2.1(a). So, for a 4×4 PV array, it requires 16 sensors for voltage measurement. In method II, the modules in each string are provided with a voltage sensor except the last module as shown in Fig.2.1(b). So, for a 4×4 PV array, it requires 12 sensors for voltage measurement. In method III, voltage sensors are connected between strings-1 and 2, strings-3 and 4 as shown in Fig.2.1(c). So, for a 4×4 PV array, it requires 8 sensors for voltage measurement. The connection of sensors in method IV is shown in Fig.2.1(d) and requires 8 voltage sensors. In method V, the voltage sensors are arranged at the lower end of strings-1,2 and strings3,4 as shown in Fig.2.1(e). It requires only 2 sensors to identify the faults in the PV array.

In method VI, there are 4 sensors arranged as shown in Fig.2.1(f). Table.2.1 gives the number of voltage sensors required for existing and the proposed DSA method implemented on a m×n PV array and for different array sizes. It is observed that, as the size of the PV array increases the number of voltage sensors required increases which makes the system more complicated and highly expensive.

Table 2.1: Comparison of various sensor placement techniques

Technique	**Number of voltage sensors required for**			
	m×n Array	**4×4**	**6×6**	**8×8**
Method I	m×n	16	36	64
Method II	(m-1)×n	12	30	56
Method III	m×n/2	8	18	32
Method IV	2×n	8	12	16
Method V	n/2	2	3	4
Method VI	m	4	6	8
Proposed Method	(n-1)	3	5	7

2.2.2 Diagonal Sensor Arrangement

A new voltage sensor placement scheme is proposed which is based on diagonal arrangement. For a m×n PV array, the sensor arrangement is shown in Fig.2.2. For a m×n PV array, there exists (m-1) cross-tie rows. The sensor-1 is connected between strings 1 and 2 in the cross-tie row-(m-1). The sensor-2 is connected between strings 2 and 3 in the cross-tie row-(m-2). This sensor arrangement continues until the strings (n-1) and n are connected. The proposed Diagonal Sensor Arrangement on a 4×4 PV array is shown in Fig.2.3. The number of sensors required for 4×4 PV array is 3. Also, there are 3 cross-tie rows for a 4×4 PV array. The arrangement of sensors is depicted in the below steps.

- The sensor 1 is connected between strings 1 and 2 in cross-tie row 3.
- The sensor 2 is connected between strings 2 and 3 in cross-tie row 2.
- The sensor 3 is connected between strings 3 and 4 in cross-tie row 1.

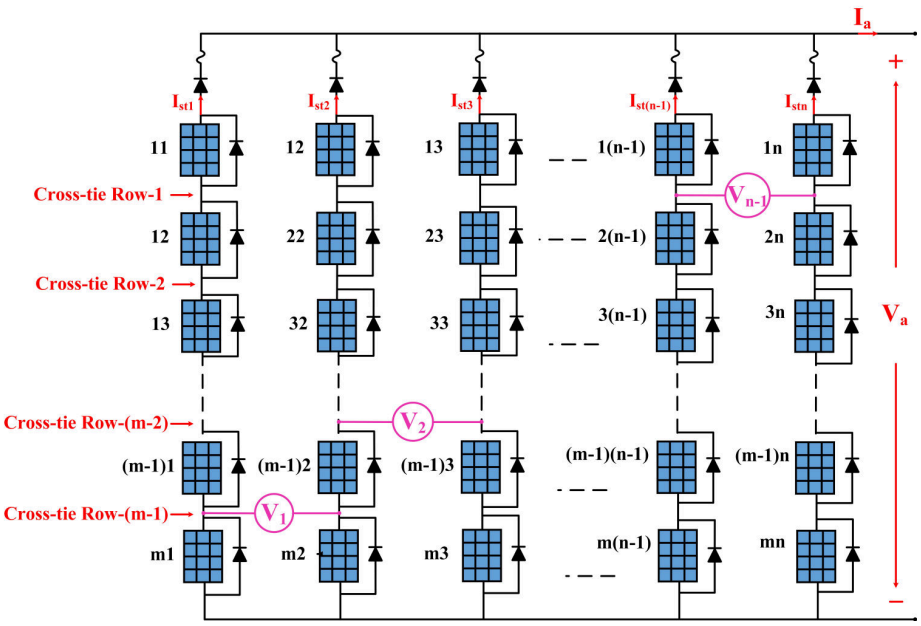

Figure 2.2: Proposed Diagonal Sensor Arrangement strategy for m×n PV Array

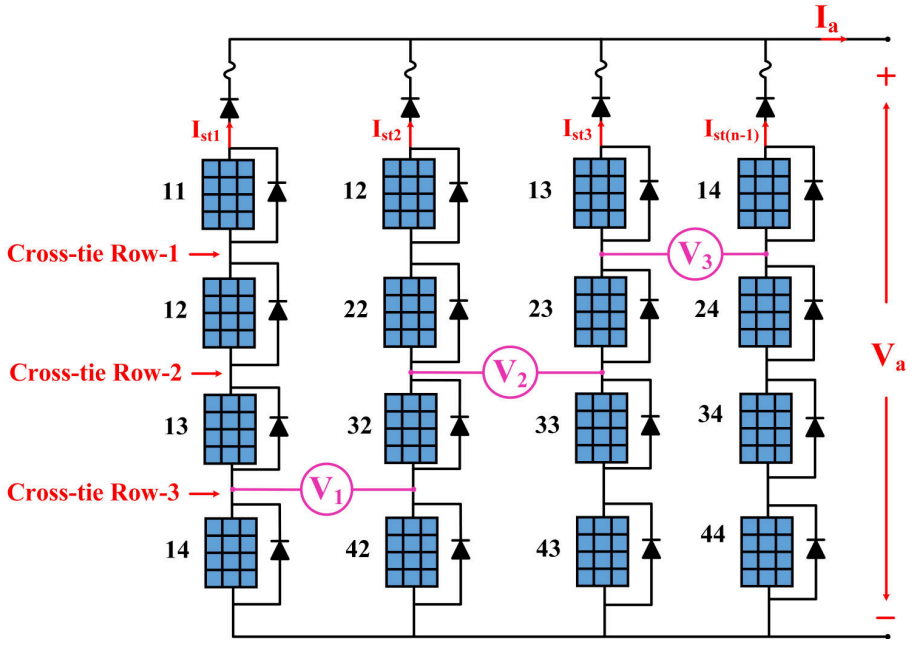

Figure 2.3: Proposed Diagonal Sensor Arrangement strategy for 4×4 PV Array

2.2.3 Detecting of Faults using the proposed Diagonal Sensor Arrangement (DSA)

The presence of faults in the PV array can be detected using the proposed DSA method. The major advantage of the proposed DSA method is its ability to identify the faulty location in the PV array. For a 4×4 PV array, the ability of the DSA method to identify the faulty location is shown in Table.2.2. For the analysis, the occurrence of a single fault at a time is considered.

Table 2.2: Identification of the faulty location

S_1	S_2	S_3	**Faulty Location**
0	0	0	Normal condition
0	0	1	String-4
0	1	0	Not Possible condition
0	1	1	String-3 or Cross Strings 3-4
1	0	0	String-1
1	0	1	Cross String 1-4 or 4-1
1	1	0	String-2, Cross String 1-2 or 2-1
1	1	1	Cross string between 1-3 or 3-1 or 2-3 or 3-2 or 2-4 or 4-2

2.3 Simulation Results

The PV array subjected to faults undergoes changes in characteristics. The analysis of characteristic curves helps in finding the faults and improving the reliability of the PV systems. Consider a 4×4 PV is considered. Here four modules each of 250W are connected in series to form a string. A set of four strings are joined in parallel to form a PV array. The specifications of PV module is given in Table. 2.3. The PV modules are numbered as PV1, PV2,.....PV16. The voltage across the PV modules is given by V_1,V_2, V_3,.....V_{16}. The current form the PV modules is given by I_1,I_2, I_3,.....I_{16}. The array output voltage is V_a and output current is I_a. The proposed Diagonal Sensor Arrangement (DSA) is implemented on a 4×4 PV array and different faults in the PV array are simulated in MATLAB/Simulink environment. The analysis of the system is carried out using the power voltage (P-V) and current-voltage (I-V) characteristics under normal operating conditions and various faulty conditions.

Table 2.3: Specifications of PV module considered for simulation

Parameters	Values
Maximum Power, $P_{mp}(W)$	250
Open Circuit Voltage, $V_{oc}(V)$	36.8
Short Circuit Current, $I_{sc}(A)$	8.71
Voltage at MPP, $V_{mp}(V)$	30.1
Current at MPP, $I_{mp}(A)$	8.1

2.3.1 Short Circuit Faults

Line-Line (LL) Faults Within the string: The Line-Line (LL) fault with one and two module mismatch is introduced in the 4×4 PV array as shown in Fig.2.4. The characteristics of the 4×4 PV under normal operating condition and LL faults with one and two module mismatches is shown in Fig.2.5. Under normal operating condition, the PV array and the string operates at the point "A" and "B" respectively. The PV array output voltage is 119.7 V and the modules of the PV array operate at MPP voltage of 30V. The voltage sensors (V_{d1}, V_{d2}, and V_{d3}) indicate zero reading indicating no fault in the PV array.

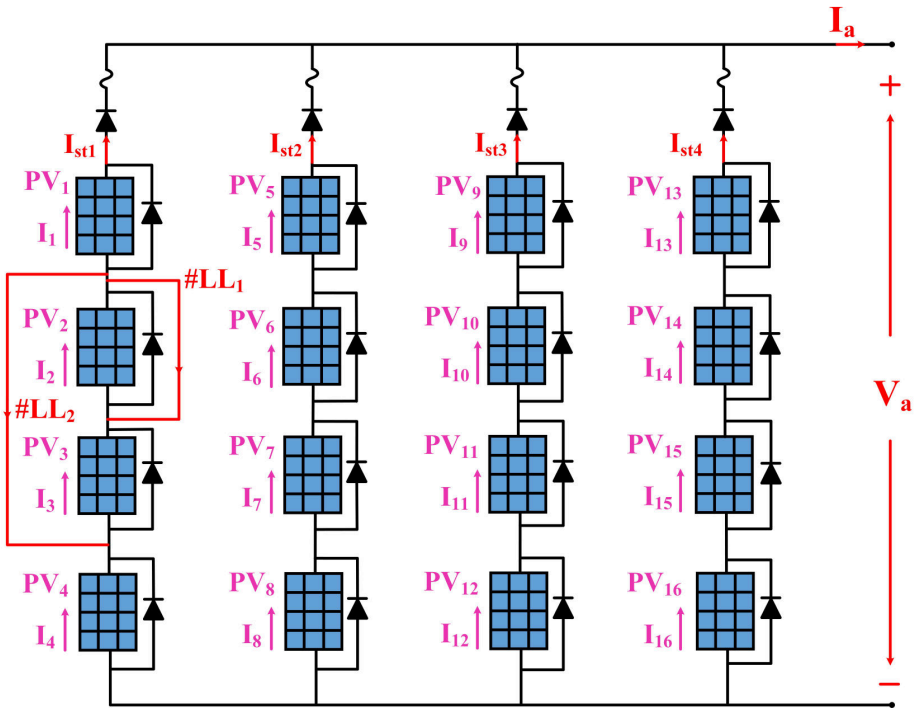

Figure 2.4: LL fault with one and two module mismatch

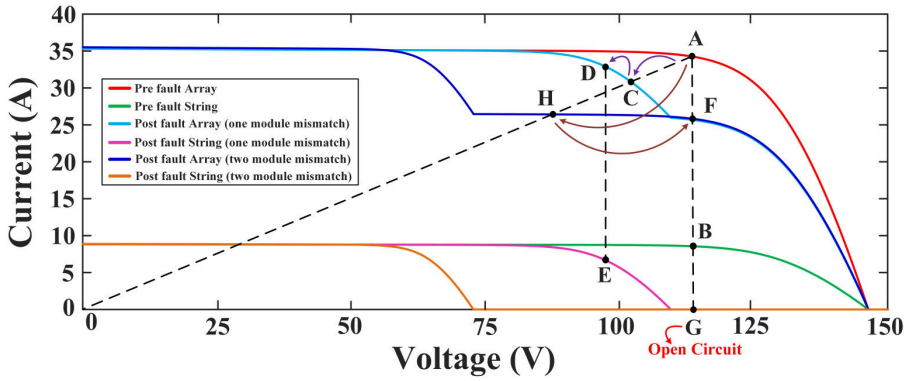

Figure 2.5: I-V characteristics of 4×4 PV array under LL fault with one and two module mismatch

In case of one module LL fault in string-1, at the instant of fault the operating point shifts from "A" to the point "C" and then settles to a new operating point "D" because of MPPT operation. At this new MPP operating point "D", the PV array operates at a reduced voltage of 97.5V, and also the faulty string (three working modules, 3×32.5 = 97.5V) and modules of the healthy string (four working modules, 4×24.375 = 97.5V) operate at the same reduced MPP voltage. It is observed that there exists voltage difference between the modules of the faulty string and healthy string. Therefore, the reading of the voltage sensor V_{d1} is 32.5-24.375 = 8.125 V, and the sensors V_{d2}, and V_{d3} reads zero. This indicates that Line-Line (LL) fault with one module mismatch has occurred in string-1. The generalized expression for voltage sensor indicator V_{d1} is given by eqn.2.1.

$$V_{d1} = \frac{V_a}{n-1} - \frac{V_a}{n} = \frac{V_a}{n(n-1)} \tag{2.1}$$

Where V_a is the array output voltage, 'n' is the number of series connected modules in a string.

In case of two module LL fault in string-1, at the instant of fault the operating point shifts from "A" to the point "H" and then settles to a new operating point "F" because of MPPT operation. Under this condition, reverse current flows in faulty string which is blocked by the blocking diode connected in series to the faulty string. The faulty string gets open circuited which is indicated by the point "G". At the new MPP operating point "F", the PV array operates at rated voltage of 119.7 V, the modules in the faulty string operates at open circuit voltage 36.8 V and the modules

Table 2.4: Voltage indicators for LL fault with one module mismatch

Faulty String	V_{d1}	V_{d2}	V_{d3}	**Faulty module**
String-1	$\frac{V_a}{n(n-1)}$	0	0	module-1 or 2 or 3
	$\frac{-V_a}{n}$	0	0	module 4
String-2	$\frac{-V_a}{n(n-1)}$	$\frac{2V_a}{n(n-1)}$	0	module-5 or 6
	$\frac{-V_a}{n(n-1)}$	$\frac{(2-n)V_a}{n(n-1)}$	0	module-7
	$\frac{V_a}{n}$	$\frac{(2-n)V_a}{n(n-1)}$	0	module-8
String-3	0	$\frac{-2V_a}{n(n-1)}$	$\frac{3V_a}{n(n-1)}$	module-9
	0	$\frac{-2V_a}{n(n-1)}$	$\frac{(3-n)V_a}{n(n-1)}$	module-10
	0	$\frac{(n-2)V_a}{n(n-1)}$	$\frac{(3-n)V_a}{n(n-1)}$	module-11 or 12
String-4	0	0	$\frac{-3V_a}{n(n-1)}$	module-13
	0	0	$\frac{(n-3)V_a}{n(n-1)}$	module-14 or 15 or 16

in the healthy string operates at rated MPP voltage of the module i.e. 30 V. It is observed that there exists voltage difference between the modules of the faulty string and healthy string. Therefore, the reading of the voltage sensor V_{d1} is 36.8-30 = 6.8 V, and the sensors V_{d2}, and V_{d3} reads zero. This indicates that Line-Line (LL) fault with two module mismatch has occurred in string-1. The generalized expression for voltage sensor indicator V_{d1} is given by eqn.2.2.

$$V_{d1} = V_{oc} - \frac{V_a}{n} \tag{2.2}$$

Similarly, for Line-Line (LL) fault with one and two module mismatches the theoretical values voltage sensor indicators are listed in Table.2.3.

Line-Line (LL) Faults between the strings: The Line-Line (LL) fault with one module mismatch is introduced in the 4×4 PV array as shown in Fig.2.6. The characteristics of the 4×4 PV under normal operating condition and LL faults with

Table 2.5: Voltage indicators for LL fault with two module mismatch

String	V_{d1}	V_{d2}	V_{d3}	Faulty module
String-1	$(V_{oc}^m - \frac{V_a}{n})$	0	0	module-(1,2) or (2,3)
	$\frac{-V_a}{n}$	0	0	module (3,4)
	$(\frac{V_a}{n}$ - $V_{oc}^m)$	$(2V_{oc}^m$ - $\frac{2V_a}{n})$	0	module-(5,6)
String-2	$(\frac{V_a}{n}$ - $V_{oc}^m)$	$(V_{oc}^m$ - $\frac{2V_a}{n})$	0	module-(6,7)
	$\frac{V_a}{n}$	$\frac{-2V_a}{n}$	0	module-(7,8)
	0	$(\frac{2V_a}{n}$ - $2V_{oc}^m)$	$(2V_{oc}^m$ - $\frac{3V_a}{n})$	module-(9,10)
String-3	0	$(\frac{2V_a}{n}$ - $V_{oc}^m)$	$(V_{oc}^m$ - $\frac{3V_a}{n})$	module-(10,11)
	0	$\frac{2V_a}{n}$	$(V_{oc}^m$ - $\frac{3V_a}{n})$	module-(11,12)
String-4	0	0	$(\frac{3V_a}{n}$ - $2V_{oc}^m)$	module-(13,14)
	0	0	$(\frac{3V_a}{n}$ - $V_{oc}^m)$	module-(14,15) or (15,16)

one and two module mismatches is shown in Fig.2.7. Irrespective of the position of the fault in the PV array, the fault characteristics are similar under one module mismatch.

For LL fault with one module mismatch between the strings 1 and 2, the PV array operates at the point "D" with reduced voltage of 97.5 V. The series connected modules-3 and 4 are in parallel with module-8, series connected modules-1 and 2 are in parallel with series connected modules-5, 6 and 7. The voltage across the modules of the faulty strings-1 and 2 are given by the eqn.2.3. The PV array output voltage is given by eqn.2.4.

$$\begin{cases} V_1 + V_2 = V_5 + V_6 + V_7 \\ V_3 + V_4 = V_8 \end{cases} \tag{2.3}$$

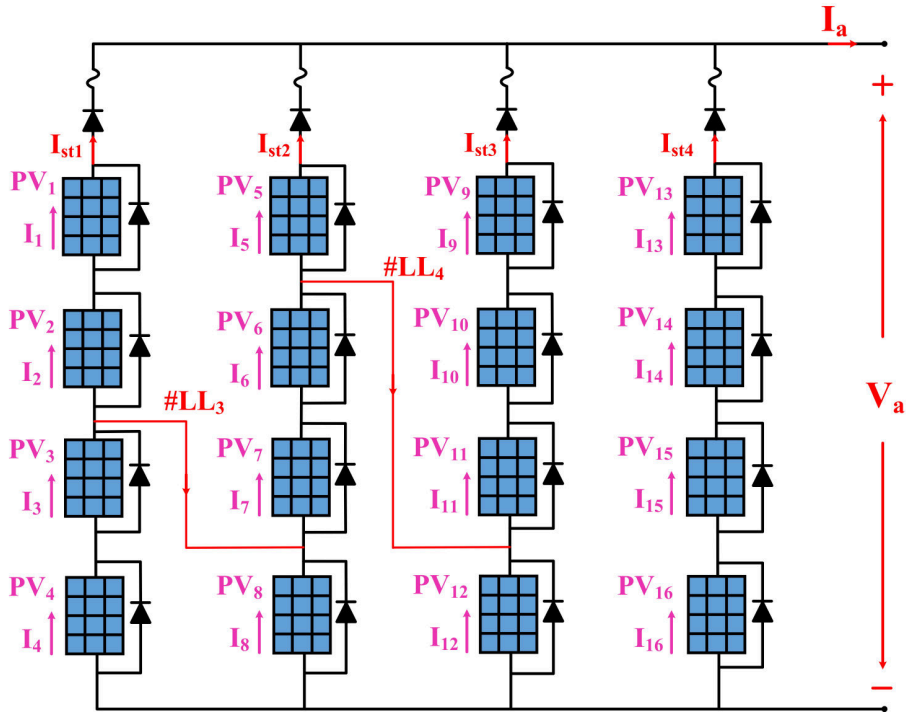

Figure 2.6: LL fault (between strings) with one and two module mismatch

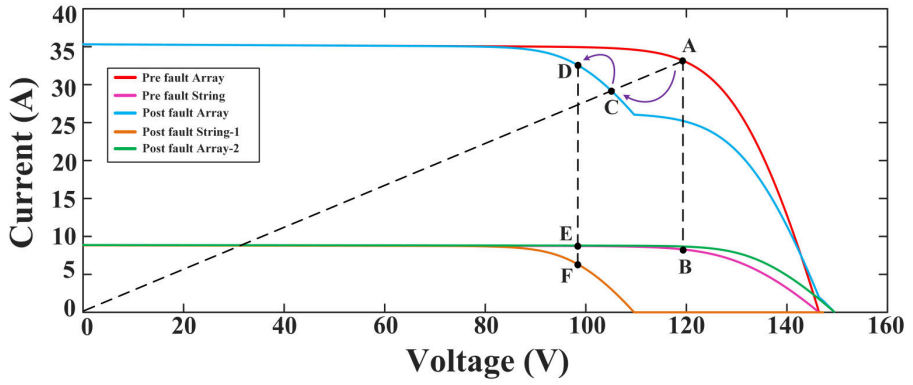

Figure 2.7: I-V characteristics of 4×4 PV array under LL fault with one module mismatch

$$\begin{cases} V_a = V_1 + V_2 + V_3 + V_4 = V_5 + V_6 + V_7 + V_8 \\ V_a = V_1 + V_2 + V_8 = V_3 + V_4 + V_5 + V_6 + V_7 \\ V_1 = V_2 = V_8 = \frac{V_a}{n-1} \\ V_3 = V_4 = V_5 = V_6 = V_7 = \frac{V_a}{n+1} \end{cases} \tag{2.4}$$

The voltage sensor indicator values are given by the eqn.2.5.

$$\begin{cases} V_{d1} = (V_4 - V_8) = \frac{V_a}{n+1} - \frac{V_a}{n-1} = \frac{-2V_a}{n^2-1} \\ V_{d2} = (V_7 + V_8) - \frac{2V_a}{n} = (\frac{2V_a}{n(n^2-1)}) \\ V_{d3} = 0 \end{cases} \tag{2.5}$$

From the fig.2.7, it is observed that the modules-5,6, and 7 in string-2 operate at lesser voltage and carry more current compared to module-8. The modules-3,4 in string-1 operate at lesser voltage and carry more current compared to modules-1,2. Therefore, the modules-1,2 and 8 operate at slightly more than the V_{mp} of the module and the remaining modules-3,4,5,6,7 and 8 operate at slightly lower than the V_{mp} of the module. From the simulate result, the values of voltage sensor indicators are V_{d1} = -13 V, V_{d2} = 3.42 V, and V_{d3} = 0.

For LL fault with two module mismatch between the strings 2 and 3 as shown in Fig.2.6, the series connected modules-6,7 and 8 are in parallel with module-12, series connected modules-9,10 and 11 are in parallel with module-5. The voltage across the modules of the faulty strings-2 and 3 are given by the eqn.2.6. The PV array output voltage is given by eqn.2.7.

$$\begin{cases} V_6 + V_7 + V_8 = V_{12} \\ V_9 + V_{10} + V_{11} = V_5 \end{cases} \tag{2.6}$$

$$\begin{cases} V_a = V_5 + V_6 + V_7 + V_8 = V_9 + V_{10} + V_{11} + V_{12} \\ V_a = V_5 + V_{12} = V_6 + V_7 + V_8 + V_9 + V_{10} + V_{11} \\ V_5 = V_{12} = \frac{V_a}{n-2} \\ V_6 = V_7 = V_8 = V_9 = V_{10} + V_{11} = \frac{V_a}{n+2} \end{cases} \tag{2.7}$$

The voltage sensor indicator values are given by the eqn.2.8.

$$\begin{cases} V_{d1} = (V_4 - V_8) = \frac{V_a}{n} - \frac{V_a}{n+2} = \frac{2V_a}{n(n+2)} \\ V_{d2} = (V_7 + V_8) - (V_{11} + V_{12}) = (\frac{-4V_a}{n^2-4}) \\ V_{d3} = (V_{10} + V_{11} + +V_{12}) - \frac{3V_a}{n} = (\frac{(12-2n)V_a}{n(n^2-4)}) \end{cases} \tag{2.8}$$

From the fig.2.7, it is observed that the modules-5,6, and 7 in string-2 operate at

lesser voltage and carry more current compared to module-8. The modules-3,4 in string-1 operate at lesser voltage and carry more current compared to modules-1,2. Therefore, the modules-1,2 and 8 operate at slightly more than the V_{mp} of the module and the remaining modules-3,4,5,6,7 and 8 operate at slightly lower than the V_{mp} of the module. From the simulate result, the values of voltage sensor indicators are V_{d1} = -13 V, V_{d2} = 13 V, and V_{d3} = 0.

2.3.2 Open Circuit Faults

Under open circuit fault in a particular string, the current flowing in that string is zero and the modules operate at open circuit voltage. The healthy operate at mpp voltage. For an open circuit fault in string-1, the voltage indicators are given by Eqn.2.9. From the simulation results, the value of V_{d1} is found to be 6.575 V and V_{d2}, V_{d3} are zero.

$$\begin{cases} V_{d1} = (V_4 - V_8) = (V_{oc} - V_{mp}) \\ V_{d2} = V_{d3} = 0 \end{cases} \tag{2.9}$$

For an open circuit fault in string-2, the voltage indicators are given by Eqn.2.10. From the simulation results, the value of $d1$ is found to be -6.575 V, V_{d2} is 13.15 V, and V_{d3} is zero.

$$\begin{cases} V_{d1} = (V_4 - V_8) = (V_{mp} - V_{oc}) \\ V_{d1} = (V_7 + V_8) - (V_{11} + V_{12}) = 2(V_{oc} - V_{mp}) \\ V_{d3} = 0 \end{cases} \tag{2.10}$$

2.3.3 Partial shading Faults

The PV modules experience variable irradiance under partial shading faults. For instance, consider shade on a 4×4 PV array as shown in Fig.2.8. The third module in string-1 experiences an irradiation of 200 W/m^2. The I-V characteristics of the 4×4 PV array under normal and PSC is shown in Fig.2.9.

Under partial shading condition, the PV array operates at the point "D" with the rated voltage of 119.7 V with reduced current of 26.55A and the faulty string operates at the point "E" with rated voltage of 119.7 V but with reduced current

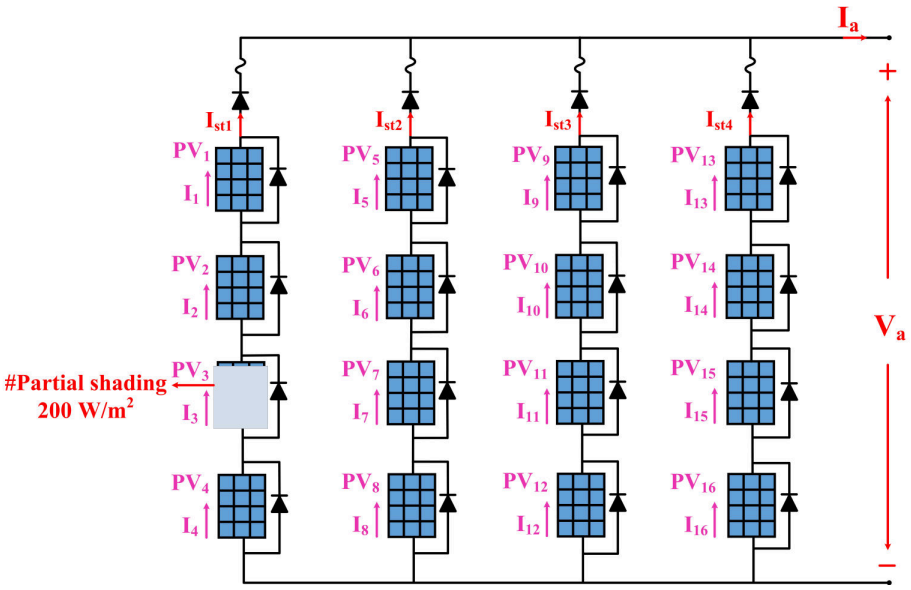

Figure 2.8: Partial shading Fault

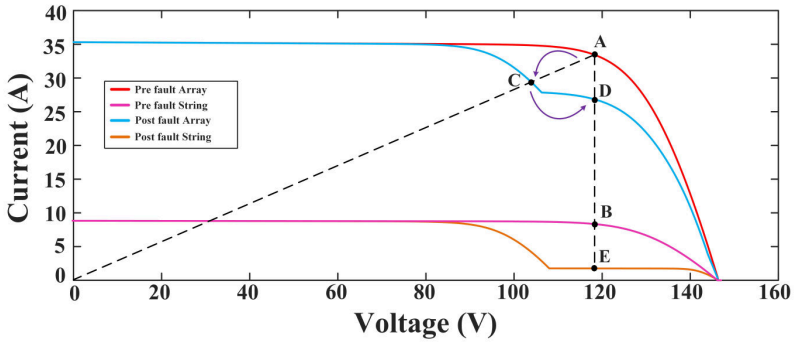

Figure 2.9: I-V characteristics of 4×4 PV array under partial shading

of 1.759 A. The voltage sensor indicators V_{d1}, V_{d2}, and V_{d3} reads zero indicating the presence of partial shading fault. Further, it can be inferred that under partial shading conditions, there exits multiple peaks in the power-voltage characteristics of the faulty string which is not seen in the case of LL faults.

2.4 Experimental Results

The proposed Diagonal sensor placement scheme is further verified in hardware considering a 4×4 PV array. The experimental set up is shown in Fig.2.10. It consists of 16 modules each of 10W (LOOM SOLAR) connected in 4×4 PV array form. The

4×4 PV array is connected to resistive load through a DC-DC converter operated in MPPT mode. To detect and localize the faults in the PV array, three differential voltage sensors modules SKU:29802 along with Arduino uno controller are connected as shown in Fig.2.10. The experiment is carried out for a period of 30 minutes from 12:10. p.m to 12:40 p.m. The fault is introduced at the instant 12:25 p.m.

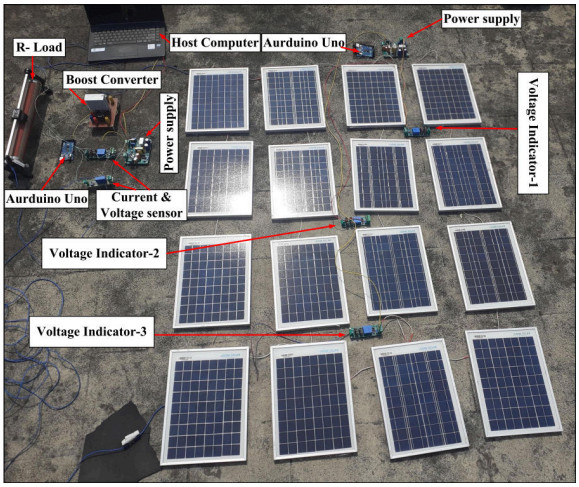

Figure 2.10: Experimental set up of 4×4 PV Array

2.4.1 Short Circuit Faults

When a line-Line (LL) fault with one module and two module mismatch are occurred in 4×4 PV array, the plot of irradiance, PV array output voltage, array output current and voltage sensor indicators is shown in Fig.2.11.

From the Fig.2.11(a) for one module mismatch, it is observed that before the fault occurrence array voltage, and current are 72.1 V, and 1.52 A. At the instant of fault, the array voltage and current drops to 55V and 1.2 A and settles at 62.2 V and 1.49 A. During healthy condition the voltage indicators (V_{d1}, V_{d2}, V_{d3}) shows zero and after the fault the voltage indicator V_{d1} shown a value of 5.54 V where as V_{d2} and V_{d3} are zero indicating the presence of fault. It is observed that the array current remains same as previous value where as the array voltage decreases.

From the Fig.2.11(b) for two module mismatch, it is observed that before the fault occurrence array voltage, and current are 73.26 V, and 1.51 A. At the instant of fault, the array voltage and current drops to 54V and 1.18 A and settles at 71.24 V and 1.22 A. During healthy condition the voltage indicators (V_{d1}, V_{d2}, V_{d3}) shows zero and

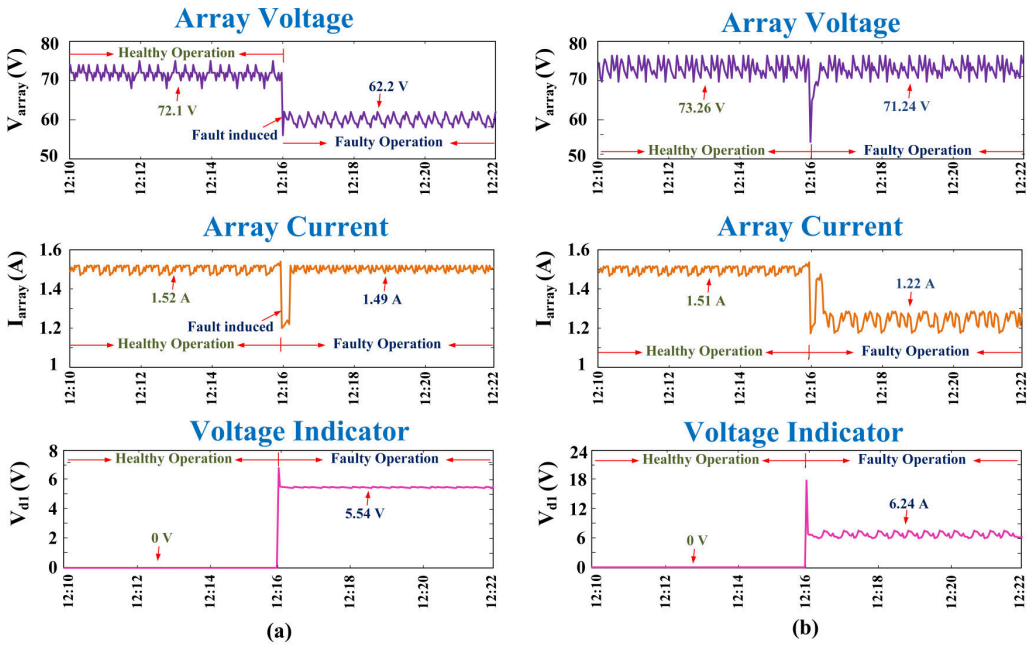

Figure 2.11: Short circuit faults (a) One module mismatch (b) Two module mismatch

after the fault the voltage indicator V_{d1} shown a value of 6.24 V where as V_{d2} and V_{d3} are zero indicating the presence of fault. It is observed that the array voltage remains same as previous value where as the array current decreases.

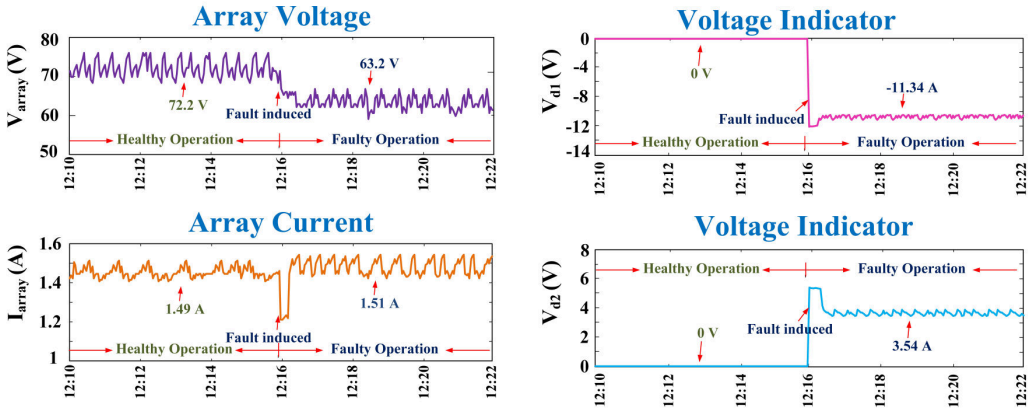

Figure 2.12: Array voltage, Current and voltage indicator

When an LL fault with one module mismatch between the strings-1,2 has occurred in 4×4 PV array, the plot of irradiance, PV array output voltage, array output current and voltage sensor indicators is shown in Fig. 2.12. It is observed that before the fault occurrence array voltage, and current are 72.2 V, and 1.49 A. At the instant

of fault, the array voltage and current drops to 62 V and 1.18 A and settles at 63.2 V and 1.51 A. During healthy condition the voltage indicators (V_{d1}, V_{d2}, V_{d3}) shows zero and after the fault the voltage indicator V_{d1} and V_{d2} shown a value of -11.34 V and 3.54 V respectively, where as V_{d3} is zero indicating the presence of fault between strings 1-2. It is observed that the array current remains same as previous value where as the array voltage decreases.

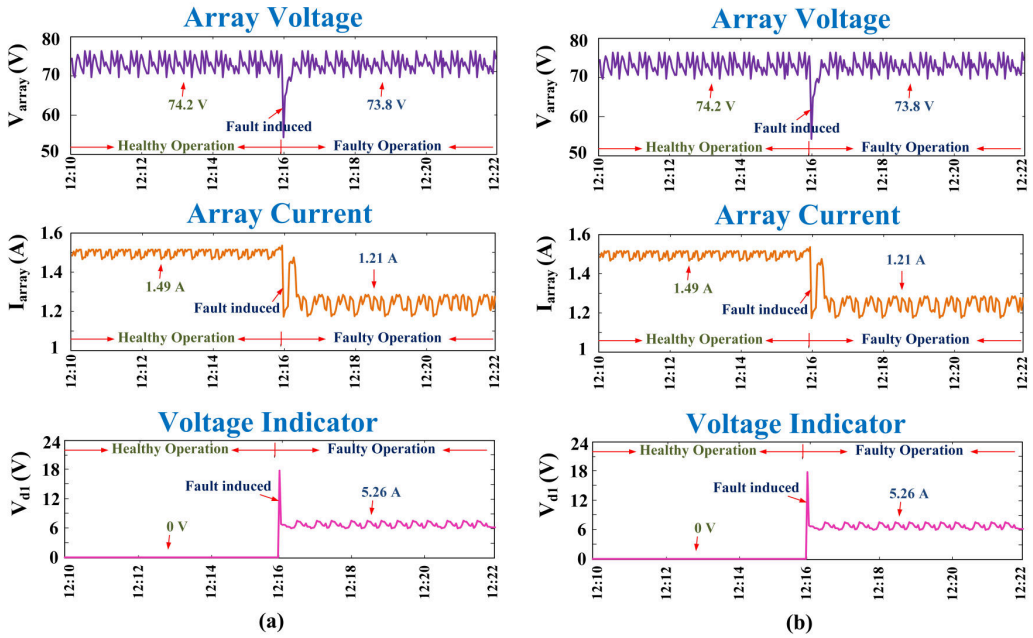

Figure 2.13: Array voltage, Current and voltage indicator

When an open circuit fault occurs in string-1 of 4×4 PV array, the plot of irradiance, PV array output voltage, array output current and voltage sensor indicators is shown in Fig. 2.13(a). It is observed that before the fault occurrence array voltage, and current are 74.2 V, and 1.49 A. At the instant of fault, the array voltage and current drops to 52 V and 1.2 A and settles at 73.8 V and 1.21 A. During healthy condition the voltage indicators (V_{d1}, V_{d2}, V_{d3}) shows zero and after the fault the voltage indicator V_{d1} shown a value of 5.26 V, where as V_{d2} and V_{d3} are zero indicating the presence of open circuit fault in string-1. It is observed that the array voltage remains same as previous value where as the array current decreases.

When partial shading occurs in string-1 of 4×4 PV array, the plot of irradiance, PV array output voltage, array output current and voltage sensor indicators is shown in Fig. 2.13(b). It is observed that before the fault occurrence array voltage, and current

are 72.2 V, and 1.49 A. At the instant of fault, the array voltage and current drops to 52.2 V and 1.18 A and settles at 73.8 V and 1.21 A. During healthy condition the voltage indicators (V_{d1}, V_{d2}, V_{d3}) shows zero and after the fault the voltage indicator V_{d1} shown a value of 5.26 V, where as V_{d2} and V_{d3} are zero indicating the presence of partial shade in string-1. It is observed that the array voltage remains same as previous value where as the array current decreases. It is similar to open circuit fault and cab distinguished based on the I-V curve where multiple peaks exits for partial shading faults.

2.5 Summary

To identify and localize the faults in the solar PV array a new Diagonal Sensor Arrangement (DSA) is proposed in this chapter. The proposed method is applicable for both square and non-square arrays of any desired size. It is implemented on 4×4 PV array in simulation and Hardware environments. DSA strategy utilizes minimal number of sensors to identify and locate the faults.

Chapter 3

Reduced Cross Tied PV Array Configuration

This chapter proposed a novel Reduced Cross Tied (RCT) configuration for extracting maximum power from a PV Array under partial shading conditions. The proposed configuration is implemented on 7×7 and 8×8 PV arrays and tested in software, hardware environments under various shading patterns. A comparative analysis is done between proposed configuration and conventional configurations Series-Parallel (SP), Bridge Link (BL), Honey Comb (HC) and Total Cross Tied (TCT) in terms of mismatch loss (ML), fill factor (FF), efficiency (η), Wiring Loss (WL) and Global Maximum Power Point (GMPP). The results replicate efficacy of proposed RCT configuration compared to existing configurations.

3.1 Introduction

The primary reason for decrease in power output from PV array is partial shading. During partial shading conditions (PSCs) PV modules experience mismatch in current and voltage generated. Also, the power voltage (P-V) characteristics of PV array possess multiple peaks under PSCs. In order to mitigate the effects caused by PSCs, configuration of the PV array is the finest solution. The major component of solar PV generation system is photovoltaic (PV) cell. A PV module is formed by series combination of PV cells. The PV modules are joined in various patterns to attain desired voltage and current. However, various factors are considered to ensure the best possible usage of PV modules. The typical PV array configurations constitute

Simple-Series (SS), Parallel (P), Series-Parallel (SP), Bridge Link (BL), Honey Comb (HC) and Total Cross Tied (TCT).

The simple-series (SS) configuration refers to connecting all PV modules in series, which offers advantages such as simplicity, high voltage, and reduced wiring losses. However, this configuration is typically suitable for small-scale PV systems. One major drawback of the simple-series configuration is its vulnerability to shading on a single module, as this can adversely impact the entire string of modules. The parallel (P) configuration involves connecting all PV modules in parallel, resulting in high current but low voltage. However, this combination of high current and low voltage is generally not ideal for most applications. To overcome these drawbacks, other configurations such as Bridge Link (BL), Honey Comb (HC) and Total Cross Tied (TCT) are proposed in the literature. According to the literature TCT configuration is able to generate more output power compared to existing configurations under partial shading conditions. However due to more number of cross ties in the TCT configuration, wiring resistance and wiring loss is more. Hence a novel Reduced Cross Tied (RCT) PV array configuration is proposed which is able to generate GMPP on-par to TCT configuration with less number of cross ties.

3.2 Modeling of 8×8 PV Array Configurations

In this section, modeling of different 8×8 solar PV array configurations is presented. To model an 8×8 PV array, 64 PV modules are considered. These 64 PV modules are connected in 8 rows and 8 columns as 8×8 matrix form. The modules are interconnected to form an array. The different conventional module arrangements are Series-Parallel (SP), Bridge Link (BL), Honey Comb (HC) and Total Cross Tied (TCT) configurations. The modules in the 8×8 PV array are numbered as PV1, PV2, PV3,.....PV64. Let V_1, V_2, V_3,...V_{64} be the PV module voltages, I_1, I_2, I_3...I_{64} be the module currents, I_{s1}, I_{s2}, I_{s3}, I_{s4}, I_{s5}, I_{s6}, I_{s7} and I_{s8} be the string currents, V_{r1}, V_{r2}, V_{r3}, V_{r4}, V_{r5}, V_{r6}, V_{r7} and V_{r8} be row voltages, V_{PV}, I_{PV} and P_{PV} are the array voltage, array current and array power.

3.2.1 Series-Parallel (SP) connected PV Array

The Series Parallel (SP) connection of PV modules is widely used arrangement in PV system applications. Here set of PV modules (string) in series are connected in parallel for the formation of PV array. It is simple and economical in design. Blocking diodes are inserted in series with each string in order to ensure no reverse current under short circuit conditions and PSCs. Every module in the PV array is provided with bypass diode to prevent local hot spots during PSCs. The array connection of SP configuration is depicted in Fig. 3.1. The PV array voltage, current and power are given by equation 3.1.

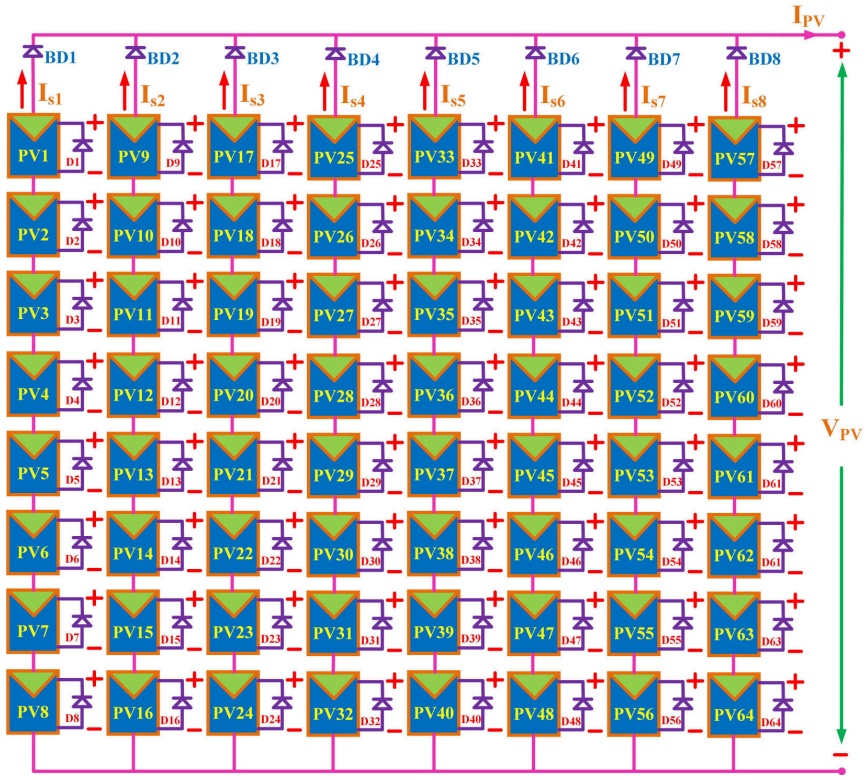

Figure 3.1: Series Parallel (SP) arrangement

$$\left.\begin{aligned} I_{PV} &= I_{s1} + I_{s2} + I_{s3} + I_{s4} + I_{s5} + I_{s6} + I_{s7} + I_{s8} = \sum_{i=1}^{8} I_{si} \\ V_{PV} &= V_1 + V_2 + V_3 + V_4 + V_5 + V_6 + V_7 + V_8 = \sum_{i=1}^{8} V_i \\ P_{PV} &= V_{PV} \times I_{PV} \end{aligned}\right\} \tag{3.1}$$

3.2.2 Bridge-Link (BL) PV Array

In case of SP configuration, the mismatch loss is more due to series connected modules. To address this issue, four modules are linked together forming a Bridge Link (BL) structure and are connected by cross ties. Voltages in series connected modules and currents in parallel connected modules are summed to produce the required output voltage and current values. The BL arrangement of the PV array is depicted in Fig.3.2 The PV array voltage, current and power are given by equation 3.2.

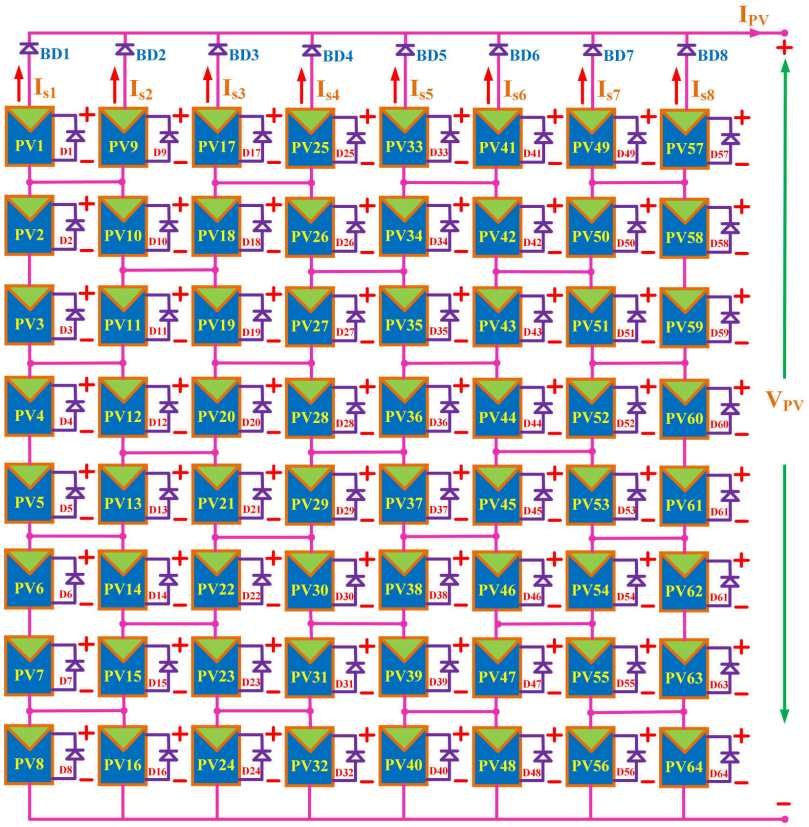

Figure 3.2: Bridge Link (BL) arrangement

$$\left.\begin{aligned} I_{PV} &= I_{s1} + I_{s2} + I_{s3} + I_{s4} + I_{s5} + I_{s6} + I_{s7} + I_{s8} = \sum_{i=1}^{8} I_{si} \\ V_{PV} &= V_1 + V_2 + V_3 + V_4 + V_5 + V_6 + V_7 + V_8 = \sum_{i=1}^{8} V_i \\ P_{PV} &= V_{PV} \times I_{PV} \end{aligned}\right\} \tag{3.2}$$

3.2.3 Honey Comb (HC) PV Array

The hexagonal shape of honey bee houses is the basic for connection of PV modules in Honey Comb (HC) configuration. In this arrangement, a hexagonal shape of honey bee house is formed with every six modules and are joined using cross ties. Here, three series connected modules are joined in parallel to another three set of series connected modules. The array connection of HC arrangement is depicted in Fig. 3.3. The PV voltage, current and power are given by equation 3.3.

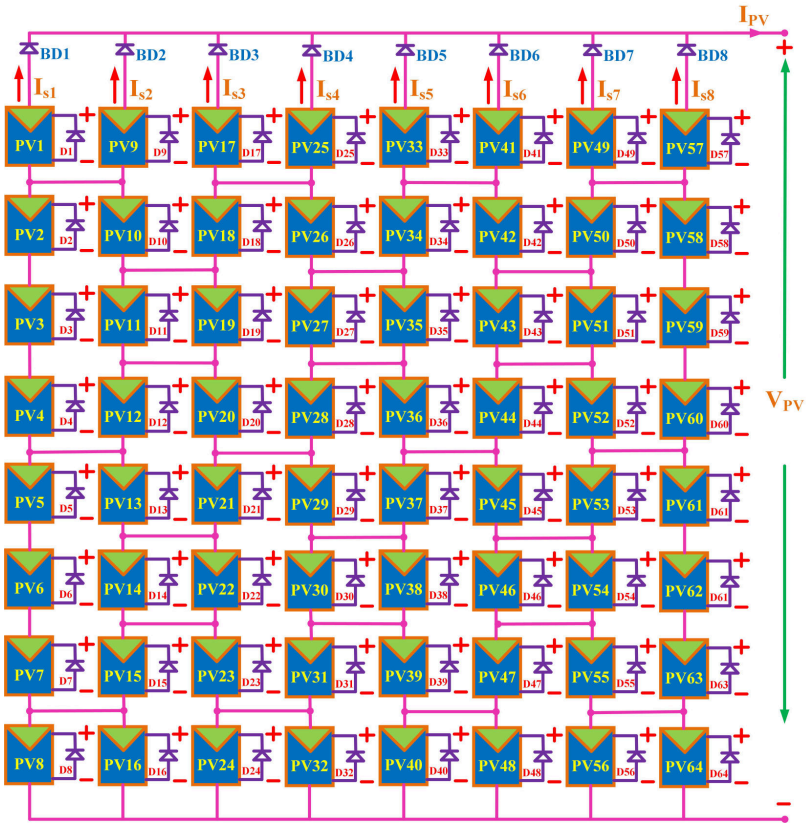

Figure 3.3: Honey Comb (HC) arrangement

$$\left.\begin{aligned} I_{PV} &= I_{s1} + I_{s2} + I_{s3} + I_{s4} + I_{s5} + I_{s6} + I_{s7} + I_{s8} = \sum_{i=1}^{8} I_{si} \\ V_{PV} &= V_1 + V_2 + V_3 + V_4 + V_5 + V_6 + V_7 + V_8 = \sum_{i=1}^{8} V_i \\ P_{PV} &= V_{PV} \times I_{PV} \end{aligned}\right\} \tag{3.3}$$

3.2.4 Total-Cross-Tied (TCT) PV Array

TCT arrangement is formed by joining cross ties at every row of the junction of Series-Parallel (SP) array. In this arrangement row and module voltages are equal. It overcomes the drawbacks of SP, BL and HC configurations. TCT configuration has more wiring loss compared to other configurations. The array arrangement of TCT arrangement is depicted in Fig. 3.4. The PV voltage, current and power are given by equation 3.4.

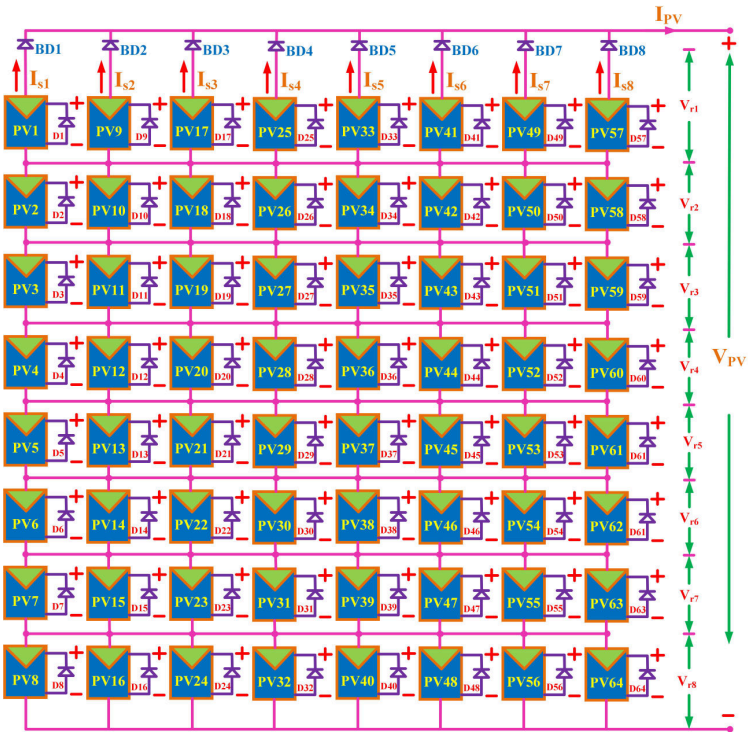

Figure 3.4: Total Cross Tied (TCT) arrangement

$$\left.\begin{aligned} I_{PV} = I_{s1} + I_{s2} + I_{s3} + I_{s4} + I_{s5} + I_{s6} + I_{s7} + I_{s8} = \sum_{i=1}^{8} I_{si} \\ V_{r1} = V_1; V_{r2} = V_2; V_{r3} = V_3; V_{r4} = V_4 \\ V_{r5} = V_5; V_{r6} = V_6; V_{r7} = V_7; V_{r8} = V_8 \\ V_{PV} = V_{r1} + V_{r2} + V_{r3} + V_{r4} + V_{r5} + V_{r6} + V_{r7} + V_{r8} = \sum_{i=1}^{8} V_{ri} \\ P_{PV} = V_{PV} \times I_{PV} \end{aligned}\right\} \quad (3.4)$$

3.3 Reduced Cross Tied PV Array Configuration

A Reduced Cross Tied (RCT) configuration is formed by modifying the TCT connected PV array with minimal number of cross ties. Consider a TCT connected PV array of size m×n as depicted in Fig. 3.5, where the number of rows and columns are equal. For an array with 'm' rows there exits (m-1) cross tie rows to be connected.

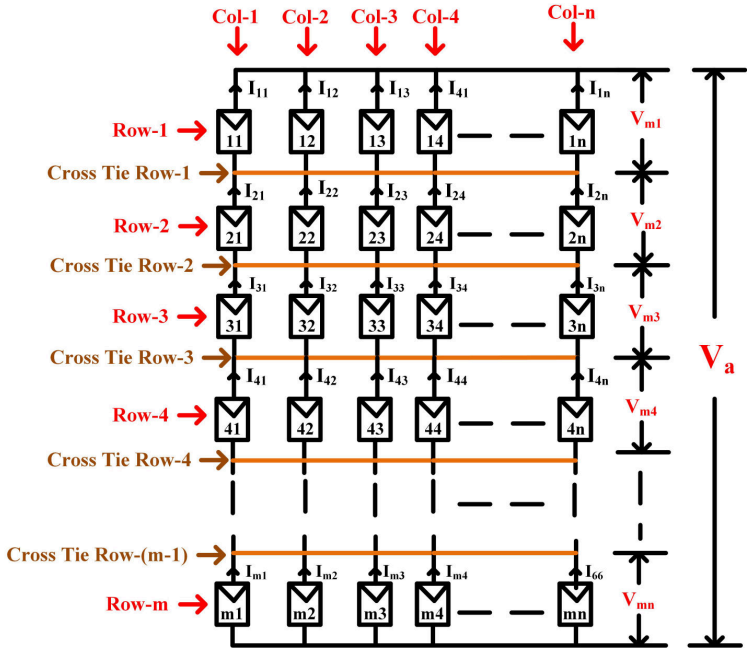

Figure 3.5: TCT connected m×n PV array

The proposed Reduced Cross Tied PV array configuration is illustrated as follows:
Case 1: For m = even, there exists odd number of cross tie rows to be connected.

- Step 1: For cross tie row-1, cross ties are connected between strings 1 and 2 leaving a gap, between strings 3 and 4 leaving a gap, between strings 5 and 6 leaving a gap .....between strings (m-1) and m.
- Step 2: For cross tie row-2, cross ties are connected between strings 1 and 2 leaving a gap, between strings 3 and 4 leaving a gap, between strings 5 and 6 leaving a gap .....between strings (m-1) and m.
- Step 3: For cross tie row-3, all the strings are cross tied together.
- Step 4: Repeat the steps-1, 2 and 3 for connecting the next cross tie rows.

The proposed Reduced Cross Tied (RCT) arrangement when applied to 8×8 PV array is shown in Fig. 3.6. The PV voltage, current and power are given by equation 3.5.

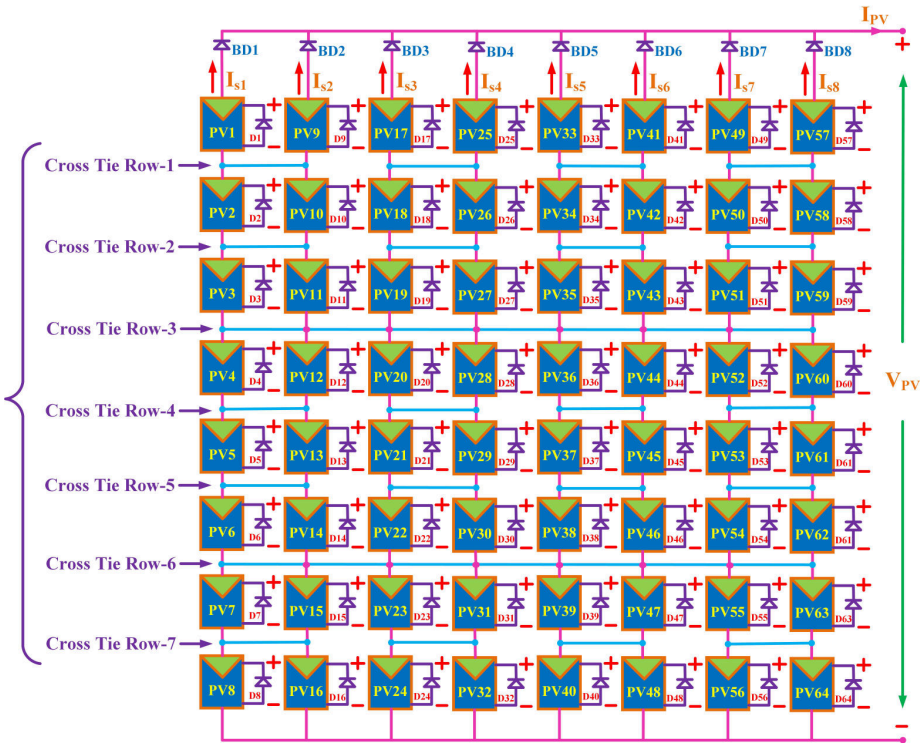

Figure 3.6: Reduced Cross Tied (RCT) 8×8 Array arrangement

$$\left.\begin{aligned} I_{PV} &= I_{s1} + I_{s2} + I_{s3} + I_{s4} + I_{s5} + I_{s6} + I_{s7} + I_{s8} \\ I_{PV} &= \sum_{i=1}^{8} I_{si} \\ V_{PV} &= V_1 + V_2 + V_3 + V_4 + V_5 + V_6 + V_7 + V_8 \\ V_{PV} &= \sum_{i=1}^{8} V_i \\ P_{PV} &= V_{PV} \times I_{PV} \end{aligned}\right\} \tag{3.5}$$

Case 2: For m = odd, there exists even number of cross tie rows to be connected. Divide the cross tie into two groups (upper half and lower half). The upper half consists of cross tie rows 1, 2, 3.....(m-1)/2 and lower half consists of cross tie rows (m+1)/2, (m+3)/2.....(m-1). For upper half, cross tie are connected as follows

- Step 1: For cross tie row-1, cross ties are connected between strings 1, 2 and 3 leaving a gap, between strings 4 and 5 leaving a gap ..... between strings (m-1) and m.

- Step 2: For cross tie row-2, cross ties are connected between strings 1 and 2 leaving a gap, between strings 3, 4 and 5 leaving a gap .....between strings (m-1) and m.

- Step 3: For cross tie row-(m-1)/2, cross ties are connected between strings 1 and 2 leaving a gap, between strings 3 and 4 leaving a gap .....between strings (m-2), (m-1) and m.

- Repeat the same procedure to connect the cross tie rows of lower half.

The proposed Reduced Cross Tied (RCT) arrangement when applied to 7×7 PV array is shown in Fig. 3.7. The PV voltage, current and power are given by equation 3.6.

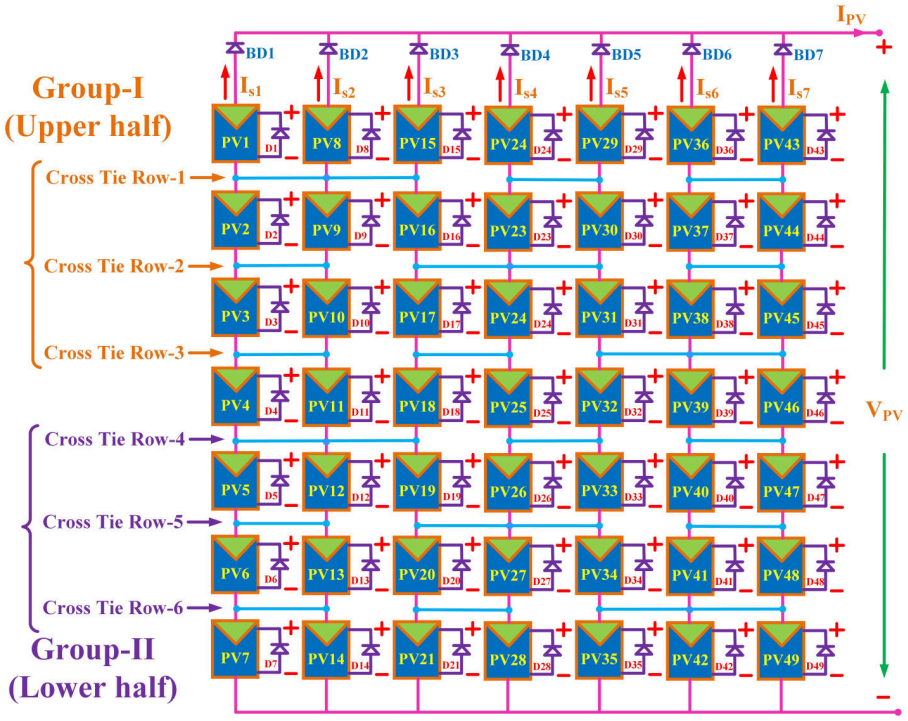

Figure 3.7: Reduced Cross Tied (RCT) 7×7 Array arrangement

$$\left.\begin{aligned} I_{PV} = I_{s1} + I_{s2} + I_{s3} + I_{s4} + I_{s5} + I_{s6} + I_{s7} = \sum_{i=1}^{7} I_{si} \\ V_{PV} = V_1 + V_2 + V_3 + V_4 + V_5 + V_6 + V_7 = \sum_{i=1}^{7} V_i \\ P_{PV} = V_{PV} \times I_{PV} \end{aligned}\right\} \tag{3.6}$$

The key advantage of the Reduced Cross Tied (RCT) configuration over TCT is reduction in cross ties. For a 7×7 PV array, the cross ties in RCT configuration are 24 where as in TCT are 36. For a 8×8 PV array, the cross ties in RCT configuration are 34 where as in TCT are 49. There is a reduction of 33.33% for 7×7 PV array and 30.61% for 8× in cross ties for RCT configuration compared to TCT configuration. Hence, the length of wire required for connecting the cross ties in RCT configuration is less compared to TCT. Also, the wiring resistance and wiring loss is less in RCT configuration compared to TCT configuration.

3.4 Simulation Results

The proposed Reduced Cross Tied (RCT) configuration is implemented on 7×7 and 8×8 PV arrays under various shading patterns such as Long & Narrow (LN), Long & Wide (LW), Short & Narrow (SN) and Short & Wide (SW). The different levels of solar insolation taken into consideration are 1000 W/m^2, 800 W/m^2, 700 W/m^2, 600 W/m^2, 500 W/m^2, 400 W/m^2, 300 W/m^2 and 200 W/m^2. The performance of the proposed RCT configuration along with conventional configurations Series-Parallel (SP), Bridge Link (BL), Honey Comb (HC) and Total Cross Tied (TCT) is presented.

3.4.1 Shading pattern - Short & Narrow (SN)

The Short & Narrow (SN) shading pattern considered is depicted in Fig. 3.8(a) & (b). The power-voltage (P-V) characteristics of 7×7 and 8×8 PV array for TCT, HC, BL, SP and RCT configurations are depicted in Fig. 3.9(a) & 3.9(b). The performance parameters are depicted in Table 3.1 in the order of decreasing GMPP. In case of 7×7 array, TCT arrangement generates highest GMPP of 8841 W and the corresponding co-ordinates of V_{mp}, I_{mp} are (224.1, 39.92). HC configuration generates lowest GMPP

of 8402 W and the corresponding co-ordinates of V_{mp}, I_{mp} are (217.36, 38.72). RCT configuration is able to generate more GMPP compared to SP, BL and HC by 191W (2.24 %), 194W(2.28 %) and 284W(3.38 %). In case of 8×8 array, SP arrangement generates highest GMPP of 12670 W and the corresponding co-ordinates of V_{mp}, I_{mp} are (231.2, 54.80). HC configuration generates lowest GMPP of 12340 W and the corresponding co-ordinates of V_{mp}, I_{mp} are (230, 53.63). RCT configuration is able to generate more GMPP compared to HC by 130W(1.01 %).

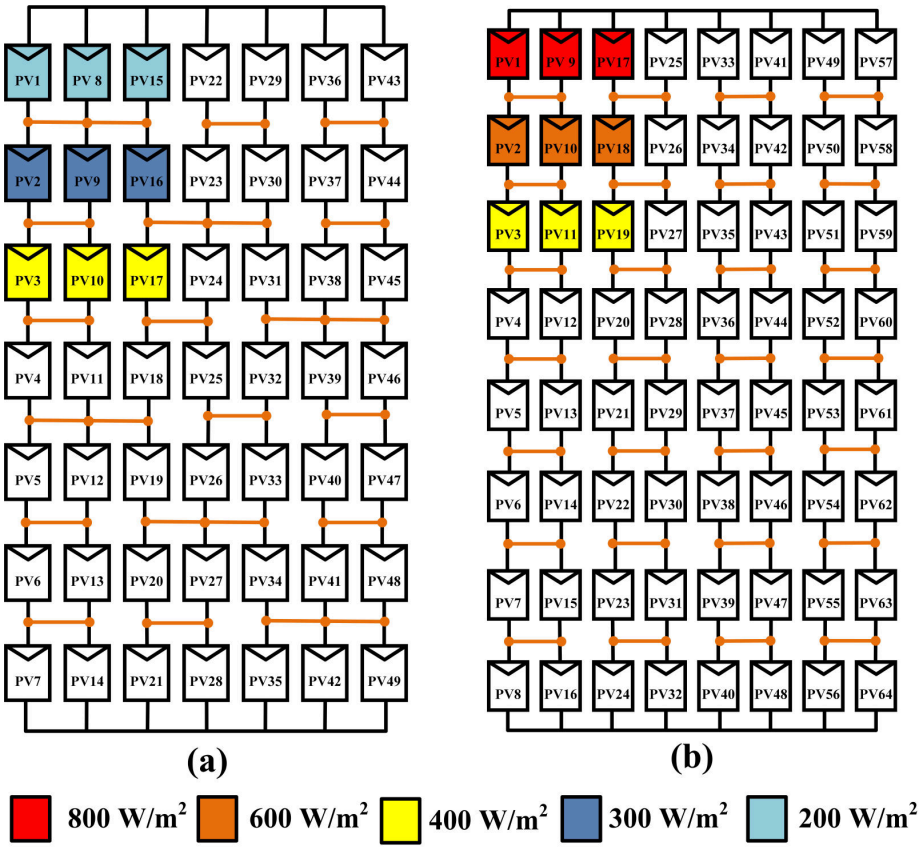

Figure 3.8: Short & Narrow (SN) shading pattern (a) 7×7 array (b) 8×8 array

3.4.2 Shading pattern - Short & Wide (SW)

The shading pattern Short & Wide (SW) considered is displayed in Fig. 3.10(a) & (b). The power-voltage (P-V) characteristics of 7×7 and 8×8 PV array for TCT, HC, BL, SP and RCT configurations are displayed in Fig. 3.11(a) & (b). The performance parameters are depicted in Table 3.2 in the order of decreasing GMPP.

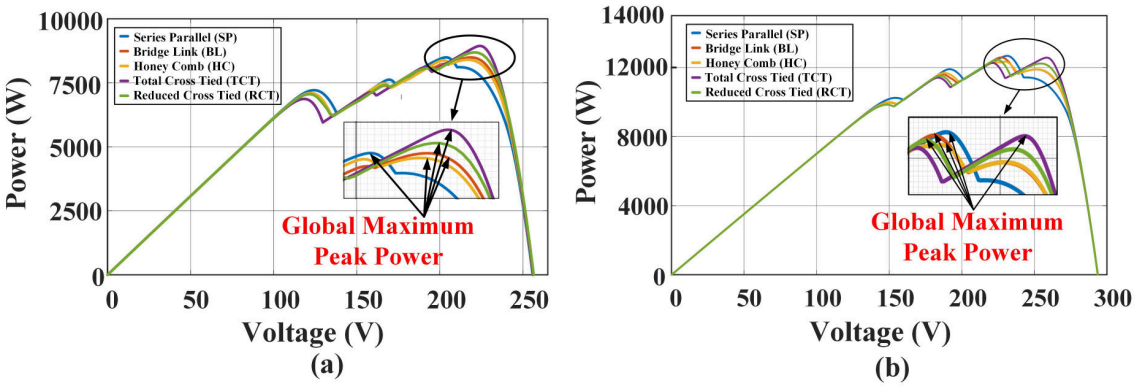

Figure 3.9: SN Shading condition (a) Power Characteristics (P-V) plot of 7×7 array (b) Power Characteristics (P-V) plot of 8×8 array

Table 3.1: Performance parameters of 7×7 & 8×8 PV array for S&N shading condition

7×7 PV Array								
Config.	$V_{OC}(V)$	$I_{SC}(A)$	$V_{mp}(V)$	$I_{mp}(A)$	$GMPP(W)$	$ML(\%)$	$FF(\%)$	$\eta(\%)$
TCT	256.16	61.77	224.10	39.92	8841	38.56	55.53	10.83
RCT	256.14	61.78	222.02	39.12	8686	41.03	54.55	10.64
BL	256.12	61.80	219.52	38.78	8492	44.25	53.33	10.40
SP	256.48	61.80	204.16	38.76	8485	44.37	53.29	10.39
HC	256.10	61.82	217.36	38.72	8402	45.80	52.77	10.29
8×8 PV Array								
Config.	$V_{OC}(V)$	$I_{SC}(A)$	$V_{mp}(V)$	$I_{mp}(A)$	$GMPP(W)$	$ML(\%)$	$FF(\%)$	$\eta(\%)$
SP	293.51	70.63	231.2	54.80	12670	26.28	60.92	11.88
BL	293.61	70.62	227.04	55.44	12580	27.19	60.49	11.80
TCT	293.55	70.61	258.42	48.64	12570	27.66	60.44	11.79
RCT	293.55	70.62	224.12	55.62	12460	28.41	59.91	11.69
HC	293.61	70.62	230.02	53.63	12340	29.66	59.34	11.57

In case of 7×7 array, TCT arrangement generates highest GMPP of 8554 W and the corresponding co-ordinates of V_{mp}, I_{mp} are (222.4, 38.46), whereas SP configuration generates lowest GMPP of 8421 W and the corresponding co-ordinates of V_{mp}, I_{mp} are (221.54, 38.12). RCT configuration is able to generate more GMPP compared to SP, BL and HC by 1.14 %, 0.23 % and 0.2 %. In case of 8×8 PV array, TCT arrangement generates highest GMPP of 11960 W and the corresponding co-ordinates of V_{mp}, I_{mp} are (251.30, 47.62), whereas SP configuration generates lowest GMPP of 11630 W and the corresponding co-ordinates of V_{mp}, I_{mp} are (249.10, 46.71). RCT configuration is

able to generate more GMPP compared to SP and HC by 1.28 %, 0.34 % and equal GMPP of 11820W compared to BL configuration.

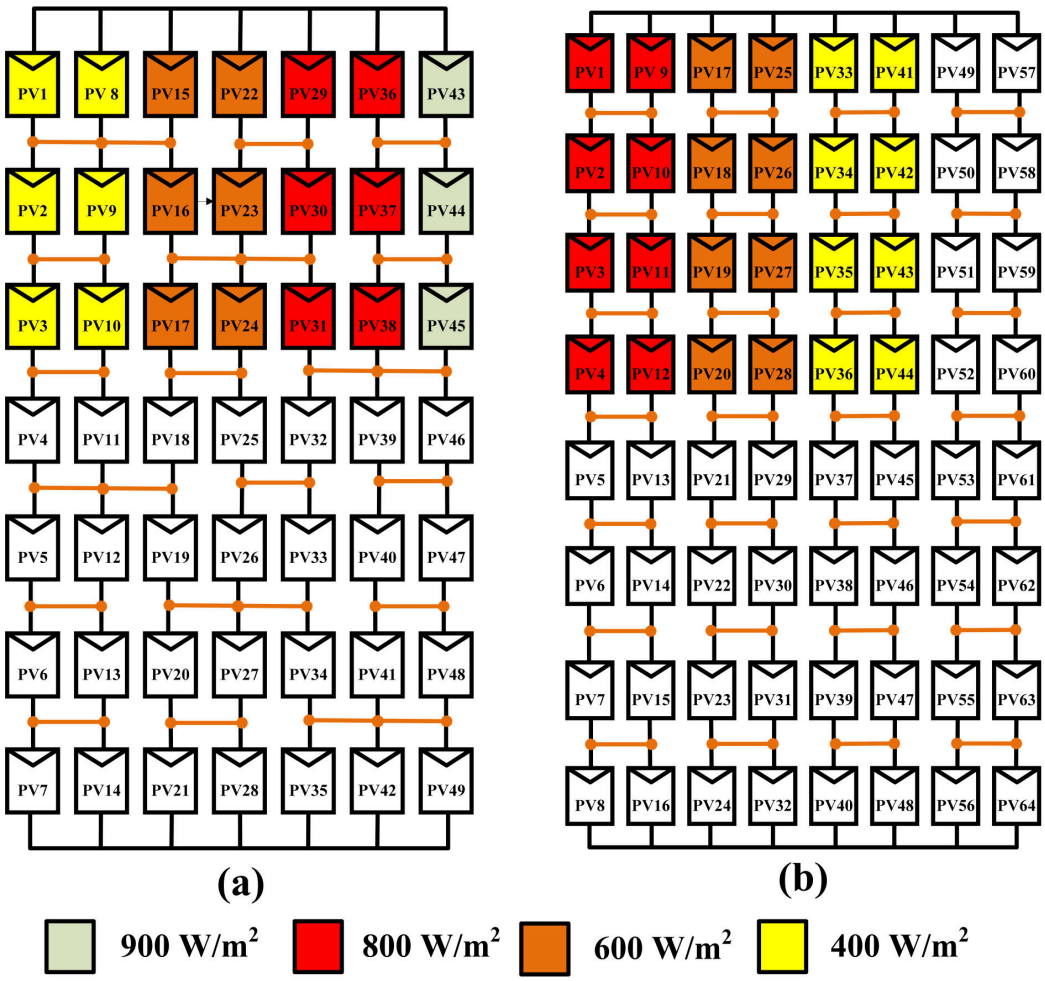

Figure 3.10: Short & Wide (SW) shading pattern (a) 7×7 array (b) 8×8 array

3.4.3 Shading pattern - Long & Narrow (LN)

The shading pattern Long & Narrow (LN) considered is displayed in Fig. 3.12(a) & (b). The power-voltage (P-V) characteristics of 7×7 and 8×8 PV array for TCT, HC, BL, SP and RCT configurations are displayed in Fig. 3.13(a) & (b). The performance parameters are depicted in Table 3.3 in the order of decreasing GMPP. In case of 7×7 PV array, TCT arrangement generates highest GMPP of 9102 W and the corresponding co-ordinates of V_{mp}, I_{mp} are (216.8, 41.98), whereas SP configuration

Table 3.2: Performance parameters of 7×7 & 8×8 PV array for S&W shading condition

7×7 PV Array								
Config.	$V_{OC}(V)$	$I_{SC}(A)$	$V_{mp}(V)$	$I_{mp}(A)$	$GMPP(W)$	$ML(\%)$	$FF(\%)$	$\eta(\%)$
TCT	256.45	61.83	222.40	38.46	8554	43.12	53.72	10.48
RCT	256.16	61.82	222.02	38.36	8517	43.83	53.49	10.43
HC	256.52	61.81	222.02	38.30	8500	44.12	53.38	10.41
BL	256.52	61.81	222.02	38.30	8497	44.17	53.37	10.41
SP	256.84	61.82	221.54	38.12	8421	45.47	52.89	10.32
8×8 PV Array								
Config.	$V_{OC}(V)$	$I_{SC}(A)$	$V_{mp}(V)$	$I_{mp}(A)$	$GMPP(W)$	$ML(\%)$	$FF(\%)$	$\eta(\%)$
TCT	292.66	70.62	251.30	47.62	11960	33.78	57.51	11.22
RCT	292.62	70.61	250.40	47.11	11840	35.82	56.64	11.05
BL	292.52	70.62	250.20	47.26	11820	35.36	56.84	11.09
HC	292.52	70.62	250.40	47.11	11780	35.82	56.64	11.05
SP	292.46	70.61	249.10	46.71	11630	37.58	55.92	10.91

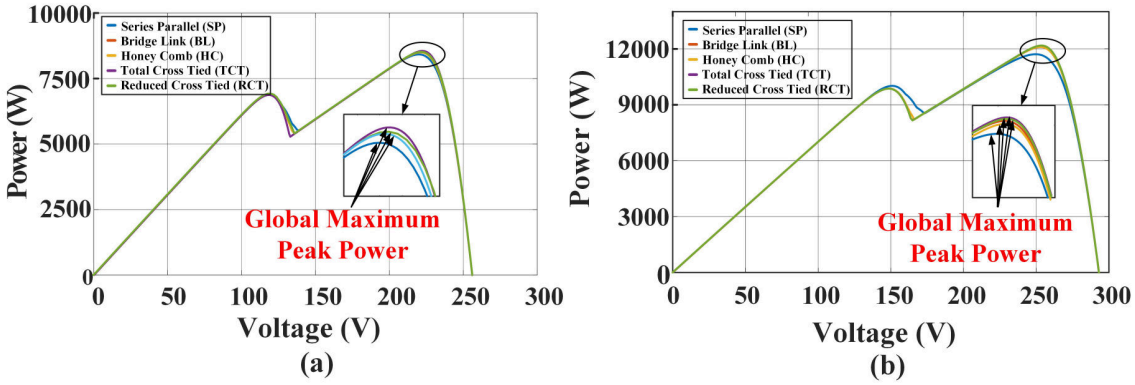

Figure 3.11: SW Shading condition (a) Power Characteristics (P-V) plot of 7×7 array (b) Power Characteristics (P-V) plot of 8×8 array

generates lowest GMPP of 7982 W and the corresponding co-ordinates of V_{mp}, I_{mp} are (214.4, 41.01). RCT configuration is able to generate more GMPP compared to SP, BL,HC by 1410W (18.82%), 73W (0.82%) and 244W (2.82%). In case of 8×8 PV array, TCT arrangement generates highest GMPP of 13190 W and the corresponding co-ordinates of V_{mp}, I_{mp} are (246.40, 53.53), whereas SP configuration generates lowest GMPP of 12530 W and the corresponding co-ordinates of V_{mp}, I_{mp} are (244.8, 51.18). RCT configuration is able to generate GMPP of 13190 W which is equal to TCT and more GMPP compared to SP, BL,HC by 660W (5.2%), 280W (2.6%) and 470W

(3.69%).

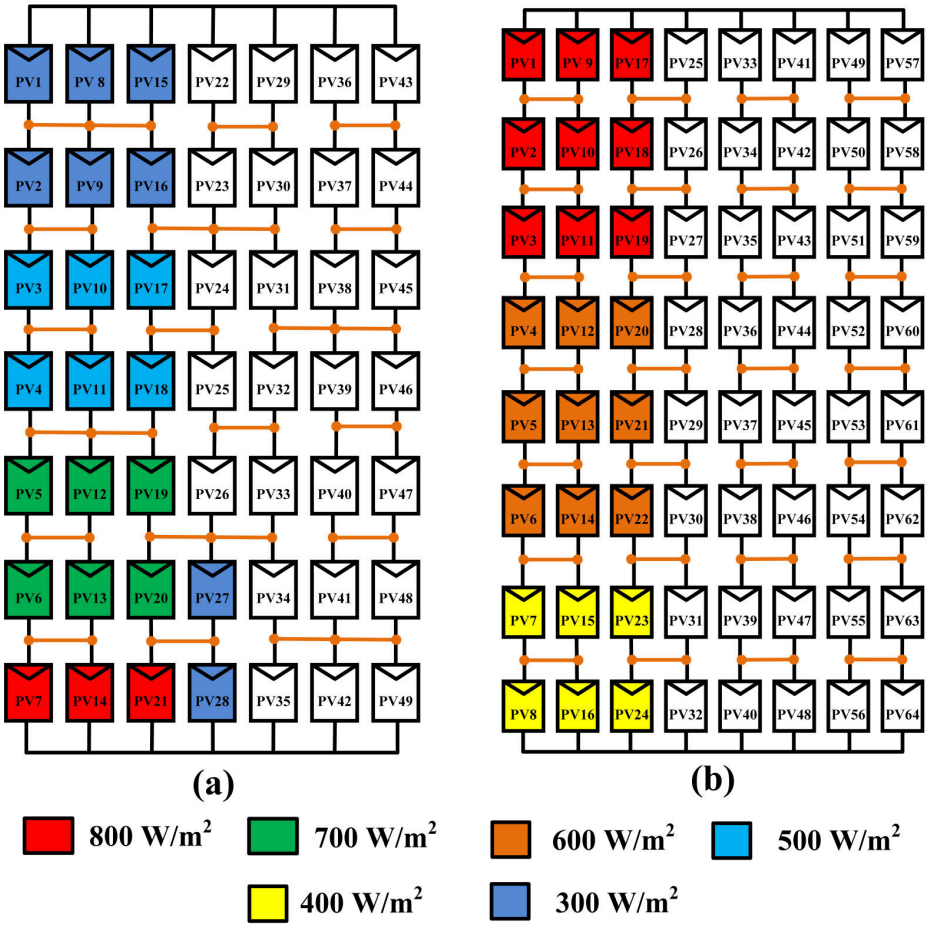

Figure 3.12: Long & Narrow (LN) shading pattern (a) 7×7 array (b) 8×8 array

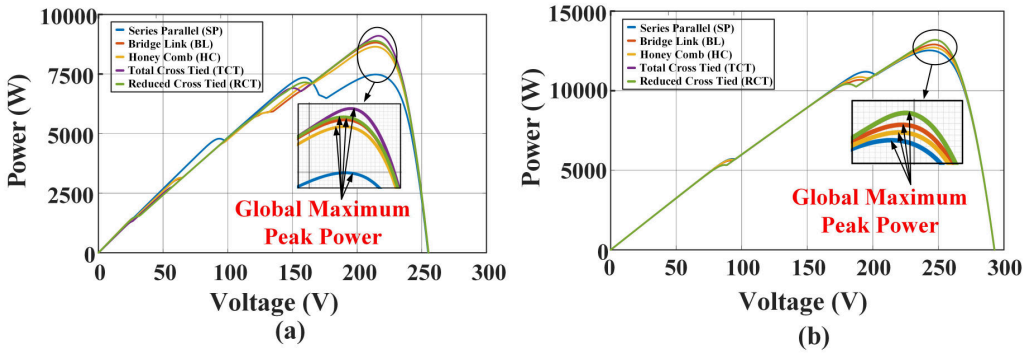

Figure 3.13: LN Shading condition (a) Power Characteristics (P-V) plot of 7×7 array (b) Power Characteristics (P-V) plot of 8×8 array

Table 3.3: Performance parameters of 7×7 & 8×8 PV array for L&N shading condition

7×7 PV Array								
Config.	$V_{OC}(V)$	$I_{SC}(A)$	$V_{mp}(V)$	$I_{mp}(A)$	$GMPP(W)$	$ML(\%)$	$FF(\%)$	$\eta(\%)$
TCT	255.4	53.75	216.8	41.98	9102	35.30	56.86	11.09
RCT	255.5	55.52	213.8	41.62	8892	37.76	55.85	10.89
BL	255.5	55.51	213.7	41.26	8819	38.90	55.39	10.80
HC	255.4	56.40	214.1	41.12	8648	41.67	54.31	10.59
SP	255.1	56.45	214.4	41.01	7982	53.47	50.13	9.78
8×8 PV Array								
Config.	$V_{OC}(V)$	$I_{SC}(A)$	$V_{mp}(V)$	$I_{mp}(A)$	$GMPP(W)$	$ML(\%)$	$FF(\%)$	$\eta(\%)$
TCT	292.62	65.29	246.40	53.53	13190	21.30	63.42	12.37
RCT	292.62	65.29	246.40	53.53	13190	21.30	63.42	12.37
BL	292.60	65.31	245.60	52.55	12910	23.93	62.08	12.11
HC	292.58	65.32	245.60	51.80	12720	25.79	61.16	11.93
SP	292.56	65.32	244.80	51.18	12530	27.69	60.25	11.75

3.4.4 Shading pattern - Long & Wide (LW)

The shading pattern Long & Wide (LW) considered is displayed in Fig. 3.14(a) & (b). The power-voltage (P-V) characteristics of 7×7 and 8×8 PV array for TCT, HC, BL, SP and RCT configurations are displayed in Fig. 3.15(a) & (b). The performance parameters are depicted in Table 3.4 in the order of decreasing GMPP. In case of 7×7 array, TCT arrangement generates highest GMPP of 7962 W and the corresponding co-ordinates of V_{mp}, I_{mp} are (220,36.19), whereas SP configuration generates lowest GMPP of 7107 W and the corresponding co-ordinates of V_{mp}, I_{mp} are (218.4,32.54). RCT configuration is able to generate more GMPP compared to SP, BL,HC by 779W (10.96%), 194W (2.52%) and 251W (3.28%). In case of 8×8 array, TCT configuration generates highest GMPP of 10760 W and the corresponding co-ordinates of V_{mp}, I_{mp} are (251.30,42.81), whereas SP configuration generates lowest GMPP of 10200 W and the corresponding co-ordinates of V_{mp}, I_{mp} are (250.20,40.79). RCT configuration is able to generate more GMPP compared to SP, BL, HC by 450W (4.44%), 175W (1.67%) and 220W (2.1%).

From the simulation results it is inferred that, for 7×7 PV array under SN, SW, LN and LW shading patterns, RCT configuration is able to generate GMPP close to TCT. RCT configuration is able to generate GMPP more than SP, BL and HC in SN, SW, LN and LW shading patterns. In case of 8×8 PV array, the proposed RCT

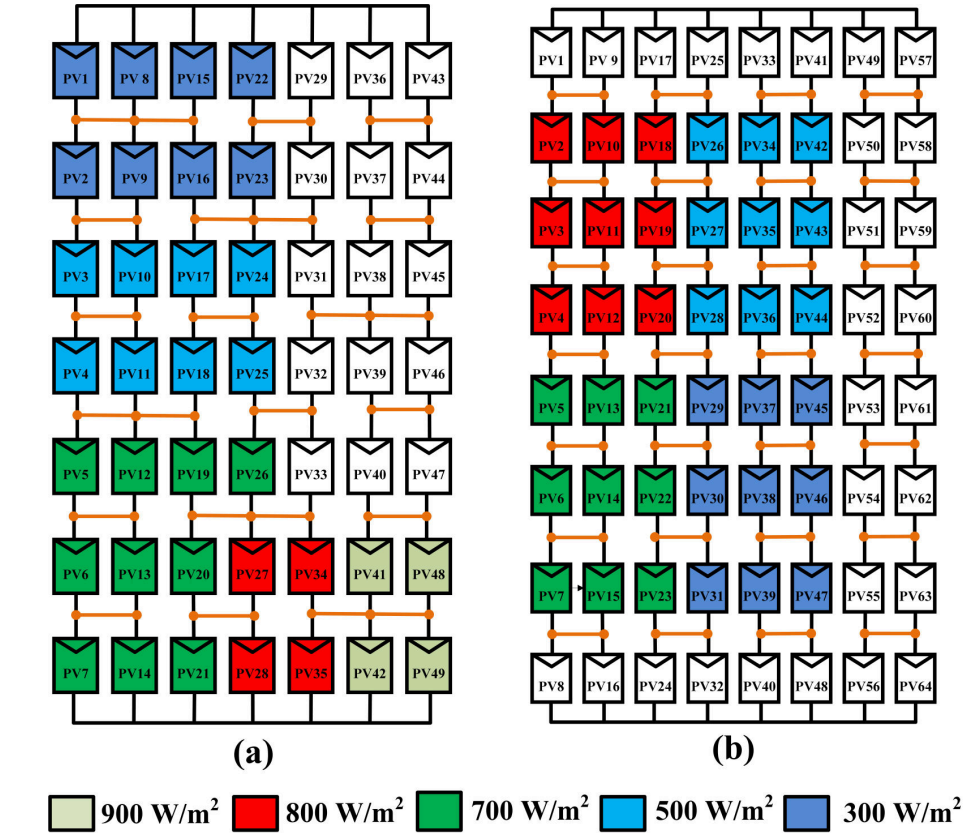

Figure 3.14: Lond & Wide (LW)shading pattern (a) 7×7 array (b) 8×8 array

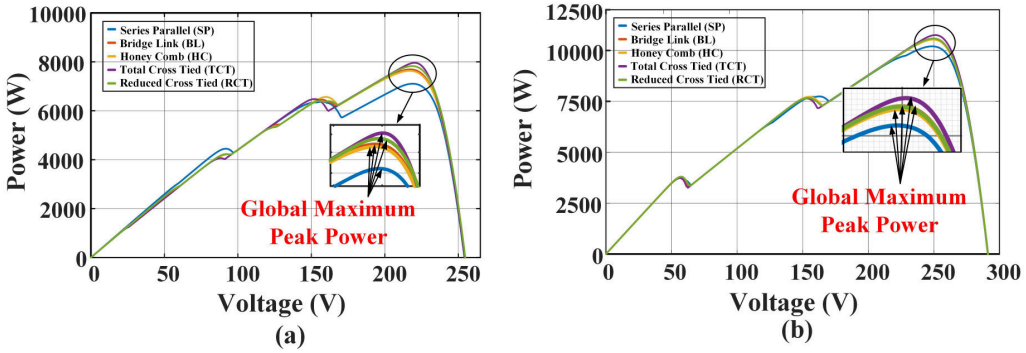

Figure 3.15: LW Shading condition (a) Power Characteristics (P-V) plot of 7×7 array (b) Power Characteristics (P-V) plot of 8×8 array

configuration is able to generate GMPP equal to TCT under LN shading pattern. Under SN, SW and LW shading patterns, RCT configuration is able to generate GMPP close to TCT. Further, RCT configuration is able to generate GMPP more than SP, BL and HC in SW, LN and LW shading patterns. The simulation results of

Table 3.4: Performance parameters of 7×7 & 8×8 PV array for L&W condition

7×7 PV Array								
Config.	$V_{OC}(V)$	$I_{SC}(A)$	$V_{mp}(V)$	$I_{mp}(A)$	$GMPP(W)$	$ML(\%)$	$FF(\%)$	$\eta(\%)$
TCT	254.30	51.16	220	36.19	7962	53.86	50.01	9.75
RCT	254.80	51.19	218	35.91	7886	55.34	49.53	9.66
BL	254.40	51.21	217.12	35.45	7692	59.26	48.31	9.42
HC	254.40	51.22	217	35.19	7635	60.45	47.95	9.35
SP	254.20	52.11	218.4	32.54	7107	72.37	44.64	8.71
8×8 PV Array								
Config.	$V_{OC}(V)$	$I_{SC}(A)$	$V_{mp}(V)$	$I_{mp}(A)$	$GMPP(W)$	$ML(\%)$	$FF(\%)$	$\eta(\%)$
TCT	291.40	70.55	251.30	42.81	10760	48.70	51.74	10.09
RCT	291.40	70.57	250.20	42.33	10680	49.81	51.36	10.02
BL	291.25	70.56	250.40	42.31	10475	51.09	50.92	9.93
HC	291.35	70.57	250.10	42.13	10430	51.95	50.63	9.88
SP	290.98	70.57	250.20	40.79	10200	56.86	49.05	9.57

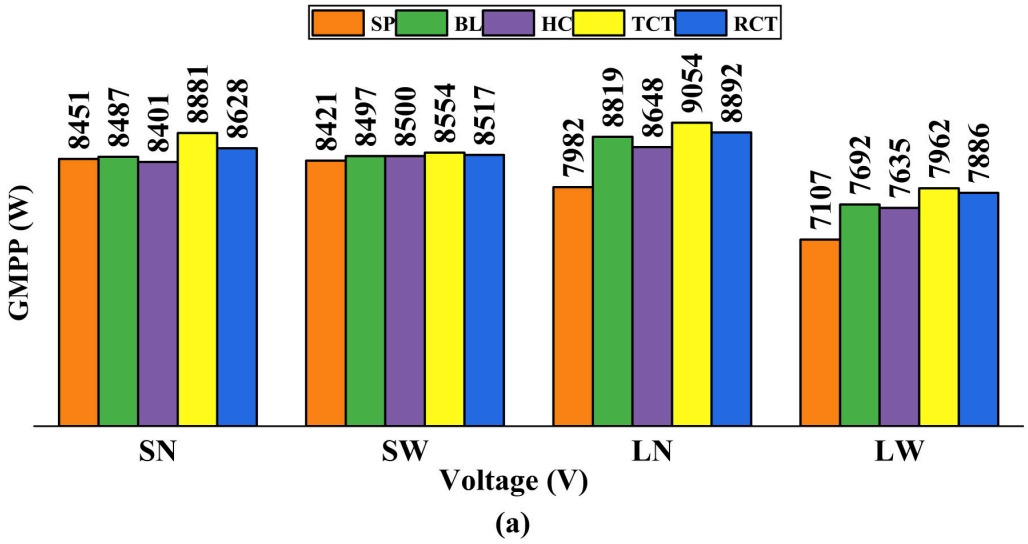

Figure 3.16: Simulation results (GMPP) for 7×7 PV Array

GMPP for 7×7 & 8×8 PV array under RCT, TCT, BL, HC and SP configurations is shown in Fig. 3.16 & 3.17.

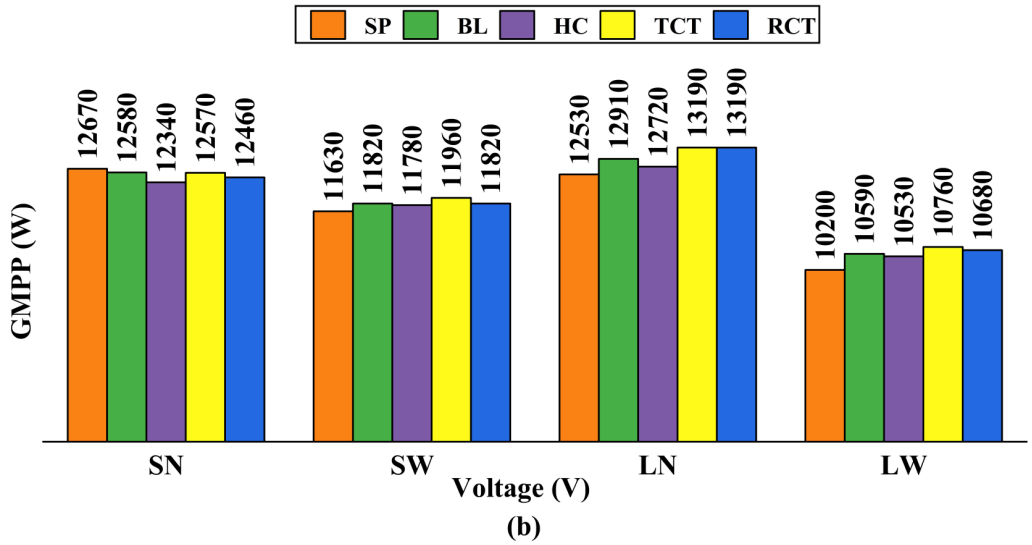

Figure 3.17: Simulation results (GMPP) for 8×8 PV Array

3.5 Experimental Results

An experimental setup of PV array shown in Fig. 3.18 is used to validate the proposed RCT configuration along with traditional TCT, SP, HC and BL configurations. It consists of PV modules of same capacity, one solar irradiance meter (FLUKE IRR1-SOL), two digital multimeters (FLUKE-17B+), resistive load, transparent sheets and connecting wires. The rating of PV module (LOOM SOLAR) considered is P_{mp} = 10W, open circuit voltage V_{oc} = 26.8 V, short circuit current I_{sc} = 0.55 A, MPP voltage, V_{mp} = 20 V, MPP current I_{mp} = 0.5A. The amount of insolation falling on the PV module ia measured by using solar irradiance meter. Various levels of solar insolation are achieved by using transparent sheets of different thickness. The output current from the PV array is measured by using multimeter connected in series to the load. The PV array output voltage is measured by using multimeter connected in parallel across the load. The output power form the PV array is obtained by multiplying the output voltage and current.The accuracy of multimeters used is ±0.5% for DC voltage and ±1.5% for DC current. The overall accuracy in measuring of PV array output power is ±2%.The experiment is conducted at 950 W/m^2 and 35^0C.

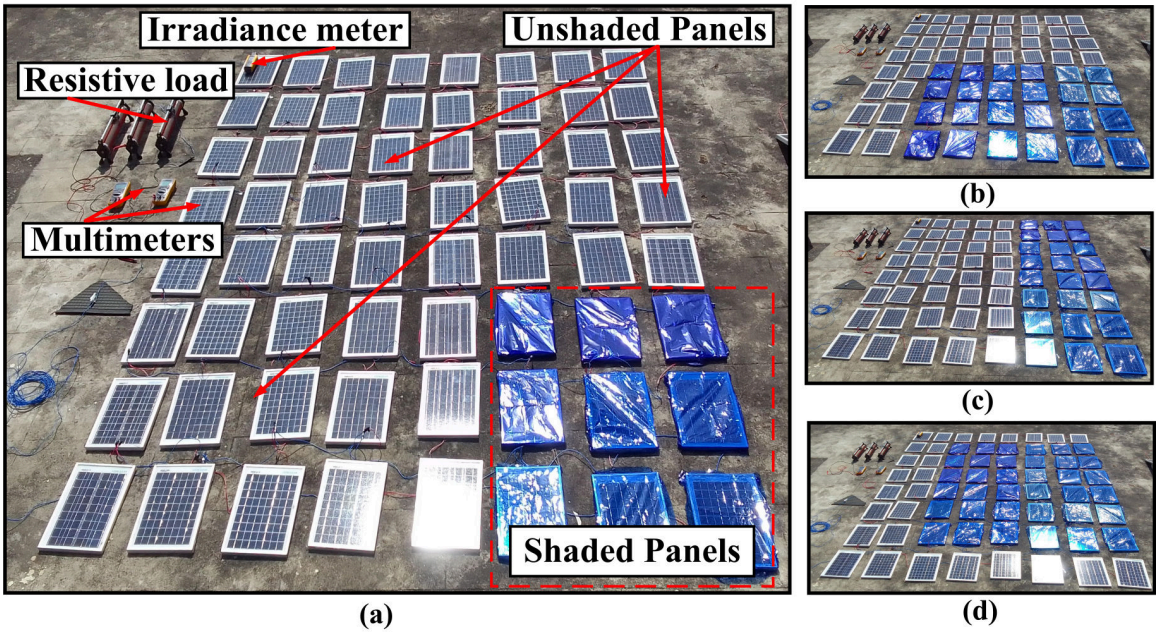

Figure 3.18: Experimental setup of 8×8 PV array (a) Short & Narrow (SN) (b) Short & Wide (SW) (c) Long & Narrow (LN) (d) Long & Wide (LW)

3.5.1 7×7 PV array

In case of 7×7 PV array, 49 PV modules are connected in TCT, SP, BL, HC and proposed RCT configuration. The power voltage (P-V) characteristics and experimental readings of GMPP for TCT, RCT, SP , BL and HC configurations is depicted in Fig. 3.19. Under SN shading pattern it is able to generate GMPP more than SP, BL and HC by 4.9%, 4.2% and 5.79%. Under SW shading pattern it is able to generate GMPP more than SP, BL and HC by 1.15%, 0.85% and 0.21%. Under LN shading pattern it is able to generate GMPP more than SP, BL and HC by 15.62%, 1.63% and 3.79%. Under LW shading pattern it is able to generate GMPP more than SP, BL and HC by 10.03%, 3.31% and 4.26%. And also, RCT configuration is able to generate GMPP close to TCT configuration under SW and LW shading patterns with reduced cross ties.

3.5.2 8×8 PV array

In case of 8×8 PV array, 64 PV modules are connected in TCT, SP, BL, HC and proposed RCT configuration. The power voltage (P-V) characteristics and experi-

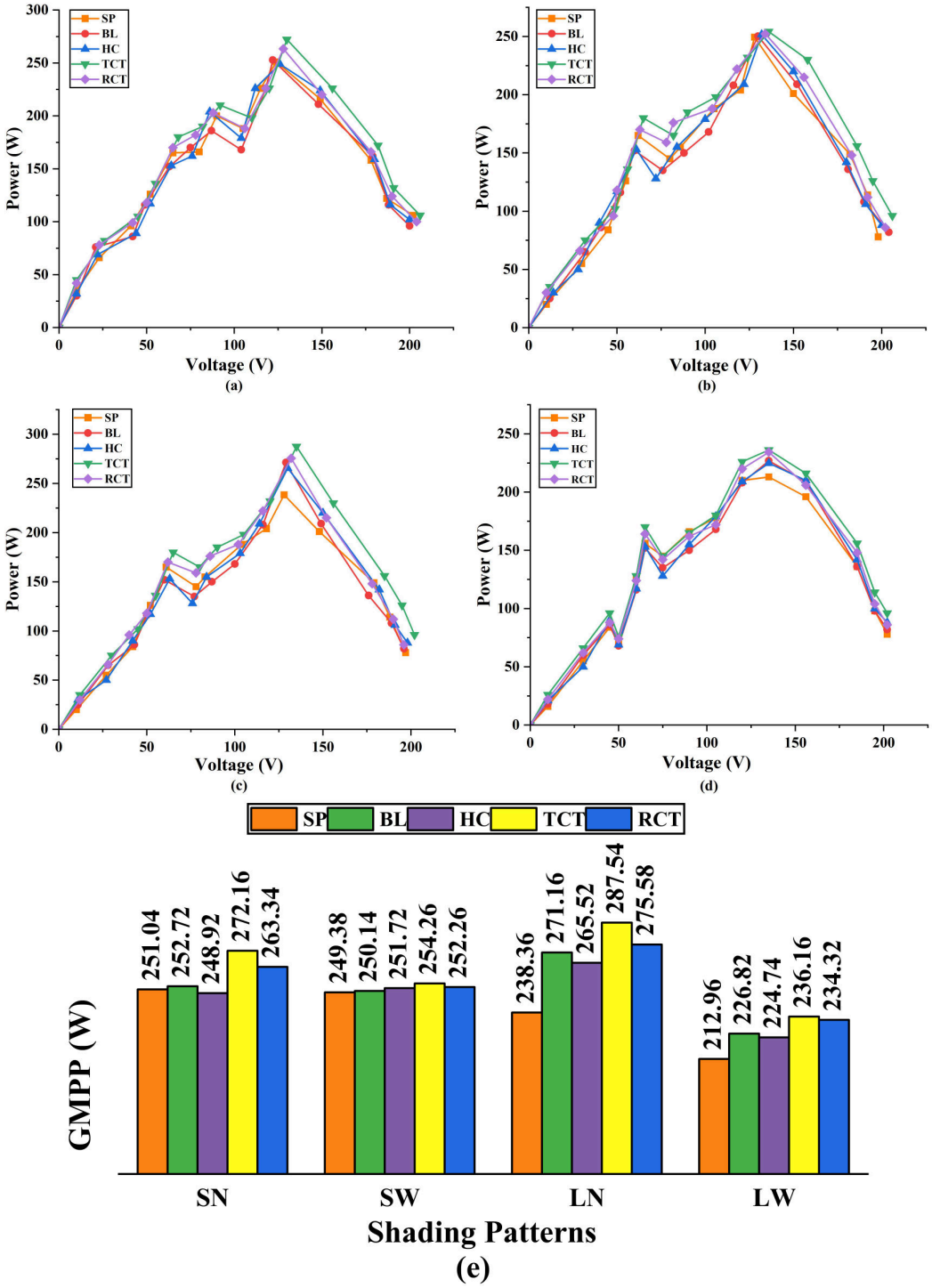

Figure 3.19: P-V characteristics of 7×7 PV array (a) SN shading pattern (b) SW shading pattern (c) LN shading pattern (d) LW shading pattern (e) GMPP of 7×7 PV array

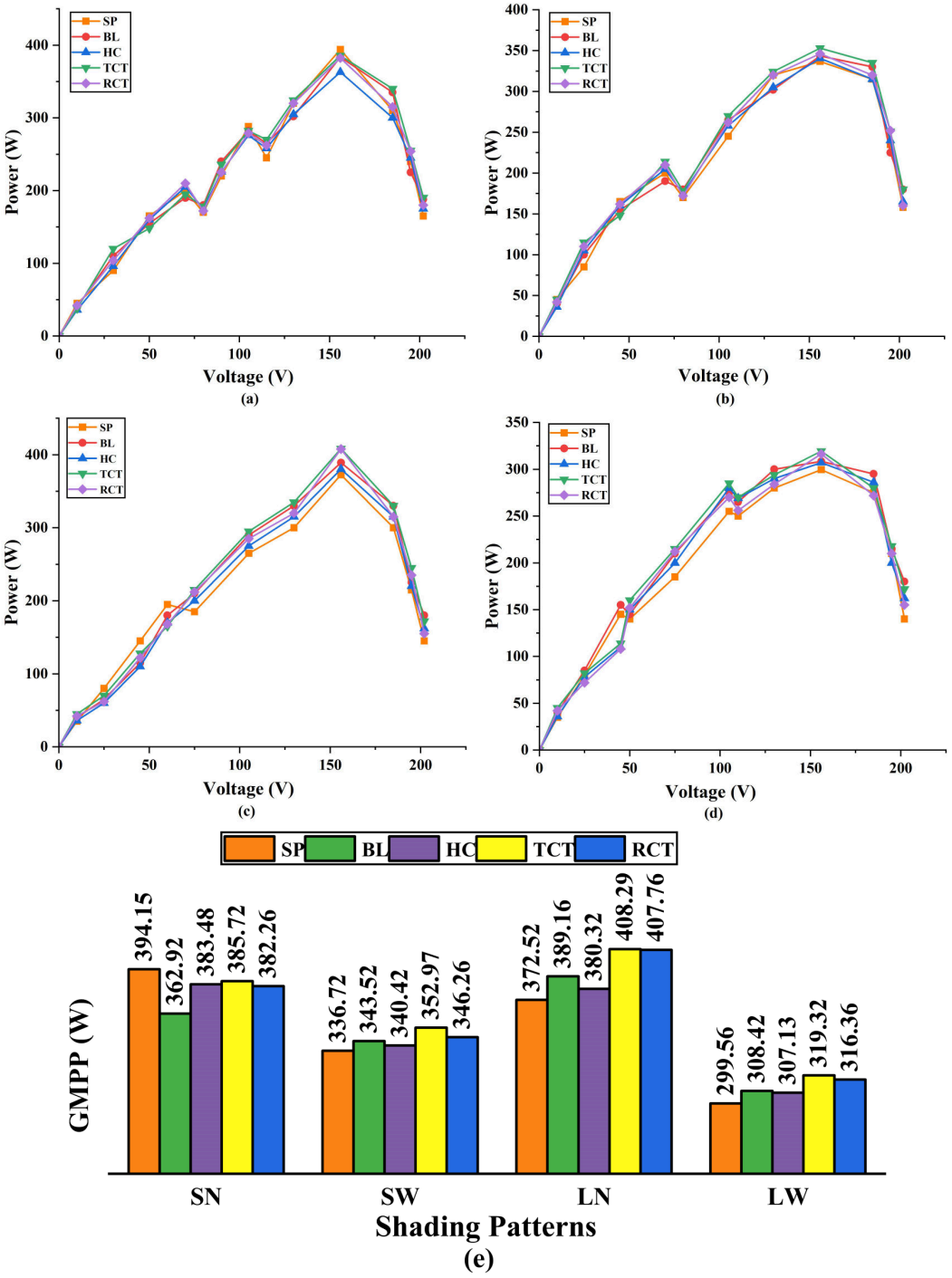

Figure 3.20: P-V characteristics of 8×8 PV array (a) SN shading pattern (b) SW shading pattern (c) LN shading pattern (d) LW shading pattern (e) GMPP of 8×8 PV array

mental readings of GMPP for TCT, RCT, SP , BL and HC configurations is depicted in Figure. 3.20. Under SN shading pattern it is able to generate GMPP more than BL configuration by 5.33%. Under SW shading pattern it is able to generate GMPP more than SP, BL and HC by 2.83%, 0.8% and 1.72%. Under LN shading pattern it is able to generate GMPP more than SP, BL and HC by 9.46%, 4.78% and 7.21%. Under LW shading pattern it is able to generate GMPP more than SP, BL and HC by 5.61%, 2.57% and 3.01%. And also RCT configuration is able to generate GMPP equal to TCT configuration under LN shading pattern with reduced cross ties.
For 7×7 PV array, RCT and TCT configuration are having total of 24 and 36 cross ties. It indicates that RCT configuration is having 33.33% lesser cross ties compared to TCT configuration. For 8×8 PV array, RCT and TCT configuration are having total of 34 and 49 cross ties. It indicates that RCT configuration is having 30.61% lesser cross ties compared to TCT configuration. The cross ties in RCT and TCT configuration for various sizes of PV array are listed in Table 3.5. along with wiring loss. RCT configuration is able to reduce the wiring loss by at least 25%.

Table 3.5: Comparison of Cross Ties in TCT and RCT PV Array configurations

Array Size	**TCT**	**RCT**	**Reduction in Cross Ties**	**Wiring Loss (%)**
5×5	16	12	4	25
6×6	25	17	8	32
7×7	36	24	12	33.33
8×8	49	34	15	30.61
9×9	64	40	24	37.5
10×10	81	57	24	29.62

3.6 Summary

In this chapter, a novel Reduced Cross Tied (RCT) PV array configuration is proposed to enhance the power output from PV array under PSCs. The conventional PV array configurations SP, HC, BL and TCT together with proposed RCT configuration are simulated for 7×7 and 8×8 symmetrical PV arrays under four different shading patterns (SN, SW, LN and LW). Further the defectiveness of the proposed RCT configuration is validated using experimental setup. From the simulation and experimental results it is observed that, RCT configuration can be considered as an

alternative to TCT configuration. And the key advantage of RCT configuration is that, it is able to generate GMPP close to TCT configuration with reduced cross ties. The proposed RCT configuration is having at least 25% reduction in cross ties compared to TCT configuration for any array size. Hence RCT configuration possess reduced wiring loss compared to TCT configuration. The RCT configuration is applicable for square array of any size. And also, the PV array configuration techniques Sudoku, Optimal Sudoku, PRMFEC, Magic Square etc. can be applied to RCT configuration in order to increase the GMPP under PSCs. Considering all the above points, for grid-connected and stand-alone PV applications RCT configuration might be an alternative to TCT configuration for improving the PV system performance.

Chapter 4

Cyclic Back Shift Method for Maximizing PV Array Power under Partial Shading

This chapter presents a static reconfiguration scheme titled Cyclic Back Shift (CBS) method to enhance PV power under partial shading conditions (PSCs). The proposed CBS method is tested on 9×9 square array in both software (20.25kW system) and hardware (0.81kW system) environments under various shading patterns. Further, a comparative analysis is carried between proposed CBS method, Reduced Cross Tied (RCT), Total Cross Tied (TCT) and different existing reconfiguration schemes. The results showed that proposed CBS method is able to generate more output power and improves efficiency of PV systems under PSCs.

4.1 Introduction

The demand for energy in the world is increasing at a rapid rate due to increase in population and economy. There is need for increasing power generation from the available resources to meet increasing energy demand. The fossil fuels are the main source of power generation. But, due to depletion of fossil fuels, there is need for alternative energy sources to generate the power. Renewable energy sources are the best alternative sources of energy which are freely available in the nature. In renewable energy sources, solar photovoltaic (PV) power generation is having more advantages

compared to other sources. However partial shading phenomena which occurs regularly limits its efficiency. Partial shading is caused by moving clouds, shadows of trees and houses. To address this issue, several solutions have been proposed which include MPPT techniques, usage of bypass diodes and array reconfiguration techniques. Among them simple and efficient solution is array reconfiguration technique which includes power generation phase without employing power converter. However, MPPT methods address PSCs by tracking the occurrence of multiple peaks and bypass diodes reduce the effect of hot spot formation. Further array reconfiguration by altering the electrical connections or physical displacement of modules reduces the occurrence of multiple peaks and increases the power output. In this regard, choosing right configuration of PV array is more important. In the literature many PV array configurations are presented namely Simple-Series (SS), Parallel (P), Series-Parallel (SP), Honey Comb (HC), Bridge Link (BL) and Total Cross Tied (TCT). Out of which TCT configuration generates more output under PSCs compared to other configurations. The TCT configuration requires more number of cross ties to be connected. Whereas RCT configuration is able to generate power on par to TCT with reduced cross ties. Hence, the proposed CBS method of module rearrangement is implemented on RCT connected PV array. The contributions made in this chapter are listed as follows

- A static reconfiguration scheme Cyclic Back Shift (CBS) method is proposed.
- The proposed CBS method is validated in software and hardware environments for 9×9 square array and 7×5 non-square array under various shading patterns.
- The performance parameters under various shading patterns by the proposed CBS method and other existing techniques in the literature are presented.
- A qualitative comparison is done between the proposed CBS method and various existing techniques in hardware and software environments.

4.1.1 Cyclic Back Shift (CBS) method

The main objective of the CBS method is to improve the power output form PV array under PSCs by distributing the shadow over the entire array. In this context, the proposed CBS method makes use of row positions of m×n PV array. The repetition

of row positions in a particular row and particular column is avoided to get a unique solution. Consider a PV array of size m×n with row and column positions as shown in Fig. 4.1

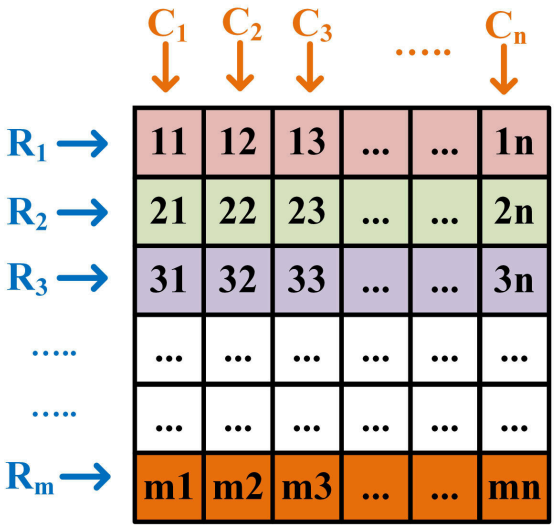

Figure 4.1: Row and Column positions of m×n RCT connected PV array

The proposed CBS method, when applied to RCT configured PV array is described as follows:
Consider $p = \lfloor \sqrt{m} \rfloor$ and $r = \text{mod}\ (m,\ p)$
Case 1: If $r = 0$

- Step-1: The row positions of modules in col-1 are unaltered.
- Step-2: The row positions of modules in col-2 are obtained by shifting row positions of previous column (col-1) backwards by 'p' steps.
- Step-3: Repeat the step-2 to obtain the row positions of next columns.
- Step-4: If any repetition of row position occurs across the row, then the row positions of particular column are obtained by shifting the row positions of previous column backwards by (p-1) steps.
- Step-5: Repeat the step-2 to obtain the row positions of next columns.

Consider a 9×9 PV array, where m = 9, n = 9 and $p = \lfloor \sqrt{9} \rfloor$ is 3. The value of r = mod(9, 3) is 0. The arrangement of modules in 9×9 PV array by implementing CBS method is shown in Fig. 4.2(a).

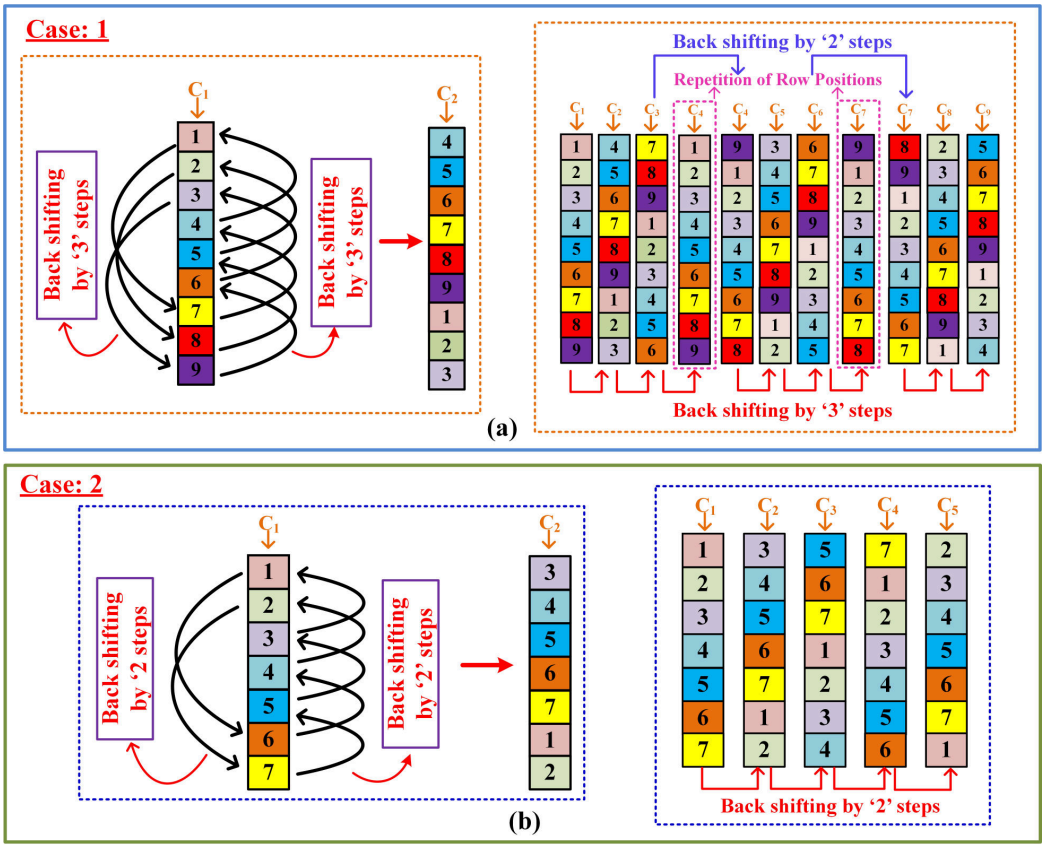

Figure 4.2: CBS arrangement (a) 9×9 PV array (b) 7×5 PV array

Case 2: If r≠0

- Step-1: The row positions of modules in col-1 are unaltered.
- Step-2: The row positions of modules in col-2 are obtained by shifting row positions of previous column (col-1) backwards by 'p' steps.
- Step-3: Repeat the step-2 to obtain the row positions of next columns.

Consider a 7×5 PV array, where m = 7, n = 5 and p = $\lfloor\sqrt{7}\rfloor$ is 2. The value of r = mod(7, 2) is 1. The arrangement of modules in 7×5 PV array by implementing CBS method is shown in Fig. 4.2(b). The flowchart of proposed CBS method is shown in Fig. 4.3.

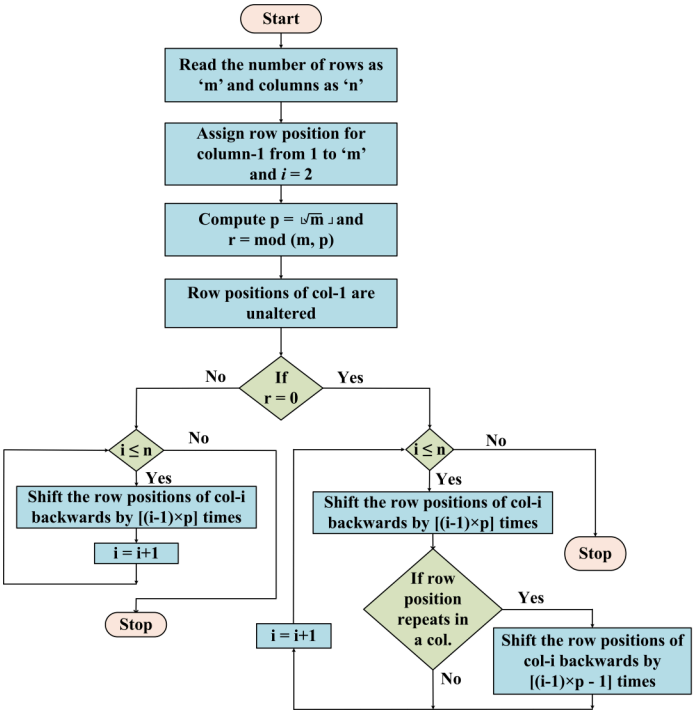

Figure 4.3: Flowchart of the proposed CBS method

4.1.2 Performance Parameters

Mismatch loss: It is the difference between maximum power point MPP_{nor} under normal condition and global maximum power point $GMPP_{PSC}$ under PSCs. It is given by equation 4.1.

$$ML(\%) = \frac{MPP_{nor} - GMPP_{PSC}}{GMPP_{PSC}} \times 100 \tag{4.1}$$

Fill Factor: It is the ratio of global maximum power output (GMPP) of the PV array to the product of open circuit voltage V_{OC} and current I_{SC} of the PV array. It is given by equation 4.2.

$$FF(\%) = \frac{GMPP_{PSC}}{V_{OC} \times I_{SC}} \tag{4.2}$$

Efficiency(η): It is the fraction of available maximum power output to the solar input power P_{in}. It is given by equation 4.3.

$$\eta(\%) = \frac{Power\ at\ GMPP}{Solar\ input\ (P_{in})} \times 100 \tag{4.3}$$

4.2 Simulation Results

To assess the performance of proposed Cyclic Back Shift (CBS) method, a square array of size 9×9 (20.25kW system) and non-square array of size 7×5 (8.75kW system) connected in RCT configuration are considered. The specifications of PV module considered for simulation is shown in Table 4.1.

Table 4.1: Specifications of PV module considered for simulation

Parameters	Values
Maximum Power, P_{mp}	250 W
Open Circuit Voltage, V_{oc}	36.8 V
Short Circuit Current, I_{sc}	8.71 A
Voltage at MPP, V_{mp}	30.1 V
Current at MPP, I_{mp}	8.1 A

4.2.1 9×9 Square Array

Shading Pattern-I: In this shading pattern, a 4×4 sub array at the bottom right corner is subjected to partial shading as shown in Fig. 4.4. The theoretical values of GMPP obtained by RCT and proposed CBS method are calculated as shown below.

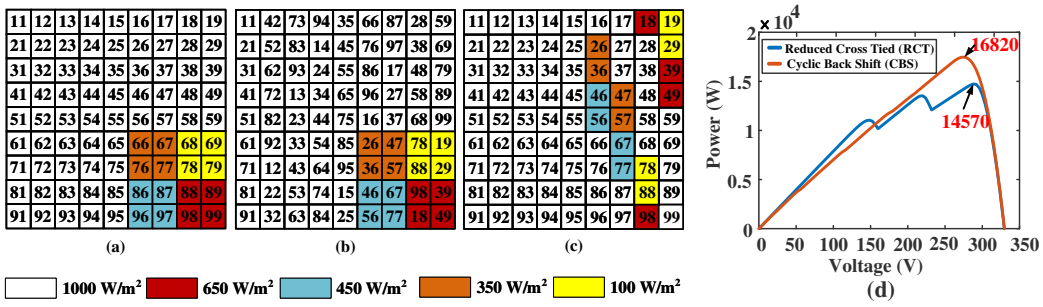

Figure 4.4: Shading Pattern-I (a) RCT arrangement (b) Cyclic Back Shift (CBS) arrangement (c) Shade dispersion by Cyclic Back Shift (CBS) method

GMPP for RCT configuration: To determine the value of GMPP, calculation of current generated by each row and corresponding array voltage is required. The

current generated by each row is given by equation 4.4.

$$\left.\begin{aligned} I_{r1} &= 9I_m \\ I_{r2} &= 9I_m \\ I_{r3} &= 9I_m \\ I_{r4} &= 9I_m \\ I_{r5} &= 9I_m \\ I_{r6} &= 5I_m + (2 \times 0.35I_m) + (2 \times 0.1I_m) = 5.9I_m \\ I_{r7} &= 5I_m + (2 \times 0.35I_m) + (2 \times 0.1I_m) = 5.9I_m \\ I_{r8} &= 5I_m + (2 \times 0.45I_m) + (2 \times 0.65I_m) = 7.2I_m \\ I_{r9} &= 5I_m + (2 \times 0.45I_m) + (2 \times 0.65I_m) = 7.2I_m \end{aligned}\right\} \tag{4.4}$$

The array voltage is $V_a = 9V_m$, if no modules are bypassed. The array current is $5.9I_m$. The array power is $P_{array} = V_a I_a = 53.1V_m I_m$. The voltage, current and power obtained for RCT arrangement is listed in Table.4.2.

GMPP for CBS configuration: The modules of the 9×9 PV array depicted in Fig. 4.4(a) are relocated based on the proposed CBS method. The current generated by each row is given by equation 4.5.

$$\left.\begin{aligned} I_{r1} &= 7I_m + (0.65I_m) + (0.1I_m) = 7.75I_m \\ I_{r2} &= 7I_m + (0.35I_m) + (0.1I_m) = 7.45I_m \\ I_{r3} &= 7I_m + (0.35I_m) + (0.65I_m) = 8I_m \\ I_{r4} &= 6I_m + (0.65I_m) + (0.45I_m) + (0.35I_m) = 7.45I_m \\ I_{r5} &= 7I_m + (0.35I_m) + (0.45I_m) = 7.8I_m \\ I_{r6} &= 8I_m + (0.45I_m) = 8.45I_m \\ I_{r7} &= 7I_m + (0.45I_m) + (0.1I_m) = 7.55I_m \\ I_{r8} &= 8I_m + (0.1I_m) = 8.1I_m \\ I_{r9} &= 8I_m + (0.65I_m) = 8.65I_m \end{aligned}\right\} \tag{4.5}$$

The array voltage is $V_a = 9V_m$, if no modules are bypassed. The array current is $7.45I_m$. The array power is $P_{array} = V_a I_a = 67.05V_m I_m$. The theoretical results are given in Table 4.2 and verified by plotting simulated PV characteristics as shown in Fig. 4.4(d). From the figure, it is inferred that GMPP for RCT and CBS method are

14570 W and 16820 W. So, CBS method generates more output power compared to RCT configuration by 15.44%.

Table 4.2: GMPP for RCT and CBS method under Shading Pattern-I

RCT arrangement				CBS arrangement			
Row	(I_a)	(V_a)	(P_a)	**Row**	(I_a)	(V_a)	(P_a)
R_6	$5.9I_m$	$9V_m$	$\mathbf{53.1}V_mI_m$	R_4	$7.45I_m$	$9V_m$	$\mathbf{67.05}V_mI_m$
R_7	$5.9I_m$	-	-	R_2	$7.45I_m$	-	-
R_8	$7.2I_m$	$7V_m$	$50.4V_mI_m$	R_7	$7.55I_m$	$7V_m$	$52.85V_mI_m$
R_9	$7.2I_m$	-	-	R_1	$7.75I_m$	$6V_m$	$46.5V_mI_m$
R_1	$9I_m$	$5V_m$	$45V_mI_m$	R_5	$7.80I_m$	$5V_m$	$39V_mI_m$
R_2	$9I_m$	-	-	R_3	$8I_m$	$4V_m$	$32V_mI_m$
R_3	$9I_m$	-	-	R_8	$8.1I_m$	$3V_m$	$24.3V_mI_m$
R_4	$9I_m$	-	-	R_6	$8.45I_m$	$2V_m$	$16.9V_mI_m$
R_5	$9I_m$	-	-	R_9	$8.65I_m$	$1V_m$	$8.65V_mI_m$

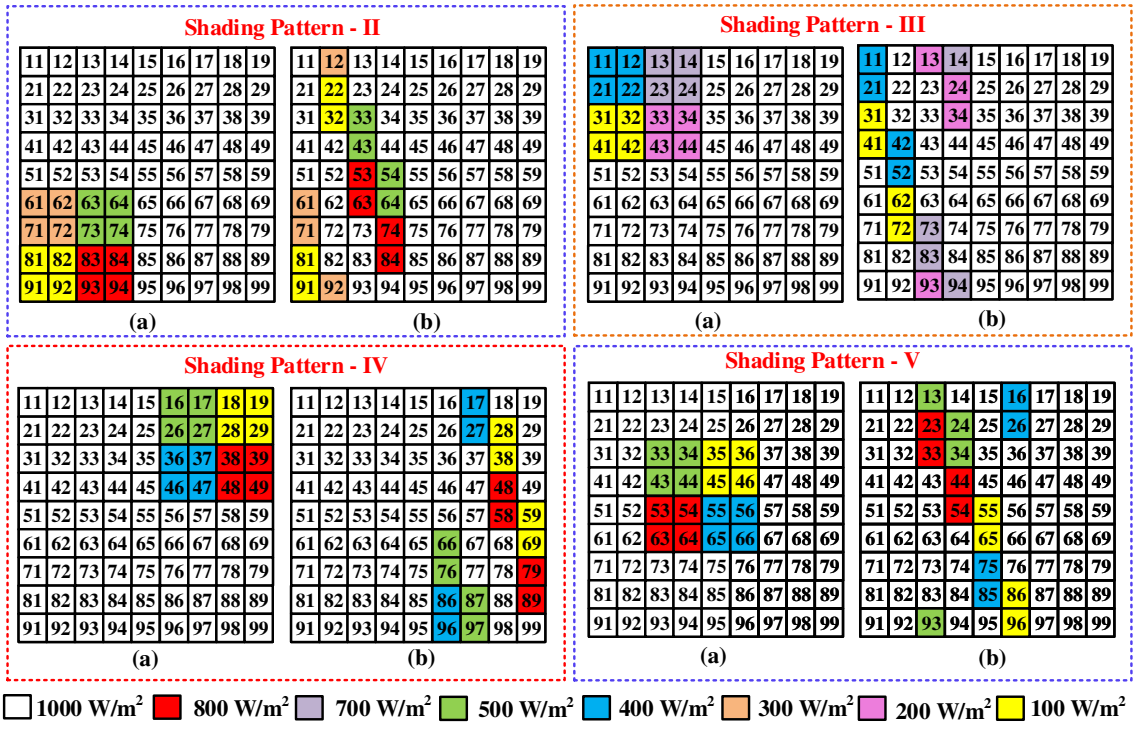

Figure 4.5: Shading Patterns - II to V (a) RCT arrangement (b) CBS arrangement

Shading Pattern-II: In this shading pattern, 4×4 sub array at the bottom left corner as depicted in Fig. 4.5 is subjected to partial shading. Table. 4.3 shows

theoretically computed value of GMPP for CBS and RCT methods. From the table, it is inferred that CBS method produces highest GMPP of 66.6 $V_m I_m$ compared to RCT (59.4 $V_m I_m$). The theoretical results are verified by plotting simulated PV characteristics as shown in Fig. 4.6. From the figure it is observed that GMPP is found to be 15740 W and 16710 W for RCT and CBS methods respectively.

Shading Pattern-III: In this shading pattern, 4×4 sub array at the top left corner as depicted in Fig. 4.5 is subjected to partial shading. Table 4.3 shows theoretically computed value of GMPP for CBS and RCT methods. From the table it is inferred that CBS method produces highest GMPP of 65.7 $V_m I_m$ compared to RCT (50.4 $V_m I_m$). The theoretical results are verified by plotting simulated PV characteristics shown in Fig. 4.6. From the figure it is observed that GMPP is found to be 14030 W and 17030 W for RCT and CBS methods respectively.

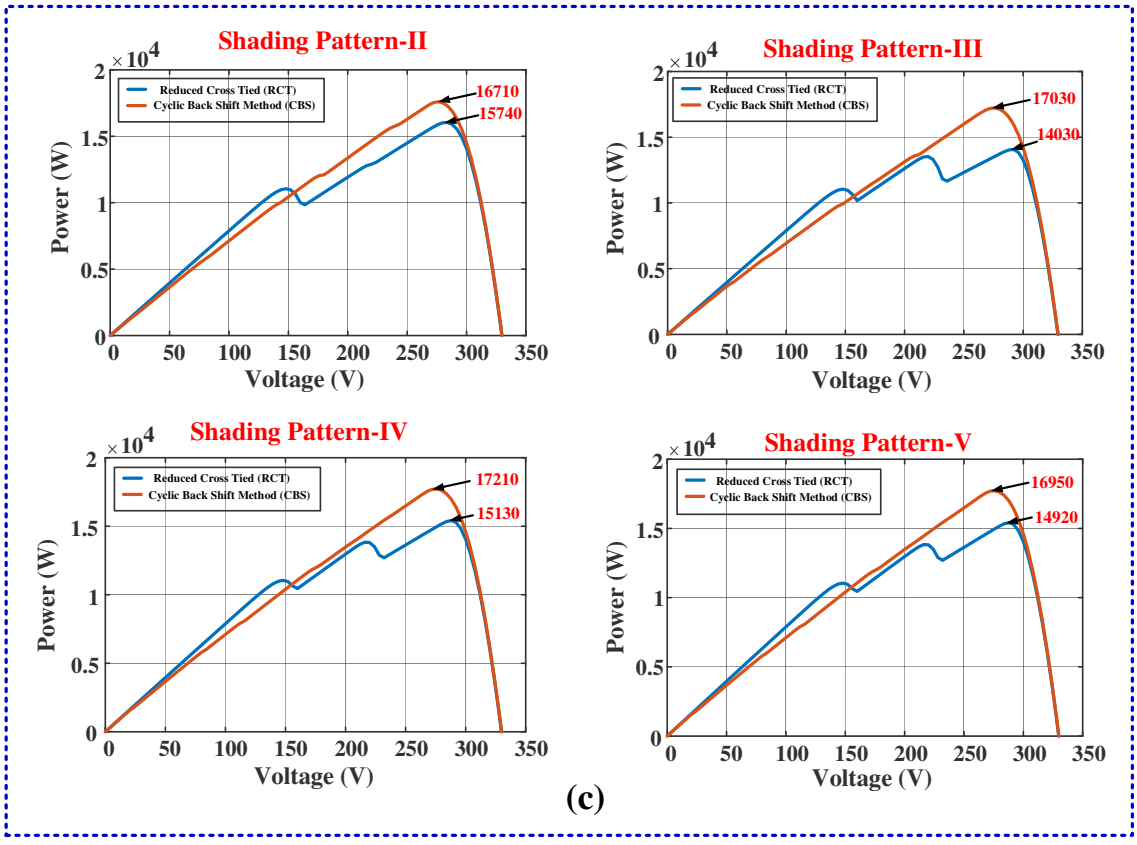

Figure 4.6: Power-voltage characteristics (a) Shading Pattern -II (b) Shading Pattern -III (c) Shading Pattern -IV (d) Shading Pattern -V

Table 4.3: GMPP for RCT and CBS method under Shading Patterns-II and III

Shading Pattern-II							
RCT arrangement				**CBS arrangement**			
Row	(I_a)	(V_a)	(P_a)	**Row**	(I_a)	(V_a)	(P_a)
R_6	6.6 I_m	$9V_m$	**59.4** V_mI_m	R_9	7.4 I_m	9 V_m	**66.66** V_mI_m
R_7	6.6 I_m	-	-	R_3	7.6 I_m	8 V_m	60.8 V_mI_m
R_8	7.8 I_m	7 V_m	54.6 V_mI_m	R_6	7.6 I_m	-	-
R_9	7.8 I_m	-	-	R_8	7.9 I_m	6 V_m	47.4 V_mI_m
R_1	9 I_m	5 V_m	45 V_mI_m	R_2	8.1 I_m	5 V_m	40.5 V_mI_m
R_2	9 I_m	-	-	R_7	8.1 I_m	-	-
R_3	9 I_m	-	-	R_1	8.3 I_m	3 V_m	24.9 V_mI_m
R_4	9 I_m	-	-	R_5	8.3 I_m	-	-
R_5	9 I_m	-	-	R_4	8.5 I_m	1 V_m	8.5 V_mI_m
Shading Pattern-III							
RCT arrangement				**CBS arrangement**			
Row	(I_a)	(V_a)	(P_a)	**Row**	(I_a)	(V_a)	(P_a)
R_3	5.9 I_m	$9V_m$	**50.4** V_mI_m	R_1	7.3 I_m	9 V_m	**65.7** V_mI_m
R_4	5.9 I_m	-	-	R_3	7.45 I_m	-	-
R_1	7.2 I_m	7 V_m	$50.4V_mI_m$	R_4	7.5 I_m	7 V_m	52.5 V_mI_m
R_2	7.2 I_m	-	-	R_2	7.6 I_m	6 V_m	45.6 V_mI_m
R_5	9 I_m	5 V_m	45 V_mI_m	R_7	7.8 I_m	5 V_m	39 V_mI_m
R_6	9 I_m	-	-	R_9	7.9 I_m	4 V_m	31.6 V_mI_m
R_7	9 I_m	-	-	R_6	8.1 I_m	3 V_m	24.3 V_mI_m
R_8	9 I_m	-	-	R_5	8.4 I_m	2 V_m	16.8 V_mI_m
R_9	9 I_m	-	-	R_8	8.7 I_m	1 V_m	8.7 V_mI_m

Shading Pattern-IV: In this shading pattern, 4×4 sub array at the top right corner as depicted in Fig. 4.5 is subjected to partial shading. Table 4.4 shows theoretically computed value of GMPP for CBS and RCT methods. From the table it is inferred that CBS method produces highest GMPP of 67.5 V_mI_m compared to RCT (55.8 V_mI_m). The theoretical results are verified by plotting simulated PV characteristics shown in Fig. 4.6. From the figure it is observed that CBS method produces highest GMPP of 17210W, which is 13.75% higher compared to RCT.

Shading Pattern-V: In this shading pattern, 4×4 sub array at the center of PV array as depicted in Fig. 4.5 is subjected to partial shading. Table 4.4 shows theoretically computed value of GMPP for CBS and RCT methods. From the table it is inferred that CBS method produces highest GMPP of 67.5 V_mI_m compared to RCT (55.8 V_mI_m). The theoretical results are verified by plotting simulated PV character-

istics shown in Fig. 4.6. From the figure it is observed that the power generated by CBS method is higher which is 16950 W compared to RCT 14920W.

Table 4.4: GMPP for RCT and CBS method under Shading Patterns-IV and V

Shading Pattern-IV							
RCT arrangement				**CBS arrangement**			
Row	(I_a)	(V_a)	(P_a)	**Row**	(I_a)	(V_a)	(P_a)
R_1	6.2 I_m	$9V_m$	**55.8** V_mI_m	R_2	7.5 I_m	9 V_m	**67.5** V_mI_m
R_2	6.2 I_m	-	-	R_6	7.6 I_m	8 V_m	60.8 V_mI_m
R_3	7.4 I_m	7 V_m	51.8 V_mI_m	R_8	7.7 I_m	7 V_m	53.9 V_mI_m
R_4	7.4 I_m	-	-	R_5	7.9 I_m	6 V_m	47.4 V_mI_m
R_5	9 I_m	5 V_m	45 V_mI_m	R_9	7.9 I_m	-	-
R_6	9 I_m	-	-	R_3	8.1 I_m	4 V_m	32.4 V_mI_m
R_7	9 I_m	-	-	R_7	8.3 I_m	3 V_m	24.9 V_mI_m
R_8	9 I_m	-	-	R_1	8.4 I_m	2 V_m	16.8 V_mI_m
R_9	9 I_m	-	-	R_4	8.8 I_m	1 V_m	8.8 V_mI_m
Shading Pattern-V							
RCT arrangement				**CBS arrangement**			
Row	(I_a)	(V_a)	(P_a)	**Row**	(I_a)	(V_a)	(P_a)
R_3	6.2 I_m	$9V_m$	**55.8** V_mI_m	R_8	7.5 I_m	9 V_m	**67.05** V_mI_m
R_4	6.2 I_m	-	-	R_9	7.6 I_m	8 V_m	60.8 V_mI_m
R_5	7.4 I_m	7 V_m	51.8 V_mI_m	R_2	7.7 I_m	7 V_m	53.9 V_mI_m
R_6	7.4 I_m	-	-	R_1	7.9 I_m	6 V_m	47.4 V_mI_m
R_1	9 I_m	5 V_m	45 V_mI_m	R_5	7.9 I_m	-	-
R_2	9 I_m	-	-	R_6	8.1 I_m	4 V_m	32.4 V_mI_m
R_7	9 I_m	-	-	R_3	8.3 I_m	3 V_m	24.9 V_mI_m
R_8	9 I_m	-	-	R_7	8.4 I_m	2 V_m	16.8 V_mI_m
R_9	9 I_m	-	-	R_4	8.8 I_m	1 V_m	8.8 V_mI_m

Table 4.5: Power Enhancement of CBS method over RCT arrangement

Shading Patterns	**RCT (W)**	**CBS (W)**	**% Power Enhancement of CBS over RCT**
SP-I	14570	16820	15.44
SP-II	15740	16710	6.16
SP-III	14030	17030	21.38
SP-IV	15130	17210	13.75
SP-V	14920	16950	13.61

The power enhancement by proposed method (CBS) over RCT is given in Table 4.5. It

Table 4.6: Simulation results (GMPP) of various reconfiguration techniques for RCT configuration

Shade	Sud	OS	Futoshiki	PRMFEC	PRFCPMFEC	ChaosMap	TTSA	ASud	CBS	RCT-CBS
SP-I	16120	16210	14680	16210	16160	15920	16110	15960	16220	16820
SP-II	16220	16140	14710	16110	16100	16050	15920	15860	15840	16710
SP-III	15750	15850	15710	16880	16920	15240	15820	15720	15860	17030
SP-IV	17090	17080	15020	17160	17110	17050	16720	16580	16660	17210
SP-V	16100	16140	15940	16450	16320	16280	15960	16120	16160	16950

is observed that the proposed CBS method is able to enhance the GMPP by minimum of 9.73% under shading pattern-II and maximum of 22.46% under shading pattern-III. Further the efficacy of the proposed CBS method is proved by performing comparative analysis between CBS method and different static reconfiguration techniques such as RCT, SuDoKu, Optimal SuDoKu, Futoshiki, PRMFEC, PRFCPMFEC, Chaos Map, Twisted two step, Tom Tom and Advanced Sudoku methods. The GMPP generated by all the afore mentioned reconfiguration techniques are graphically plotted in Table.4.6. It is observed that CBS method generates more output power compared to above mentioned techniques in the literature under the shading patterns considered.

4.3 Experimental Results

To verify the proposed CBS method, an experimental laboratory setup shown in Fig. 4.7 was built and tested under the above said PSCs for 9×9 square array (0.81kW system). The experiment was performed in real-time on the rooftop of the Electrical and Electronics Engineering department building at the National Institute of Technology (13.0108° latitude North, 74.7943° longitude East), Karnataka, India in January 2023. It consists of PV modules, one solar irradiance meter (FLUKE IRR1-SOL), two digital multimeters (FLUKE-17B+), resistive load, transparent sheets and connecting wires. The rating of PV module (LOOM SOLAR) considered is P_{mp} = 10W, open circuit voltage V_{oc} = 26.8 V, short circuit current I_{sc} = 0.55 A, MPP voltage, V_{mp} = 20 V, MPP current I_{mp} = 0.5A.

4.3.1 9×9 Square array

In this case, 81 PV modules each of 10 W are assembled to form 9×9 array as shown in Fig. 4.7(a). The experimental procedure is described as follows:

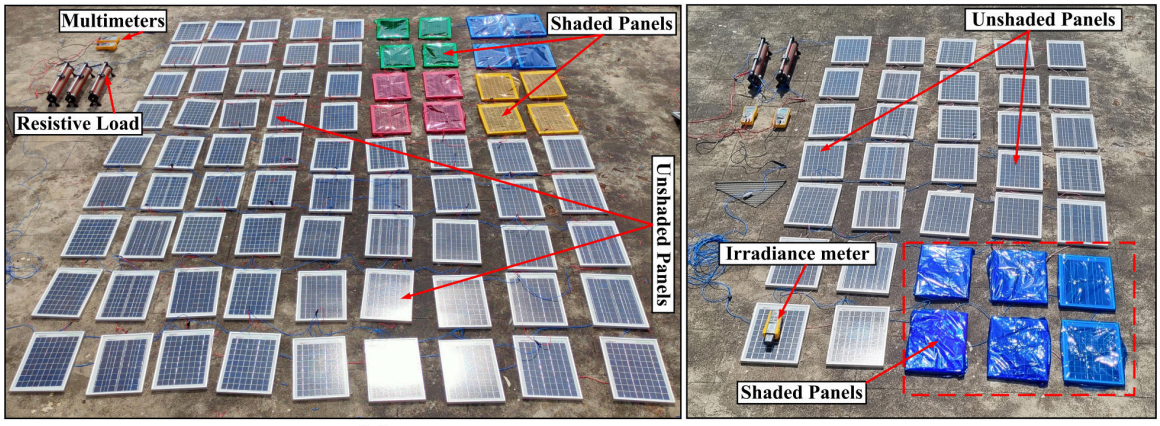

Figure 4.7: Experimental setup (a) 9×9 square array (b) 7×5 non-square array

- The PV panels are connected in 9×9 array configuration is connected across a resistive load.
- One multimeter is connected in parallel to the load to measure the array output voltage (V) and one multimeter is connected in series to the load to measure the array output current (I). The accuracy of multimeters used is ±0.5% for DC voltage and ±1.5% for DC current.
- The amount of irradiation falling on the PV module is measured using an irradiance meter. It has a high-precision mono-crystalline solar sensor that can measure the instantaneous solar irradiation. It is observed that irradiance falling on the PV module is 950 W/m^2.
- To get reduced irradiance level, the PV module is covered with a transparent sheet of thickness 200 μm. The amount of irradiation falling on the PV panel is measured by irradiance meter. The reading shown by the irradiance meter is 790 W/m^2. It is observed that the irradiance level has fallen from 950 W/m^2 to 790 W/m^2 when a single transparent sheet is used.
- In a similar manner the PV module is covered with two, three, and four layers of transparent sheets, and the values of irradiance levels are measured as 610 W/m^2, 430 W/m^2, and 210 W/m^2 respectively. When the transparent sheets are placed one on the other as layers, the irradiation level falling on the PV modules decreases. Therefore, it is observed that the desired irradiation levels

to carry out the experimental work can be achieved by using transparent sheets. The experiment is conducted at 950 W/m^2 and 35^0C.

- Now the resistive load is varied from 0 Ω to 200 Ω. A total of 36 data points for array voltage and array current are measured at every instant of load variation.
- The array output power (P) is measured by multiplying the values array voltage (V), and array current (I) at every instant of load variation. The accuracy in measuring of PV array output power is ±2%.
- The values of array voltage (V), array current (I), and array power (P) are tabulated.
- Considering voltage on the x-axis (V) and power (P) on the y-axis, the P-V characteristic graph is plotted by using an appropriate quadratic polynomial curve fitting technique.

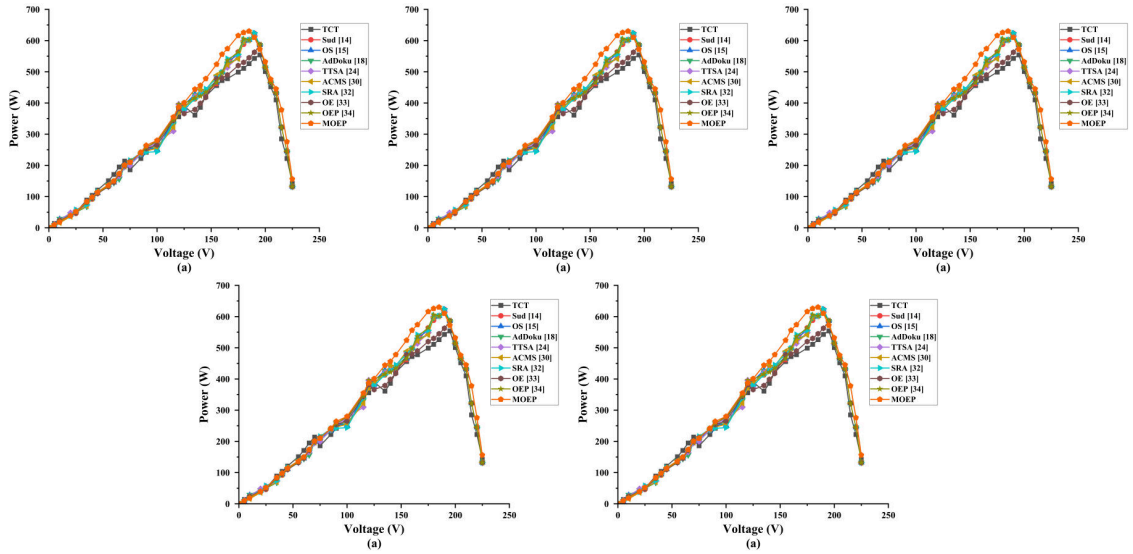

Figure 4.8: Hardware results of 9×9 PV array (0.81kW system) P-V characteristics

The power-voltage (P-V) curves obtained in the hardware are plotted as shown in Fig. 4.8. The experimental readings of GMPP for proposed CBS method and RCT configuration is listed in Table. 4.7. From the table it is inferred that CBS method is able to generate more GMPP compared to RCT arrangement by 18.14%, 11.83%, 18.78%, 12.06% and 13% under the five shading patterns. It is clear that CBS method

Table 4.7: Power Enhancement of CBS method over RCT arrangement

Shading	RCT (W)	CBS (W)	% Power Enhancement of CBS over RCT
SP-I	525.32	620.59	18.14
SP-II	561.49	627.94	11.83
SP-III	516.54	613.56	18.78
SP-IV	556.96	624.12	12.06
SP-V	556.26	628.56	13.00

Table 4.8: Experimental results (GMPP) of various reconfiguration techniques for RCT configuration

Shade	Sud	OS	Futoshiki	PRMFEC	PRFCPMFEC	ChaosMap	TTSA	ASud	CBS	RCT-CBS
SP-I	562.24	564.46	522.86	564.44	563.64	556.12	554.24	552.24	556.48	571.32
SP-II	564.12	562.86	514.56	562.58	562.38	552.86	550.26	542.34	540.26	556.74
SP-III	551.26	552.94	551.46	572.68	573.88	543.64	565.48	556.86	562.84	582.56
SP-IV	572.58	571.64	520.18	572.32	571.44	577.56	572.26	568.24	570.42	575.62
SP-V	561.78	561.96	553.96	568.46	567.36	559.42	538.34	540.24	542.36	579.18

improves the GMPP by minimum 11.83% and maximum of 18.78% compared to RCT arrangement which is a significant improvement. Further the efficacy of the proposed CBS method is proved by performing comparative analysis between CBS method and different static reconfiguration techniques such as RCT, SuDoKu, Optimal SuDoKu, Futoshiki, PRMFEC, PRFCPMFEC, Chaos Map, Twisted two step, Tom Tom and Advanced Sudoku methods. The GMPP generated by all the afore mentioned reconfiguration techniques are shown in Table.4.8. It is observed that the proposed CBS method generates GMPP greater than afore mentioned techniques under the shading patterns considered.

4.4 Comparative Analysis

To further verify the effectiveness of the proposed CBS method, the performance parameters like Fill factor, mismatch loss and efficiency for the proposed CBS method and various existing techniques in the literature under the above said five shading patterns are graphically plotted in Fig. 4.9. These parameters are plotted from the GMPP obtained in the hardware environment. The proposed CBS method is able to achieve highest fill factor, efficiency and lower mismatch loss compared to TCT, SuDoKu, Optimal SuDoKu, Futoshiki, PRMFEC, PRFCPMFEC, Chaos Map,

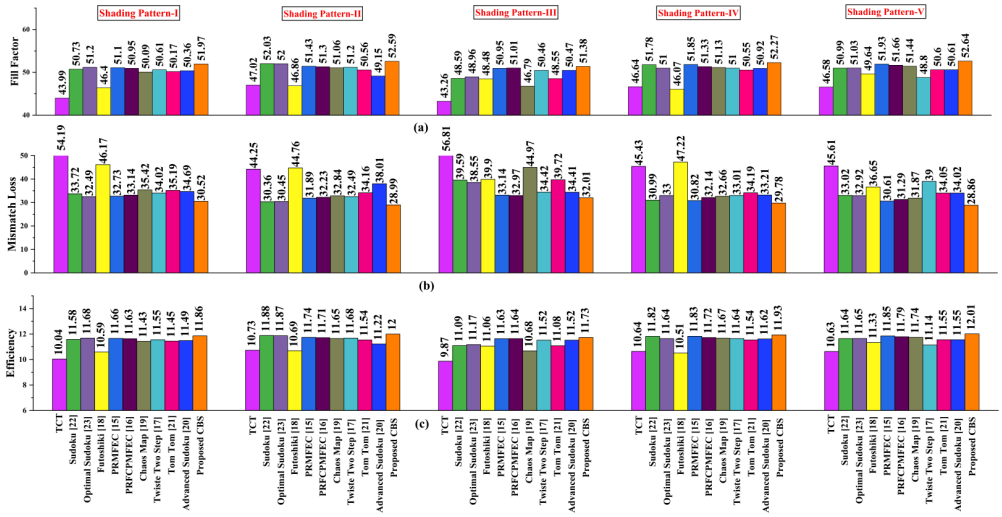

Figure 4.9: Performance Parameters (a) Fill Factor (b) Mismatch Loss (c) Efficiency

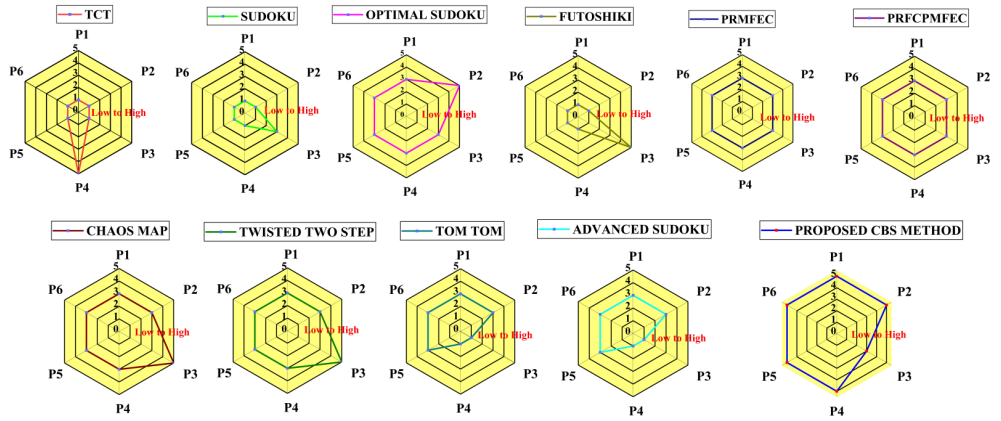

Figure 4.10: Radar chart describing performance comparison of proposed CBS method and other existing techniques. (P1) Ability to generate maximum power (P2) Shade dispersion capability (P3) Wiring complexity (P4) Applicability for any array size (P5) Revenue generation (P6) Efficiency

Twisted two step, Tom Tom and Advanced Sudoku methods.

From the simulation and experimental results, it is observed that the proposed CBS method is capable of generating GMPP more than the existing techniques by at least 1% under the shading patterns considered. This shows tat CBS method has greater shade dispersion capability and efficiency. The proposed CBS is applicable for both square and non-square PV arrays. A qualitative analysis is carried out between the existing techniques and proposed CBS method considering the following param-

eters, P1 - Ability to generate maximum power, P2 - Shade dispersion capability, P3 - Wiring complexity, P4 - Applicability for any array size, P5 - Revenue generation, P6 - Efficiency which is shown in Table.4.9 The parameters are analyzed on a scale of 1 to 5, where Low(L) - 1, Medium(M) - 3 and High(H) - 5. For clear understanding of the metrics in Table. VI, a radar chart describing the performance comparison of the proposed CBS method and other existing techniques is depicted in Fig. 4.10. From the diagram analysis, it is observed that CBS method outperforms the existing techniques under the shading patterns considered for analysis.

Table 4.9: Qualitative Comparison of CBS method over existing techniques (L - Low (1), M - Medium (3), H - High (5))

Techniques	**P1**	**P2**	**P3**	**P4**	**P5**	**P6**
TCT	L	L	L	H	L	L
Sudoku	L	L	M	L	L	L
Optimal Sudoku	M	H	M	M	M	M
Futoshiki	L	L	H	L	L	L
PRMFEC	M	M	M	M	M	M
PRFCPMFEC	M	M	M	M	M	M
Chaos Map	M	M	H	M	M	M
Twisted Two Step	M	H	H	M	M	M
Tom-Tom	M	M	L	L	M	M
Advanced Sudoku	H	M	L	L	M	M
Proposed CBS	H	H	M	H	H	H

4.5 CBS method applied to TCT configuration

The GMPP generated by 9×9 TCT connected PV array under simulation and hardware environments by implementing the proposed CBS method are listed in Table.4.10 and Table.4.11. Further, PV array reconfiguration techniques SuDoKu, Optimal SuDoKu, Futoshiki, PRMFEC, PRFCPMFEC, Chaos Map and proposed CBS method is implemented on TCT connected 9×9 PV array. The GMPP generated by above mentioned reconfiguration techniques under five different shading pattern for 9×9 PV array in both software (20.25kW system) and hardware (0.81kW system) are listed in Tables.4.12 and 4.13. It is observed that CBS method improves the GMPP of PV array compared to other reconfiguration techniques.

Table 4.10: Power Enhancement of CBS method over TCT arrangement

Shading	TCT (W)	CBS (W)	% Power Enhancement
SP-I	14740	17470	18.52
SP-II	16040	17600	9.73
SP-III	14070	17230	22.46
SP-IV	15420	17720	14.92
SP-V	15380	17760	15.47

Table 4.11: Power Enhancement of CBS method over TCT arrangement

Shading	TCT (W)	CBS (W)	% Power Enhancement
SP-I	525.32	620.59	18.14
SP-II	561.49	627.94	11.83
SP-III	516.54	613.56	18.78
SP-IV	556.96	624.12	12.06
SP-V	556.26	628.56	13.02

Table 4.12: Simulation results (GMPP) of various reconfiguration techniques

Shade	Sud	OS	Futoshiki	PRMFEC	PRFCPMFEC	ChaosMap	TTSA	ASud	CBS	RCT-CBS
SP-I	17090	17180	15320	17180	17120	16860	17060	16960	17220	17470
SP-II	17520	17430	15560	17240	17200	17110	17070	17010	16960	17600
SP-III	16490	16520	16250	17120	17160	15500	17040	16590	17180	17230
SP-IV	17420	17110	15260	17430	17240	17230	17050	17130	17480	17720
SP-V	17100	17140	16740	17530	17320	17310	16540	17110	17330	17760

Table 4.13: Experimental results (GMPP) of various reconfiguration techniques

Shade	Sud	OS	Futoshiki	PRMFEC	PRFCPMFEC	ChaosMap	TTSA	ASud	CBS	RCT-CBS
SP-I	605.72	611.35	554.12	610.24	608.36	598.12	604.36	599.12	601.35	620.59
SP-II	621.35	620.88	559.54	614.12	612.56	609.74	611.36	603.74	586.88	627.94
SP-III	580.24	584.62	578.96	608.36	609.12	558.72	602.56	579.72	602.62	613.56
SP-IV	618.36	609.02	550.18	619.16	612.96	610.58	608.96	603.58	608.02	624.12
SP-V	608.92	609.36	592.72	620.12	616.92	614.24	582.72	604.24	604.36	628.56

4.6 Summary

To mitigate the effects caused by partial shading, a static reconfiguration technique Cyclic Back Shift (CBS) is proposed in this chapter. In CBS method, the module rearrangement is based on back shifting of row positions in a particular column. During installation, it is a one-time rearrangement made without changing the electrical connections between the PV modules. So, dispersion of shade occurs over the entire array which results in increased GMPP under PSCs. It is very simple, economical and applicable for square and non-square arrays. This technique is implemented in

software (9×9 square array of 20.25kW system) and hardware (9×9 square array of 0.81kW system) environments. In case of 9×9 array, CBS method is able to achieve power increment of 18.52%, 9.73%, 22.46%, 14.92%, 15.47% in software environment and 18.14%, 11.83%, 18.78%, 12.06%, 13% in hardware platform under five shading patterns considered. In comparison to the other existing reconfiguration schemes Sudoku, Optimal Sudoku, Futoshiki, PRMFEC, PRFCPMFEC, Chaos Map, Twisted Two step, Tom Tom and Advanced Sudoku, the proposed CBS method of arrangement clearly generates at least 1% more power output under the shading patterns considered in both simulation and hardware. In addition to GMPP, the proposed CBS method increases fill factor and efficiency, reduces mismatch loss of PV systems under PSCs. Also, the proposed CBS method applied to RCT configured PV array is able to increase the GMPP compared to other techniques. Therefore, it can be said that CBS method of module rearrangement can be an effective solution in reducing the effects caused by PSCs.

Chapter 5

Modified Odd Even Prime Pattern for Effective Dispersion of Shade over the PV Array under Partial Shading Conditions

This chapter presents an effective shade dispersion technique titled Modified Odd Even Prime (MOEP) pattern to address the issue of Partial Shading in solar photovoltaic systems. The proposed MOEP technique is applied on 9×9 and 8×8 PV arrays, tested in both software and hardware environments under various shading patterns. A comparative analysis is carried between proposed MOEP technique, Total Cross Tied (TCT), Odd Even (OE) and Odd Even Prime (OEP) techniques. A detailed study on energy savings from the proposed MOEP method is made on hourly, daily and yearly basis. From the experimental results obtained, it is observed that MOEP method generates a significant improvement in GMPP, efficiency and reduces the mismatch loss compared to TCT, OE and OEP methods.

5.1 Introduction

The world's population and economic growth are driving an explosive rise in energy demand. To meet the demand for energy, it is necessary to increase the amount of electricity generated from the available resources. The primary means of generating

electricity are fossil fuels. However, there is a need for alternative energy sources to generate power due to the depletion of fossil resources. The best alternative energy sources accessible for free in nature are renewable energy sources . In renewable sources of energy, solar photovoltaic (PV) power generation offers greater benefits than other sources. Solar photovoltaic energy is clean, Eco-friendly and requires less maintenance. The factors affecting the PV array's output are temperature and incident irradiance. However, due to partial shading, the incident irradiance on the PV array is not uniform. Moving clouds, the shadows of trees and tall buildings contribute to partial shading on the PV array. Under partial shading, the power voltage (P-V) characteristic curve has numerous peaks, making it challenging for the maximum power point tracking (MPPT) algorithm to track the global maximum power point (GMPP). The amount of power loss due to partial shading depends on the type of shading pattern, module configuration and position of the shaded modules within the PV array. Among these, PV module configuration significantly affects the maximum power production. Therefore, it is more crucial to choose the proper PV array configuration. The literature presents a variety of PV array topologies which includes series (S), series-parallel (SP), honeycomb (HC), bridge link (BL), and total cross linked (TCT). The effectiveness of the S, SP, HC, BL, and TCT array designs is examined in under various partial shading scenarios. TCT configuration has demonstrated superior performance compared to other configurations. However, TCT configuration is not able to generate more power when the modules in a row are shaded. To address this issue, the researchers suggested different reconfiguration strategies to lessen the impact of partial shading by dividing the shade into distinct rows under PSCs. These methods are divided into static and dynamic reconfiguration strategies. The contributions made in this chapter are listed as follows

- A new Modified Odd Even Prime (MOEP) pattern of module arrangement for total cross tied (TCT) connection is presented in this chapter to mitigate the effects of partial shading.

- The proposed MOEP method is implemented on 9×9 and 8×8 PV arrays and validated in software (9×9 array - 20.25kW system and 8×8 array - 16kW system) and hardware (9×9 array - 0.81kW system and 8×8 array - 0.64kW system) environments under various shading patterns.

- The performance of proposed MOEP method along with TCT, OE and OEP

are evaluated in terms of GMPP, mismatch power loss (MPL), Fill Factor (FF), and Efficiency (η).

- A detailed study on energy savings from the proposed MOEP method is made on hourly, daily and yearly basis and compared with TCT,OE and OEP patterns.

Firstly in this chapter description of the proposed MOEP CBS method is presented. Then simulation and experimental results of 9×9 and 8×8 PV arrays under different shading conditions are presented. Further, a detailed study on energy savings from the proposed MOEP method is made on hourly, daily and yearly basis and compared with TCT,OE and OEP patterns.

5.2 System Description

5.2.1 Total Cross Tied (TCT) PV array

Total Cross-tied (TCT) PV array [29] configuration is a modified version of a series parallel configuration. It is obtained by connecting cross ties across each row of the junctions for a series-parallel connection. The arrangement of PV modules in a m×9n TCT-connected PV array is shown in Fig. 5.1.

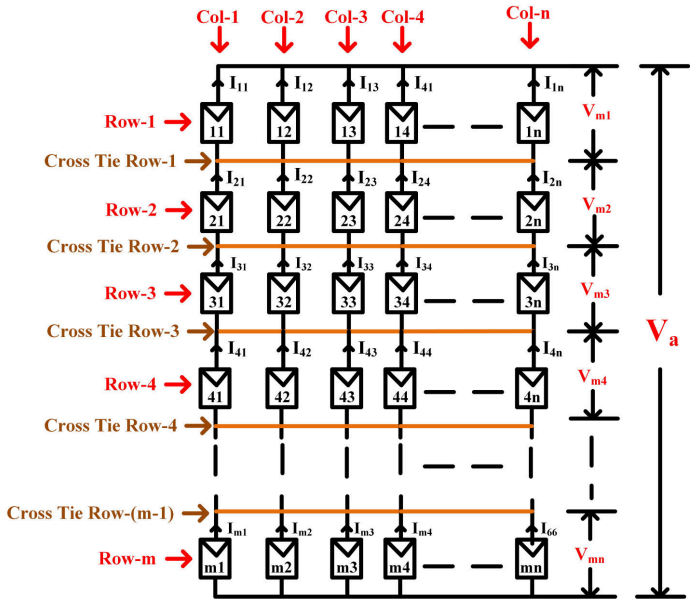

Figure 5.1: m×n TCT connected PV Array

5.2.2 Odd Even (OE) pattern

In this arrangement, the row and column positions are divided into two categories odd and even numbers. The row and column positions are numbered as odd-odd, even-even, odd-even, and even-odd combinations of row and column positions. The odd-even arrangement [29] for a 9×9 PV array is shown in Fig. 5.2(a).

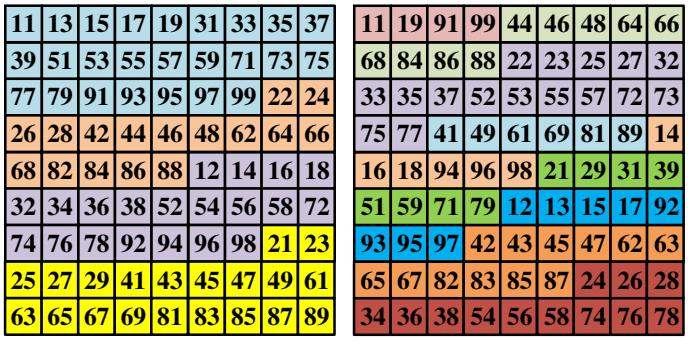

Figure 5.2: (a) Odd Even arrangement of 9×9 PV array (b) Odd Even Prime arrangement of 9×9 PV array

5.2.3 Odd Even Prime (OEP) pattern

For odd even prime arrangement [29], row and column positions are divided into nine groups odd-odd, even-even, prime-prime, even-odd, odd-even, prime-odd, odd-prime, even-prime, and prime-even. The row and column positions of 9×9 PV array under the Odd-Even-Prime (OEP) pattern is shown in Fig. 5.2(b). From the OE and OEP patterns, the observations are summarized as follows:

- The modules in a particular column are displaced to other columns, which results in increased wiring loss, wire length, and cost of the wire.
- The electrical connection of PV modules in the PV array is difficult.
- The row positions in a particular row and column are not unique. Hence, the shade in a particular column is not dispersed effectively over the array.
- There exists more number of 2×2, 2×3, 3×2 and 3×3 sub arrays with repeated row psitions. The shade on these sub-arrays reduces the row current and GMPP from the array.

5.2.4 Modified Odd Even Prime (MOEP) method

To illustrate the proposed MOEP method a m×n PV array is considered, where 'm' denotes number of rows and 'n' denotes number of columns. Each module of the PV array is represented as 'xy' as shown in Fig. 5.3(a) where 'x' denotes row position of the module (x = 1,2,3,4.....m) and 'y' denotes column position of the module (y = 1,2,3,4.....n). The row positions of the m×n PV array is shown in Fig. 5.3(b).

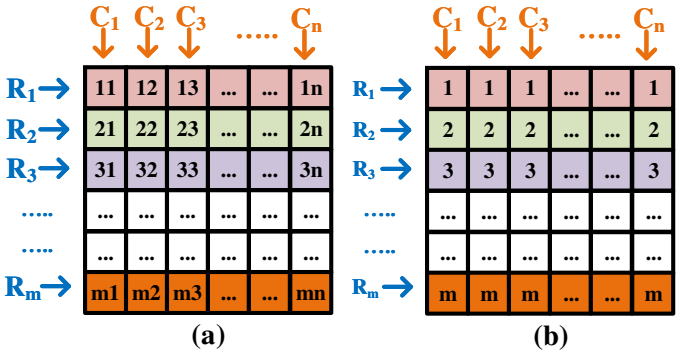

Figure 5.3: (a) Row and Column positions of m×n PV array (b) Row positions of m×n PV array

The module rearrangement by MOEP method is based on row positions of the m×n PV array. Firstly, the row positions are made into three groups such that in every group the row positions are arranged in increased order.
Group-I: Odd (1,9,.....)
Group-II: Even (4,6,8,.....)
Group-III: Prime (2,3,5,7,.....)
The proposed MOEP method of rearrangement is as follows:
Case 1: For m = Odd

- Step-1: The row positions of modules in col-1 are rearranged in the order of Group-I (Odd), Group-II (Even) and Group-III (Prime) in increasing order.
- Step-2: Consider k = $\lfloor \frac{m}{2} \rfloor$, where $\lfloor . \rfloor$ indicates greatest integer function.
- Step-3: The row positions of modules in col-2 are obtained by circular shifting of row positions of previous column (col-1) by 'k' steps.
- Step-4: Repeat the step-3 to obtain the row positions of next columns.

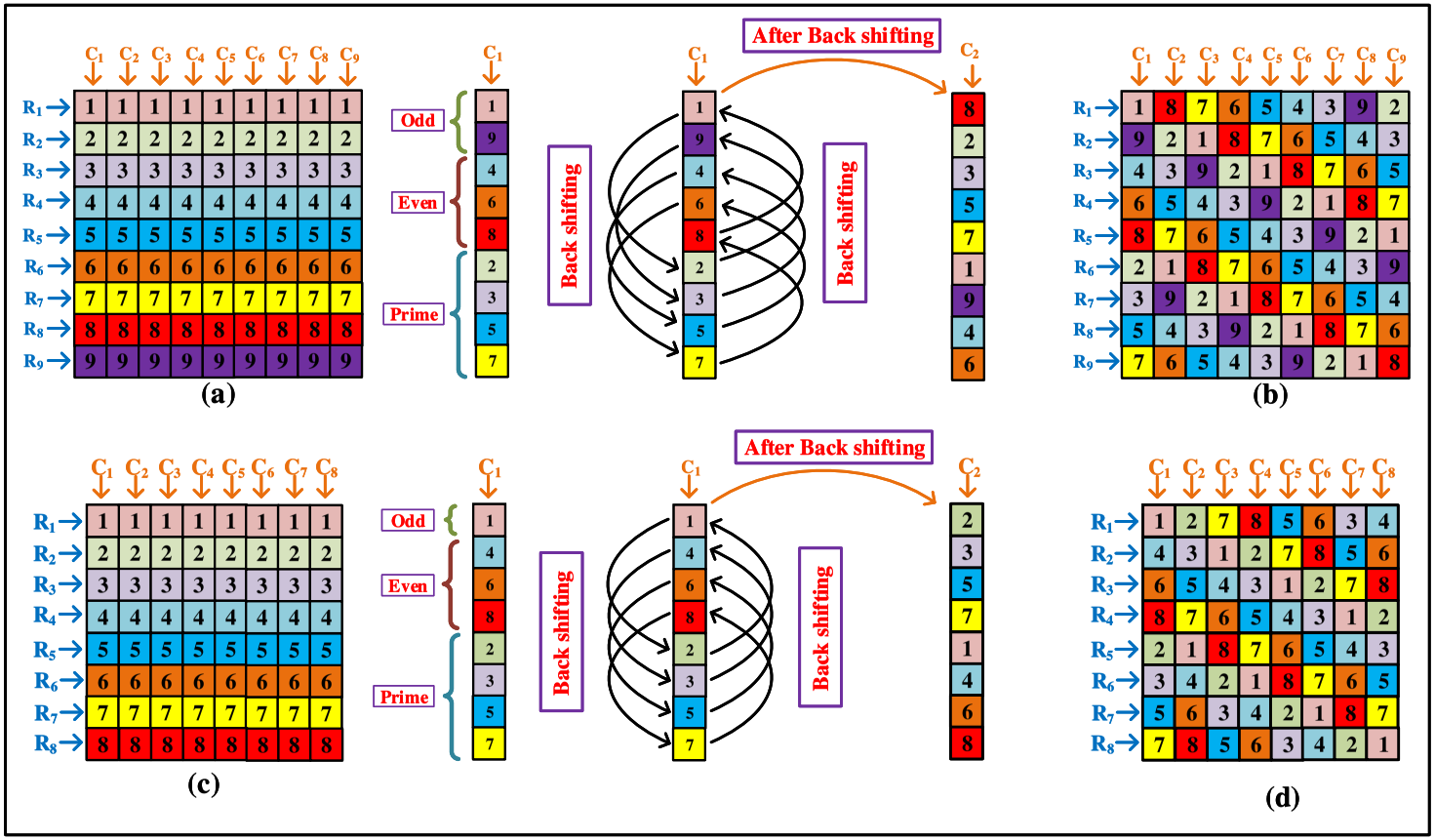

Figure 5.4: (a) 9×9 PV array with row positions (b) 9×9 PV array with row positions after rearrangement by MOEP method (c) 8×8 PV array with row positions (d) 8×8 PV array with row positions after rearrangement by MOEP method

To illustrate the above case, a 9×9 PV array is considered as shown in Fig. 5.4(a), where m = 9 and n = 9. The value of k = $\lfloor \frac{9}{2} \rfloor$ is 4. The row positions of 9×9 PV array in Fig. 5.4(a) are rearranged by applying MOEP method. The modified 9×9 PV array is shown in Fig. 5.4(b).
Case 2: For m = Even

- Step-1: The row positions of modules in col-1 are rearranged in the order of Group-I (Odd), Group-II (Even) and Group-III (Prime) in increasing order.
- Step-2: Consider k = $\lfloor \frac{m}{2} \rfloor$, where $\lfloor . \rfloor$ indicates greatest integer function.
- Step-3: The row positions of modules in col-2 are obtained by circular shifting of row positions of previous column (col-1) by 'k' steps.
- Step-4: If any repetition of row position occurs across a particular row, the row positions of particular column are obtained by circular shifting of row positions of previous column by (k - 1) steps.
- Step-5: Repeat the step-3 to obtain the row positions of next columns.

To illustrate the above case, a 8×8 PV array is considered as shown in Fig. 5.4(c), where m = 8 and n = 8. The value of k = $\lfloor \frac{8}{2} \rfloor$ is 4. The row positions of 8×8 PV array in Fig. 5.4(c) are rearranged by applying MOEP method. The modified 8×8 PV array is shown in Fig. 5.4(d). The flowchart of proposed MOEP method is shown in Fig. 5.5

5.2.5 Performance Parameters

Mismatch Power loss: It is the deviation of maximum power point (MPP_{nor}) under normal condition to global maximum power point ($GMPP_{PSC}$) under PSCs. It is given by equation 5.1.

$$MPL(\%) = \frac{MPP_{nor} - GMPP_{PSC}}{GMPP_{PSC}} \times 100 \tag{5.1}$$

Fill Factor: It is the ratio of global maximum power output (GMPP) of the PV array under PSCs to the product of voltage (V_{OC}) and current (I_{SC}). It is given ny equation 5.2.

$$FF(\%) = \frac{GMPP_{PSC}}{V_{OC} \times I_{SC}} \times 100 \tag{5.2}$$

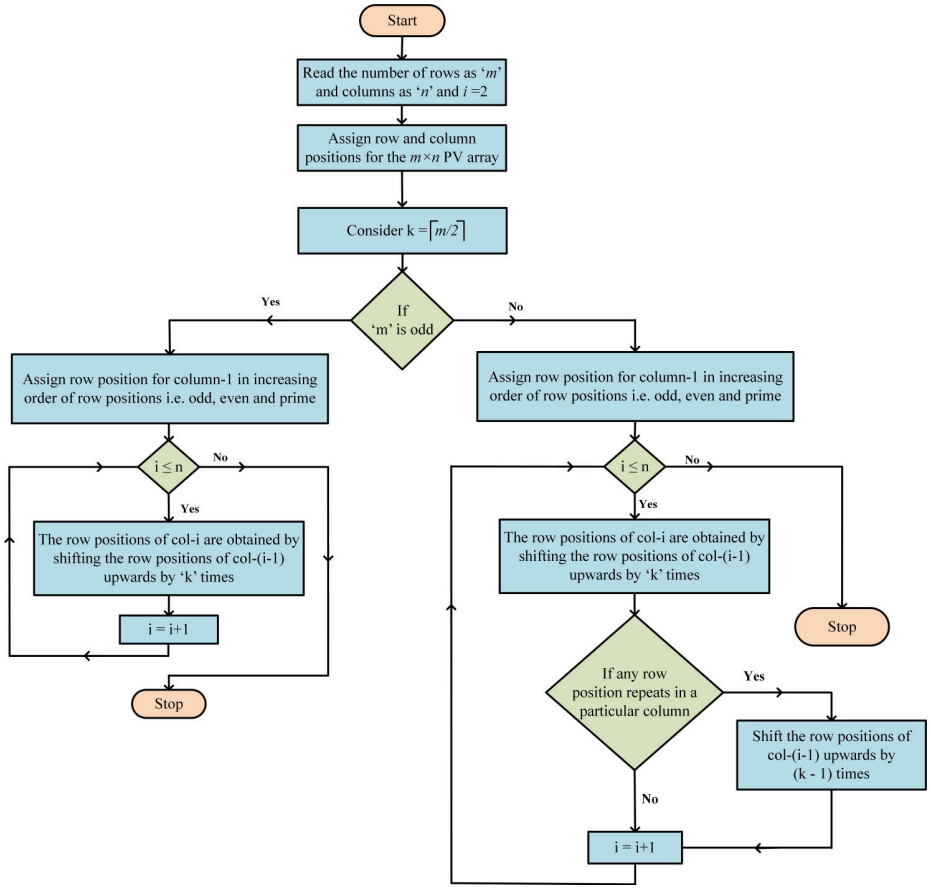

Figure 5.5: Flowchart of the proposed MOEP method

Efficiency: It is fraction of power output at GMPP to the solar input power (P_{in}). It is given by equation 5.3.

$$\%\eta = \frac{Power\ at\ GMPP}{Solar\ input(P_{in})} \times 100 \tag{5.3}$$

Shade Dispersion Ratio (SDR): It is the factor which describes the efficiency of shade dispersion. The lower value of SDR indicates the more efficient shade dispersion. It is the difference in maximum sum of irradiance (SIR) in a row to minimum sum of irradiance (SIR) in a row expressed as percentage of maximum sum of irradiance (SIR) in a row. It is given by equation 5.4.

$$SDR = \frac{(max\ SIR) - (min\ SIR)}{(max\ SIR)} \tag{5.4}$$

5.3 Simulation Results

To verify the effectiveness of the proposed MOEP method, two arrays of size 9×9 and 8×8 are tested under various shading conditions. The theoretical computations of GMPP for TCT, OE, OEP and MOEP methods and performance parameters under various shading conditions are presented in the subsequent sections.

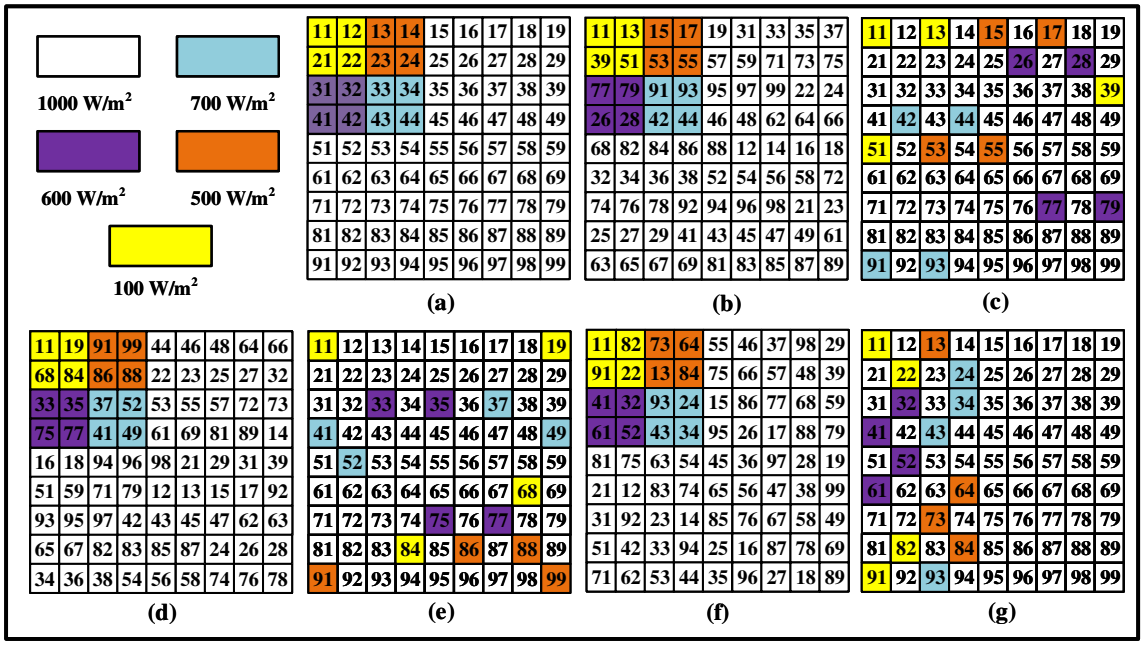

Figure 5.6: Shading Pattern-I (a) TCT arrangement (b) OE arrangement (c) Shade dispersion by OE method (d) OEP arrangement (e) Shade dispersion by OEP method (f) MOEP arrangement (g) Shade dispersion by MOEP method.

5.3.1 9×9 PV Array

Shading Pattern-I: In this shading pattern, the top left corner 4×4 sub array is subjected to different insolation levels as shown in Fig. 5.6(a). The module rearrangement and shade dispersion under OE, OEP and MOEP arrangements is shown in Fig. 5.6(b) to (g). The Power-Voltage(P-V) characteristics and performance parameters under shading pattern-I is shown in Fig. 5.7(a) and (b). The theoretical values of GMPP under TCT, OE, OEP and MOEP arrangements is shown in Table. 5.1.

GMPP for TCT configuration: To find the location of GMPP, it is necessary to

calculate the current generated by each row and voltage of the PV array. The current generated by modules in each row of the PV array in TCT configuration is given by equation 5.5. The current generated by each row, array voltage and power are listed in Table. 5.1. It is observed that GMPP occurs at I_a= $6.2I_m$. Therefore V_a= $9V_m$ and GMPP = $55.8V_mI_m$.

$$\left.\begin{aligned} I_{r1} &= 5I_m + (0.2I_m) + (1.0I_m) = 6.2I_m \\ I_{r2} &= 5I_m + (0.2I_m) + (1.0I_m) = 6.2I_m \\ I_{r3} &= 5I_m + (2 \times 0.6I_m) + (2 \times 0.7I_m) = 7.6I_m \\ I_{r4} &= 5I_m + (2 \times 0.6I_m) + (2 \times 0.7I_m) = 7.6I_m \\ I_{r5} &= 9.0I_m \\ I_{r6} &= 9.0I_m \\ I_{r7} &= 9.0I_m \\ I_{r8} &= 9.0I_m \\ I_{r9} &= 9.0I_m \end{aligned}\right\} \tag{5.5}$$

GMPP for OE configuration: The current generated by modules in each row of PV array for OE configuration under shading pattern-I is given by equation 5.6. From the Table. 5.1, it is observed that GMPP occurs at I_a= $7.1I_m$. Therefore V_a= $8V_m$ and GMPP = $56.8V_mI_m$.

$$\left.\begin{aligned} I_{r1} &= 5I_m + (2 \times 0.1I_m) + (2 \times 0.5I_m) = 6.2I_m \\ I_{r2} &= 7I_m + (2 \times 0.6I_m) = 8.2I_m \\ I_{r3} &= 8I_m + (0.1I_m) = 8.1I_m \\ I_{r4} &= 7I_m + (2 \times 0.7I_m) = 8.4I_m \\ I_{r5} &= 6I_m + (0.1I_m) + (2 \times 0.5I_m) = 7.1I_m \\ I_{r6} &= I_{r8} = 9.0I_m \\ I_{r7} &= 7I_m + (2 \times 0.6I_m) = 8.2I_m \\ I_{r8} &= 9.0I_m \\ I_{r9} &= 7I_m + (2 \times 0.7I_m) = 8.4I_m \end{aligned}\right\} \tag{5.6}$$

GMPP for OEP configuration: The current generated by modules in each row

of PV array for OEP configuration under shading pattern-I is given by equation 5.7. From the Table. 5.1, it is observed that GMPP occurs at I_a= $7.1I_m$. Therefore V_a= $9V_m$ and GMPP = $63.9V_mI_m$.

$$\left.\begin{aligned} I_{r1} &= 7I_m + (2 \times 0.1I_m) = 7.2I_m \\ I_{r2} &= 9I_m \\ I_{r3} &= 6I_m + (2 \times 0.6I_m) + (0.7I_m) = 7.9I_m \\ I_{r4} &= 7I_m + (2 \times 0.7I_m) = 8.4I_m \\ I_{r5} &= 8I_m + (0.7I_m) = 8.7I_m \\ I_{r6} &= 8I_m + (0.1I_m) = 8.1I_m \\ I_{r7} &= 7I_m + (2 \times 0.6I_m) = 8.2I_m \\ I_{r8} &= 6I_m + (0.1I_m) + (2 \times 0.5I_m) = 7.1I_m \\ I_{r9} &= 7I_m + (2 \times 0.5I_m) = 8I_m \end{aligned}\right\} \tag{5.7}$$

GMPP for MOEP configuration: The current generated by modules in each row of PV array for MOEP configuration under shading pattern-I is given by equation 5.8. From Table. 5.1, it is observed that GMPP occurs at I_a= $7.6I_m$. Therefore V_a= $9V_m$ and GMPP = $68.4V_mI_m$.

$$\left.\begin{aligned} I_{r1} = I_{r8} &= 7I_m + (0.1I_m) + (0.5I_m) = 7.6I_m \\ I_{r2} = I_{r9} &= 7I_m + (0.1I_m) + (0.7I_m) = 7.8I_m \\ I_{r3} = I_{r4} &= 7I_m + (0.6I_m) + (0.7I_m) = 8.3I_m \\ I_{r5} &= 8I_m + (0.6I_m) = 8.6I_m \\ I_{r6} &= 7I_m + (0.6I_m) + (0.5I_m) = 8.1I_m \\ I_{r7} &= 8I_m + (0.5I_m) = 8.5I_m \end{aligned}\right\} \tag{5.8}$$

The simulation results shows that GMPP generated by TCT, OE, OEP and MOEP arrangements are 15440W, 15630W, 17240W and 17850W respectively. It is observed that MOEP method of arrangement is able to enhance the GMPP by 2410W, 2220W and 610W compared to TCT, OE and OEP arrangements. And also, it has highest efficiency, fill factor of 13.23%, 67.82% and lowest mismatch loss of 13.45% compared to TCT, OE and OEP arrangements. The SDR for TCT, OE, OEP and MOEP arrangements is 0.311, 0.311, 0.211 and 0.116, which indicates that MOEP arrangement is able to disperse shade more effectively.

Table 5.1: GMPP for TCT, OE, OEP and MOEP schemes for Shading Pattern-I

TCT arrangement			**OE arrangement**		
I_a	V_a	P_a	I_a	V_a	P_a
R_1 - $6.2I_m$	$9V_m$	$\mathbf{55.8}V_mI_m$	R_5 - $7.1I_m$	$8V_m$	$\mathbf{56.8}V_mI_m$
R_2 - $6.2I_m$	-	-	R_1 - $6.2I_m$	$9V_m$	$55.8V_mI_m$
R_3 - $7.6I_m$	$7V_m$	$53.2V_mI_m$	R_3 - $8.1I_m$	$7V_m$	$56.7V_mI_m$
R_4 - $7.6I_m$	-	-	R_2 - $8.2I_m$	$6V_m$	$49.2V_mI_m$
R_5 - $9.0I_m$	$5V_m$	$45.0V_mI_m$	R_7 - $8.2I_m$	-	-
R_6 - $9.0I_m$	-	-	R_4 - $8.4I_m$	$4V_m$	$33.6V_mI_m$
R_7 - $9.0I_m$	-	-	R_9 - $8.4I_m$	-	-
R_8 - $9.0I_m$	-	-	R_6 - $9.0I_m$	$2V_m$	$18V_mI_m$
R_9 - $9.0I_m$	-	-	R_8 - $9.0I_m$	-	-
OEP arrangement			**MOEP arrangement**		
I_a	V_a	P_a	I_a	V_a	P_a
R_8 - $7.1I_m$	$9V_m$	$\mathbf{63.9}V_mI_m$	R_1 - $7.6I_m$	$9V_m$	$\mathbf{68.4}V_mI_m$
R_1 - $7.2I_m$	$8V_m$	$57.6V_mI_m$	R_8 - $7.6I_m$	-	-
R_3 - $7.9I_m$	$7V_m$	$53.2V_mI_m$	R_3 - $7.8I_m$	$7V_m$	$56.7V_mI_m$
R_9 - $8.0I_m$	$6V_m$	$48.0V_mI_m$	R_9 - $7.8I_m$	-	-
R_6 - $8.1I_m$	$5V_m$	$40.5V_mI_m$	R_6 - $8.1I_m$	$5V_m$	$40.5V_mI_m$
R_7 - $8.2I_m$	$4V_m$	$32.8V_mI_m$	R_3 - $8.3I_m$	$4V_m$	$33.2V_mI_m$
R_4 - $8.4I_m$	$3V_m$	$25.2V_mI_m$	R_4 - $8.3I_m$	-	-
R_5 - $8.7I_m$	$2V_m$	$17.4V_mI_m$	R_5 - $8.6I_m$	$2V_m$	$17.2V_mI_m$
R_2 - $9.0I_m$	$1.0V_m$	$9.0V_mI_m$	R_7 - $8.6I_m$	-	-

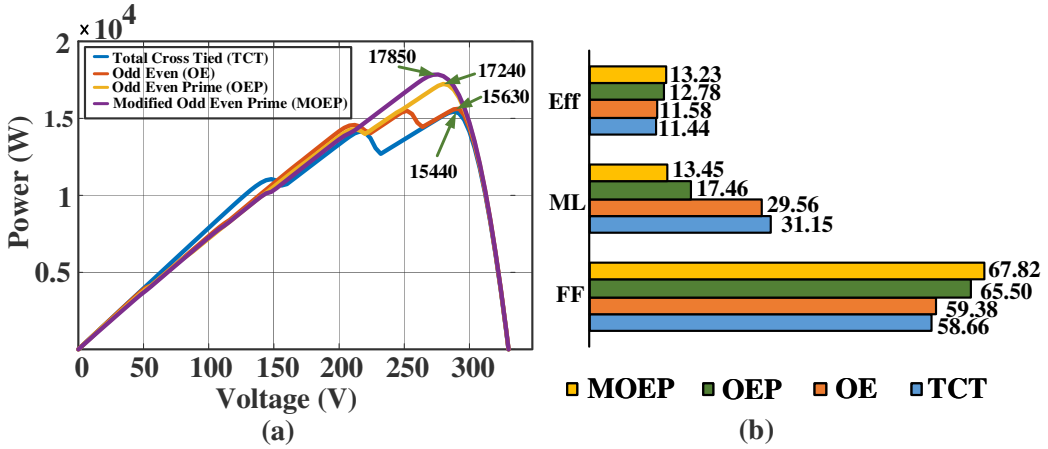

Figure 5.7: Shading pattern-I (a)Power-Voltage (P-V) characteristics (b) Performance parameters

Shading Pattern-II: In this shading pattern, the top right corner 4×4 sub array 9×9 PV array is subjected to different insolation levels as shown in Fig. 5.8(a). The module rearrangement and shade dispersion of the 9×9 array under OE, OEP and MOEP arrangements is shown in Fig. 5.8(b) to (g).The power-voltage (P-V) characteristics and performance parameters of 9×9 PV under shading pattern-II is shown in Fig. 5.9(a) and (b). The theoretical values of GMPP under TCT, OE, OEP and MOEP arrangements is shown in Table. 5.2.

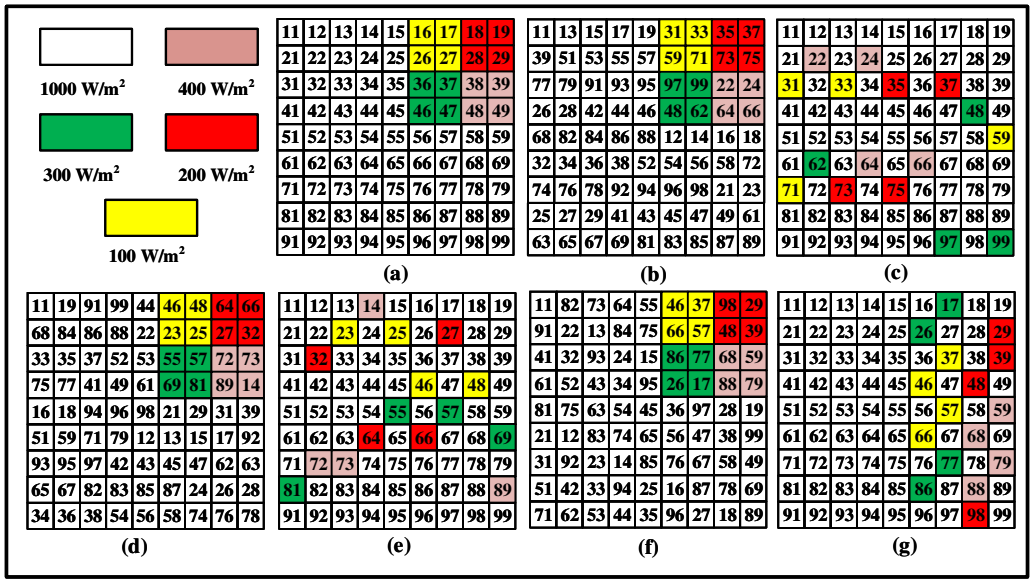

Figure 5.8: Shading Pattern-II (a) TCT PV array arrangement (b) OE arrangement (c) Shade dispersion by OE method (d) OEP arrangement (e) Shade dispersion by OEP method (f) MOEP arrangement (g) Shade dispersion by MOEP method.

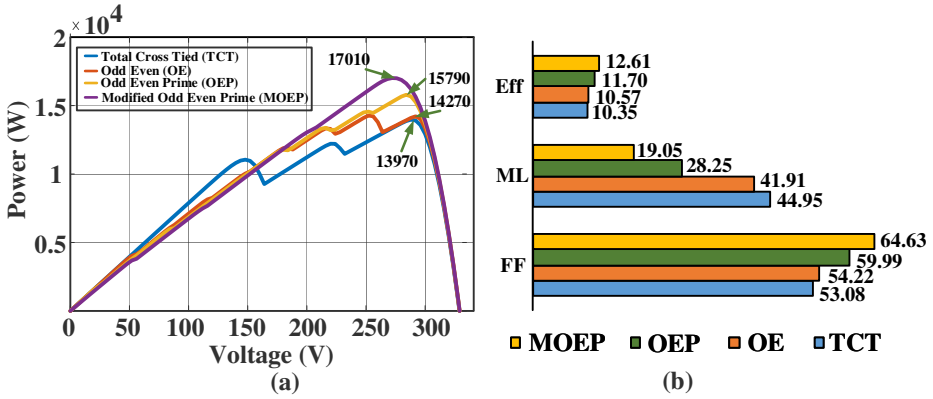

Figure 5.9: Shading pattern-II (a)P-V characteristics (b) Performance parameters

The simulation results shows that GMPP generated by TCT, OE, OEP and MOEP arrangements are 13970W, 14270W, 15790W and 17010W respectively. It is observed that MOEP method of arrangement is able to enhance GMPP by 21.76%, 19.2% and 7.73% compared to TCT, OE and OEP arrangements . And also, it has highest efficiency, fill factor of 12.61%, 64.63% and lowest mismatch loss of 19.05% compared to TCT, OE and OEP arrangements. TCT arrangement has highest SDR of 0.377 and MOEP arrangement has lowest SDR of 0.12. Therefore, efficient shade dispersion is achieved by MOEP arrangement.

Table 5.2: GMPP for TCT, OE, OEP and MOEP schemes for Shading Pattern-II

TCT arrangement			**OE arrangement**		
I_a	V_a	P_a	I_a	V_a	P_a
R_1 - $5.6I_m$	$9V_m$	$\mathbf{50.4}V_mI_m$	R_7 - $6.5I_m$	$8V_m$	$\mathbf{52}V_mI_m$
R_2 - $5.6I_m$	-	-	R_3 - $5.6I_m$	$9V_m$	$50.4V_mI_m$
R_3 - $6.4I_m$	$7V_m$	$44.8V_mI_m$	R_6 - $7.1I_m$	$7V_m$	$49.7V_mI_m$
R_4 - $6.4I_m$	-	-	R_9 - $7.6I_m$	$6V_m$	$45.6V_mI_m$
R_5 - $9.0I_m$	$5V_m$	$45.0V_mI_m$	R_2 - $7.8I_m$	$5V_m$	$39V_mI_m$
R_6 - $9.0I_m$	-	-	R_5 - $8.1I_m$	$4V_m$	$32.4V_mI_m$
R_7 - $9.0I_m$	-	-	R_4 - $8.3I_m$	$3V_m$	$24.9V_mI_m$
R_8 - $9.0I_m$	-	-	R_1 - $9.0I_m$	$2V_m$	$18V_mI_m$
R_9 - $9.0I_{0m}$	-	-	R_8 - $9.0I_m$	-	-
OEP arrangement			**MOEP arrangement**		
I_a	V_a	P_a	I_a	V_a	P_a
R_2 - $6.4I_m$	$9V_m$	$\mathbf{57.6}V_mI_m$	R_3 - $7.3I_m$	$9V_m$	$\mathbf{65.7}V_mI_m$
R_6 - $6.7I_m$	$8V_m$	$53.6V_mI_m$	R_4 - $7.3I_m$	-	-
R_4 - $7.2I_m$	$7V_m$	$50.4V_mI_m$	R_2 - $7.5I_m$	$7V_m$	$52.5V_mI_m$
R_5 - $7.6I_m$	$6V_m$	$45.6V_mI_m$	R_5 - $7.5I_m$	-	-
R_8 - $7.7I_m$	$5V_m$	$38.5V_mI_m$	R_6 - $7.5I_m$	-	-
R_7 - $7.8I_m$	$4V_m$	$31.2V_mI_m$	R_7 - $7.7I_m$	$4V_m$	$30.8V_mI_m$
R_3 - $8.2I_m$	$3V_m$	$24.6V_mI_m$	R_8 - $7.7I_m$	-	-
R_1 - $8.4I_m$	$2V_m$	$16.8V_mI_m$	R_9 - $8.2I_m$	$2V_m$	$16.4V_mI_m$
R_9 - $9.0I_m$	$1V_m$	$9.0V_mI_m$	R_1 - $8.3I_m$	$1V_m$	$8.3V_mI_m$

Shading Pattern-III: In this shading pattern, the bottom right corner 4×4 sub array 9×9 PV array is subjected to different insolation levels as shown in Fig. 5.10(a). The module rearrangement and shade dispersion of the 9×9 array under OE, OEP and MOEP arrangements is shown in Fig. 5.10(b) to (g).The power-voltage (P-V) characteristics and performance parameters of 9×9 PV under shading pattern-II is

shown in Fig. 5.11(a) and (b). The theoretical values of GMPP under TCT, OE, OEP and MOEP arrangements is shown in Table. 5.3.

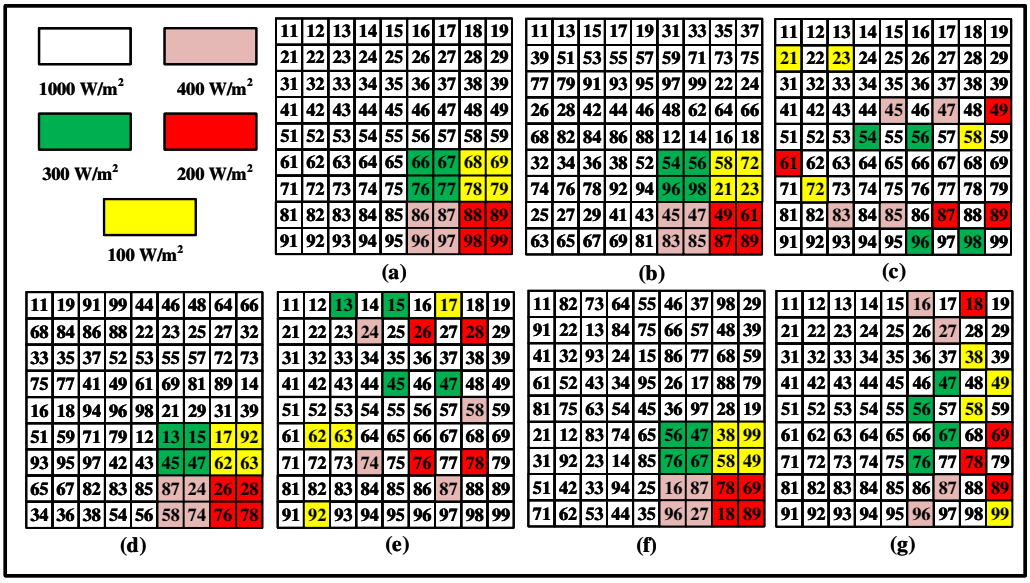

Figure 5.10: Shading Pattern-III (a) TCT PV array arrangement (b) OE arrangement (c) Shade dispersion by OE method (d) OEP arrangement (e) Shade dispersion by OEP method (f) MOEP arrangement (g) Shade dispersion by MOEP method.

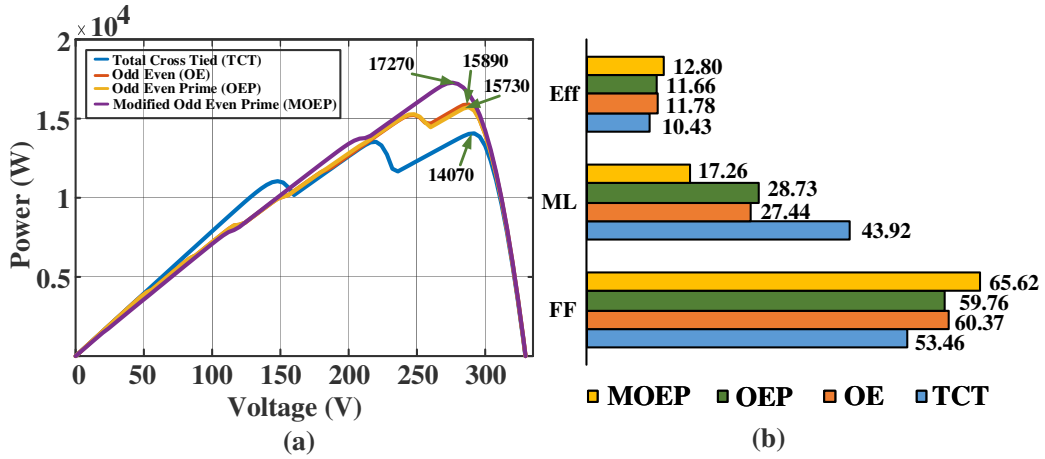

Figure 5.11: Shading pattern-III (a) P-V characteristics (b) Performance parameters

The simulation results shows that GMPP generated by TCT, OE, OEP and MOEP arrangements are 14330W, 15390W, 16160W and 17070W respectively. It is observed that MOEP method of arrangement is able to enhance the GMPP by 19.12%, 10.92%

and 5.63% compared to TCT, OE and OEP arrangements. And also, it has highest efficiency, fill factor of 12.65%, 64.86% and lowest mismatch loss of 18.63% compared to TCT, OE and OEP arrangements. The SDR for TCT, OE, OEP and MOEP arrangements is 0.355, 0.311, 0.255 and 0.119 which indicates that MOEP arrangement is able to disperse shade more effectively.

Table 5.3: GMPP for TCT, OE, OEP and MOEP method for Shading Pattern-III

TCT arrangement			**OE arrangement**		
I_a	V_a	P_a	I_a	V_a	P_a
R_6 - $5.8I_m$	$9V_m$	$\mathbf{52.2}V_mI_m$	R_8 - $6.2I_m$	$9V_m$	$\mathbf{55.8}V_mI_m$
R_7 - $5.8I_m$	-	-	R_5 - $6.7I_m$	$8V_m$	$53.6V_mI_m$
R_8 - $6I_m$	$7V_m$	$42V_mI_m$	R_4 - $7I_m$	$7V_m$	$49V_mI_m$
R_9 - $6I_m$	-	-	R_2 - $7.2I_m$	$6V_m$	$43.2V_mI_m$
R_1 - $9.0I_m$	$5V_m$	$45.0V_mI_m$	R_9 - $7.6I_m$	$5V_m$	$38V_mI_m$
R_2 - $9.0I_m$	-	-	R_7 - $8.1I_m$	$4V_m$	$32.4V_mI_m$
R_3 - $9.0I_m$	-	-	R_6 - $8.2I_m$	$3V_m$	$24.6V_mI_m$
R_4 - $9.0I_m$	-	-	R_1 - $9.0I_m$	$2V_m$	$18V_mI_m$
R_5 - $9.0I_m$	-	-	R_3 - $9.0I_m$	-	-
OEP arrangement			**MOEP arrangement**		
I_a	V_a	P_a	I_a	V_a	P_a
R_1 - $6.7I_m$	$9V_m$	$\mathbf{60.3}V_mI_m$	R_4 - $7.4I_m$	$9V_m$	$\mathbf{66.66}V_mI_m$
R_2 - $6.8I_m$	$8V_m$	$54.4V_mI_m$	R_5 - $7.4I_m$	-	-
R_7 - $6.8I_m$	-	-	R_6 - $7.5I_m$	$7V_m$	$52.5V_mI_m$
R_6 - $7.2I_m$	$6V_m$	$43.2V_mI_m$	R_7 - $7.5I_m$	-	-
R_4 - $7.6I_m$	$5V_m$	$38V_mI_m$	R_9 - $7.5I_m$	-	-
R_9 - $8.1I_m$	$4V_m$	$32.4V_mI_m$	R_1 - $7.6I_m$	$4V_m$	$30.4V_mI_m$
R_5 - $8.4I_m$	$3V_m$	$25.2V_mI_m$	R_8 - $7.6I_m$	-	-
R_8 - $8.4I_m$	-	-	R_3 - $8.1I_m$	$2V_m$	$16.2V_mI_m$
R_3 - $9.0I_m$	$1.0V_m$	$9.0V_mI_m$	R_2 - $8.4I_m$	$1V_m$	$8.4V_mI_m$

Shading Pattern-IV: In this shading pattern, the bottom right corner 4×4 sub array 9×9 PV array is subjected to different insolation levels as shown in Fig. 5.12(a). The module rearrangement and shade dispersion of the 9×9 array under OE, OEP and MOEP arrangements is shown in Fig. 5.12(b) to (g). The power-voltage (P-V) characteristics and performance parameters of 9×9 PV under shading pattern-II is shown in Fig. 5.13(a) and (b). The theoretical values of GMPP under TCT, OE, OEP and MOEP arrangements is shown in Table. 5.4. The simulation results shows that GMPP generated by TCT, OE, OEP and MOEP arrangements are 14000W,

14200W, 15790W and 17080W respectively. It is observed that MOEP method of arrangement is able to enhance the GMPP by 22.01%, 20.28% and 8.17% compared to TCT, OE and OEP arrangements. And also, it has highest efficiency, fill factor of 12.66%, 64.89% and lowest mismatch loss of 18.56% compared to TCT, OE and OEP arrangements. TCT arrangement has highest SDR of 0.377 and MOEP arrangement has lowest SDR of 0.12. Therefore, efficient shade dispersion is achieved by MOEP arrangement.

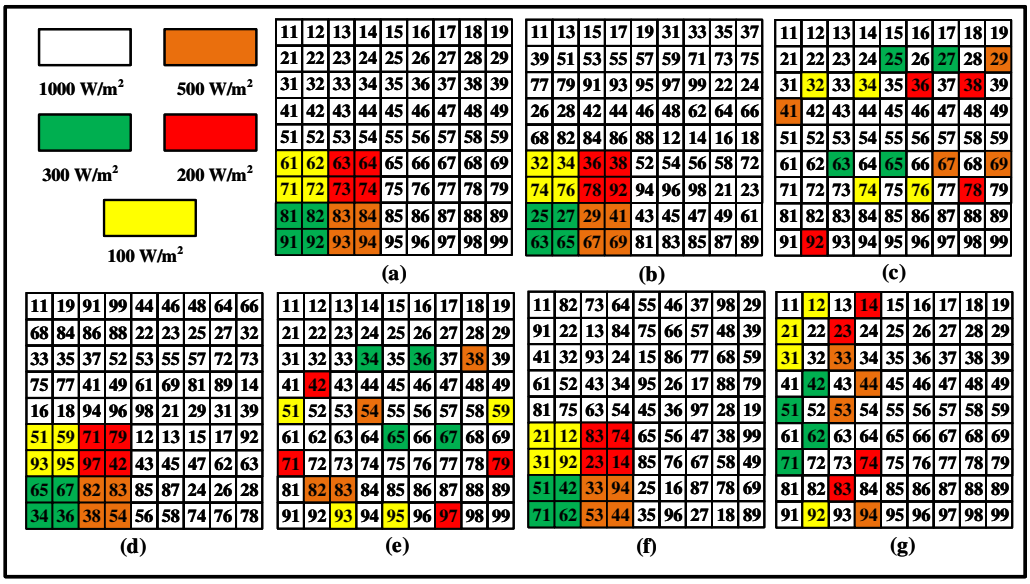

Figure 5.12: Shading Pattern-IV (a) TCT PV array arrangement (b) OE arrangement (c) Shade dispersion by OE method (d) OEP arrangement (e) Shade dispersion by OEP method (f) MOEP arrangement (g) Shade dispersion by MOEP method.

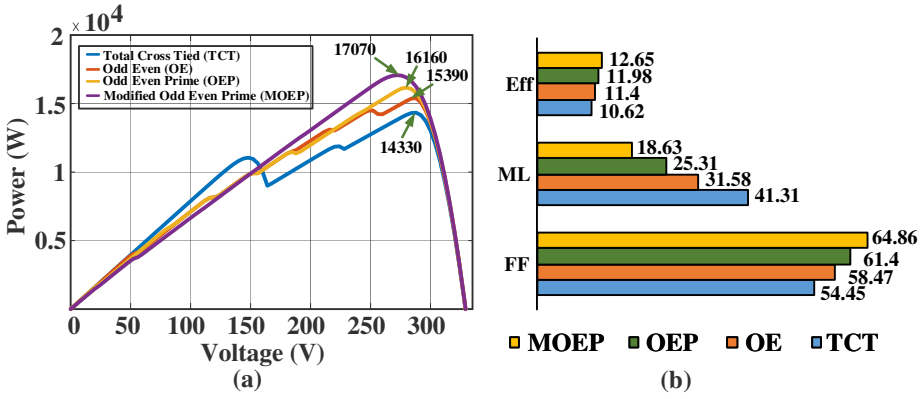

Figure 5.13: Shading pattern-IV (a) P-V characteristics (b) Performance parameters

Table 5.4: GMPP for TCT, OE, OEP and MOEP method for Shading Pattern-IV

TCT arrangement			**OE arrangement**		
I_a	V_a	P_a	I_a	V_a	P_a
R_6 - $5.6I_m$	$9V_m$	**50.4**V_mI_m	R_7 - $6.4I_m$	$8V_m$	**51.2**V_mI_m
R_7 - $5.6I_m$	-	-	R_3 - $5.6I_m$	$9V_m$	$50.4V_mI_m$
R_8 - $6.6I_m$	$7V_m$	$46.2V_mI_m$	R_6 - $6.6I_m$	$7V_m$	$46.2V_mI_m$
R_9 - $6.6I_m$	-	-	R_2 - $7.1I_m$	$6V_m$	$42.6V_mI_m$
R_5 - $9.0I_m$	$5V_m$	$45.0V_mI_m$	R_9 - $8.2I_m$	$5V_m$	$41V_mI_m$
R_6 - $9.0I_m$	-	-	R_4 - $8.5I_m$	$4V_m$	$34V_mI_m$
R_7 - $9.0I_m$	-	-	R_1 - $9I_m$	$3V_m$	$27V_mI_m$
R_8 - $9.0I_m$	-	-	R_5 - $9.0I_m$	-	-
R_9 - $9.0I_m$	-	-	R_8 - $9.0I_m$	-	-
OEP arrangement			**MOEP arrangement**		
I_a	V_a	P_a	I_a	V_a	P_a
R_9 - $6.4I_m$	$9V_m$	**57.6**V_mI_m	R_1 - $7.3I_m$	$9V_m$	**65.7**V_mI_m
R_5 - $6.7I_m$	$8V_m$	$53.6V_mI_m$	R_2 - $7.3I_m$	-	-
R_3 - $7.1I_m$	$7V_m$	$49.7V_mI_m$	R_7 - $7.5I_m$	$7V_m$	$52.5V_mI_m$
R_7 - $7.4I_m$	$6V_m$	$44.4V_mI_m$	R_3 - $7.6I_m$	$6V_m$	$45.6V_mI_m$
R_6 - $7.6I_m$	$5V_m$	$38V_mI_m$	R_9 - $7.6I_m$	-	-
R_8 - $8I_m$	$4V_m$	$32V_mI_m$	R_4 - $7.8I_m$	$4V_m$	$31.2V_mI_m$
R_4 - $8.2I_m$	$3V_m$	$24.6V_mI_m$	R_5 - $7.8I_m$	-	-
R_1 - $9.0I_m$	$2V_m$	$18V_mI_m$	R_8 - $8.2I_m$	$2V_m$	$16.4V_mI_m$
R_2 - $9.0I_m$	-	-	R_6 - $8.3I_m$	$1V_m$	$8.3V_mI_m$

Shading Pattern-V: In this shading pattern, the bottom right corner 4×4 sub array 9×9 PV array is subjected to different insolation levels as shown in Fig. 5.14(a). The module rearrangement and shade dispersion of the 9×9 array under OE, OEP and MOEP arrangements is shown in Fig. 5.14(b) to (g).The power-voltage (P-V) characteristics and performance parameters of 9×9 PV under shading pattern-II is shown in Fig. 5.15(a) and (b). The theoretical values of GMPP under TCT, OE, OEP and MOEP arrangements is shown in Table. 5.5. The simulation results shows that GMPP generated by TCT, OE, OEP and MOEP arrangements are 14070W, 15890W, 15730W and 17270W respectively. It is observed that MOEP method of arrangement is able to enhance the GMPP by 22.74%, 8.68% and 9.79% compared to TCT, OE and OEP arrangements. And also, it has highest efficiency, fill factor of 12.8%, 65.82% and lowest mismatch loss of 17.26% compared to TCT, OE and OEP arrangements. The SDR for TCT, OE, OEP and MOEP arrangements is 0.355,

0.288, 0.3 and 0.141, which indicates that MOEP arrangement is able to disperse shade more effectively.

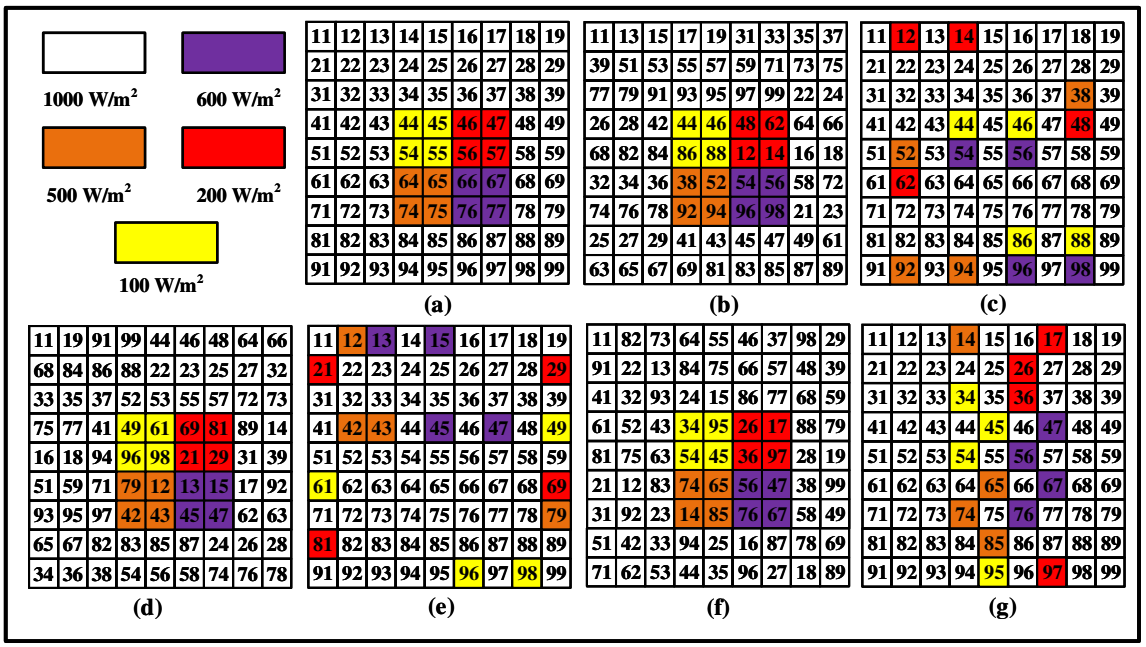

Figure 5.14: Shading Pattern-V (a) TCT PV array arrangement (b) OE arrangement (c) Shade dispersion by OE method (d) OEP arrangement (e) Shade dispersion by OEP method (f) MOEP arrangement (g) Shade dispersion by MOEP method.

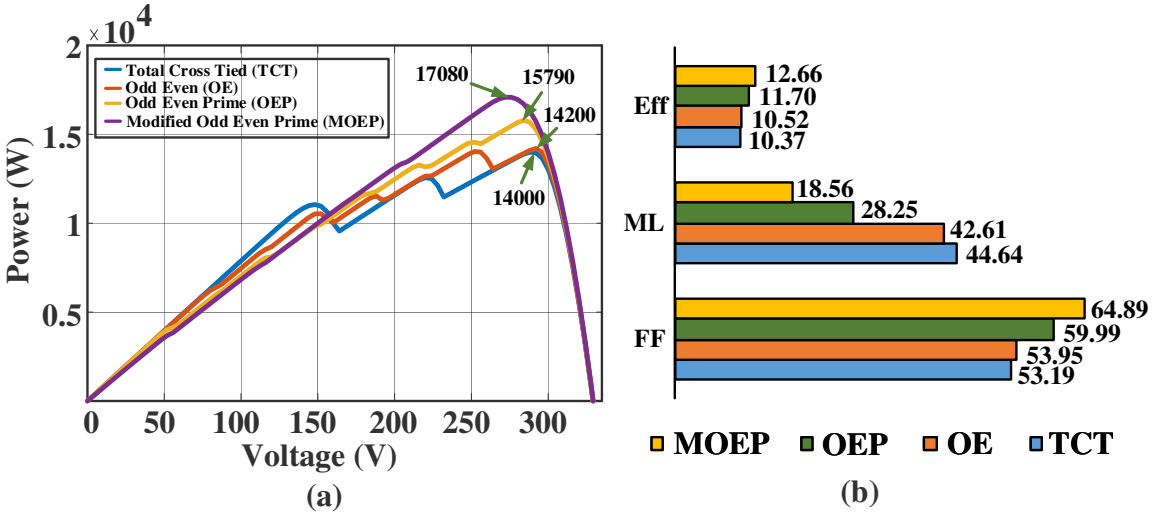

Figure 5.15: Shading pattern-V (a)Power-Voltage (P-V) characteristics (b) Performance parameters

Table 5.5: GMPP for TCT, OE, OEP and MOEP method for Shading Pattern-V

TCT arrangement			**OE arrangement**		
I_a	V_a	P_a	I_a	V_a	P_a
R_4 - $5.6I_m$	$9V_m$	**50.4**V_mI_m	R_4 - $6.4I_m$	$9V_m$	**57.6**V_mI_m
R_5 - $5.6I_m$	-	-	R_8 - $7.2I_m$	$8V_m$	$57.6V_mI_m$
R_6 - $7.2I_m$	$7V_m$	$50.4V_mI_m$	R_9 - $7.2I_m$	-	-
R_7 - $7.2I_m$	-	-	R_1 - $7.4I_m$	$6V_m$	$44.4V_mI_m$
R_1 - $9.0I_m$	$5V_m$	$45.0V_mI_m$	R_5 - $7.7I_m$	$5V_m$	$38.5V_mI_m$
R_2 - $9.0I_m$	-	-	R_6 - $8.2I_m$	$4V_m$	$32.8V_mI_m$
R_3 - $9.0I_m$	-	-	R_3 - $8.5I_m$	$3V_m$	$25.5V_mI_m$
R_8 - $9.0I_m$	-	-	R_2 - $9.0I_m$	$2V_m$	$18V_mI_m$
R_9 - $9.0I_m$	-	-	R_7 - $9.0I_m$	-	-
OEP arrangement			**MOEP arrangement**		
I_a	V_a	P_a	I_a	V_a	P_a
R_9 - $7.2I_m$	$8V_m$	**57.6**V_mI_m	R_3 - $7.3I_m$	$9V_m$	**65.7**V_mI_m
R_4 - $6.3I_m$	$9V_m$	$56.7V_mI_m$	R_9 - $7.3I_m$	-	-
R_8 - $7.3I_m$	$7V_m$	$51.1V_mI_m$	R_1 - $7.6I_m$	$7V_m$	$53.2V_mI_m$
R_2 - $7.4I_m$	$6V_m$	$44.4V_mI_m$	R_4 - $7.7I_m$	$6V_m$	$46.2V_mI_m$
R_1 - $7.7I_m$	$5V_m$	$38.5V_mI_m$	R_5 - $7.7I_m$	-	-
R_8 - $8.2I_m$	$4V_m$	$32.8V_mI_m$	R_7 - $8.1I_m$	$4V_m$	$32.4V_mI_m$
R_7 - $8.5I_m$	$3V_m$	$25.5V_mI_m$	R_8 - $8.1I_m$	-	-
R_3 - $9.0I_m$	$2V_m$	$18V_mI_m$	R_2 - $8.2I_m$	$2V_m$	$16.4V_mI_m$
R_5 - $9.0I_m$	-	-	R_8 - $8.5I_m$	$1V_m$	$8.5V_mI_m$

Table 5.6: Simulation results (GMPP) of 9×9 array and % Power Enhancement of MOEP method

Shade	GMPP (W)				% Power Enhancement of MOEP over		
	TCT	OE	OEP	MOEP	TCT	OE	OEP
SP-I	15440	15630	17240	17850	15.61	14.2	3.54
SP-II	13970	14270	15790	17010	21.76	19.2	7.73
SP-III	14330	15390	16160	17070	19.12	10.92	5.63
SP-IV	14000	14200	15790	17080	22.01	20.28	8.17
SP-V	14070	15890	15730	17270	22.74	8.68	9.79

The SDR of TCT, OE, OEP and MOEP methods under all the five shading patterns is shown in Fig. 5.16. It is observed that, MOEP method has lowest SDR compared to TCT, OE and OEP methods. Further, MOEP method is able to decrease the SDR by at least 50% compared to TCT, OE and OEP methods. This indicates that MOEP method has better shade dispersion capability compared to TCT, OE and

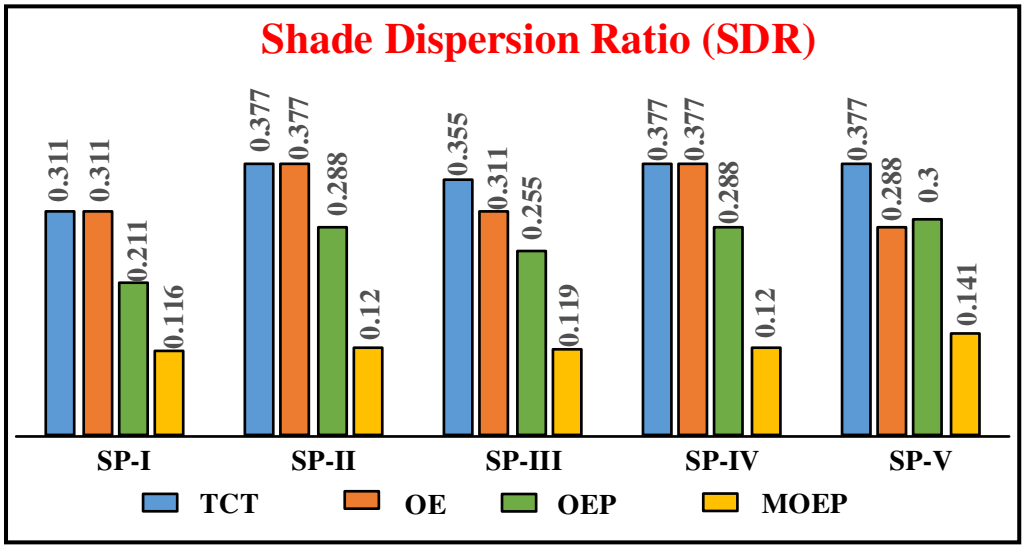

Figure 5.16: Shade Dispersion Ration under various shading patterns -I to V

OEP methods. The GMPP of TCT, OE, OEP and MOEP methods under all the five shading patterns considered is tabulated in Table. 5.6. It is observed that MOEP method improves the GMPP by at least 15.61%, 8.68% and 3.54% compared to TCT, OE and OEP methods. And also the maximum power enhancement by MOEP method is 22.74%, 20.28% and 9.79% compared to TCT, OE and OEP methods under the five shading patterns considered.

5.3.2 8×8 PV Array

The proposed MOEP method is applicable to any array size. In this regard, 8×8 TCT connected PV array is rearranged according to OE, OEP and MOEP methods and analyzed under short & narrow (S&N), short & wide (S&W), long & narrow (L&N) and long & wide (L&W) shading patterns. The shading patterns are shown in Fig. 5.17.

The GMPP generated by TCT, OE, OEP and proposed MOEP methods under short & narrow (S&N), short & wide (S&W), long & narrow (L&N) and long & wide (L&W) shading patterns is given in Table. 5.7. For S&N shading pattern, the GMPP generated by TCT, OE, OEP and MOEP methods are 13700W, 13700W, 14620W and 14830W. The power enhancement by proposed MOEP method is 8.25%, 8.25% and 1.44% compared to TCT, OE and OEP methods. For S&W shading pattern,

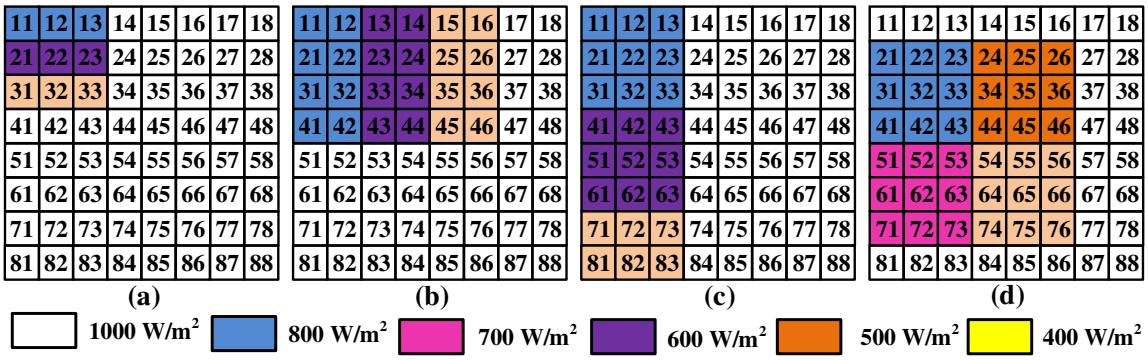

Figure 5.17: Shading Patterns (a) Short & Narrow (SN) (b) Short & Wide (SW) (c) Long & Narrow (LN) (d) Long & Wide (LW)

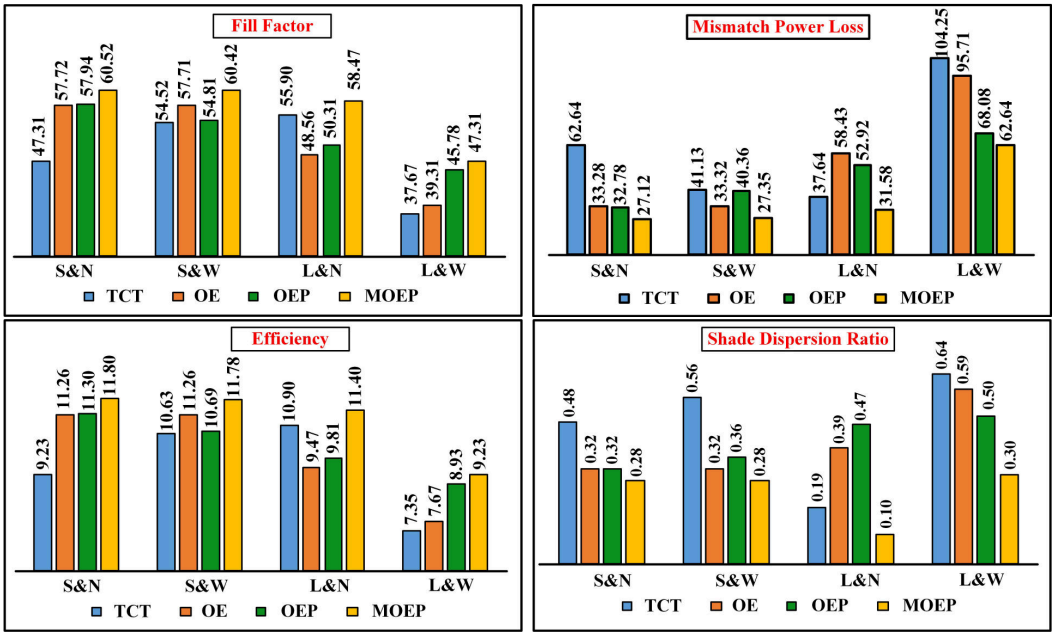

Figure 5.18: Performance parameters of 8×8 PV array

the GMPP generated by TCT, OE, OEP and MOEP methods are 11390W, 13400W, 13230W and 13790W. The power enhancement by proposed MOEP method is 21.07%, 2.91% and 4.23% compared to TCT, OE and OEP methods. For L&N shading pattern, the GMPP generated by TCT, OE, OEP and MOEP methods are 13220W, 11270W, 12620W and 13790W. The power enhancement by proposed MOEP method is 3.33%, 21.21% and 8.24% compared to TCT, OE and OEP methods. For L&W shading pattern, the GMPP generated by TCT, OE, OEP and MOEP methods are 11300W, 11600W, 10710W and 12190W. The power enhancement by proposed MOEP

method is 7.88%, 5.09% and 13.82% compared to TCT, OE and OEP methods. Further the performance parameters FF, ML and efficiency are shown in Fig. 5.18.

Table 5.7: Simulation results of 8×8 array and % Power Enhancement of MOEP method

Shade	GMPP (W)				Power Enhancement of MOEP over		
	TCT	OE	OEP	MOEP	TCT (%)	OE (%)	OEP (%)
SN	13700	13700	14620	14830	8.25	8.25	1.44
SW	11390	13400	13230	13790	21.07	2.91	4.23
LN	13220	11270	12620	13660	3.33	21.21	8.24
LW	11300	11600	10710	12190	7.88	5.09	13.82

5.4 Experimental Results

To validate the theoretical and simulation results for TCT, OE, OEP and proposed MOEP methods, an experimental set up is made as shown in Fig. 5.19. It consists of PV modules of same capacity, one solar irradiance meter (FLUKE IRR1-SOL), two digital multi meters (FLUKE-17B+), resistive load, transparent sheets and connecting wires.

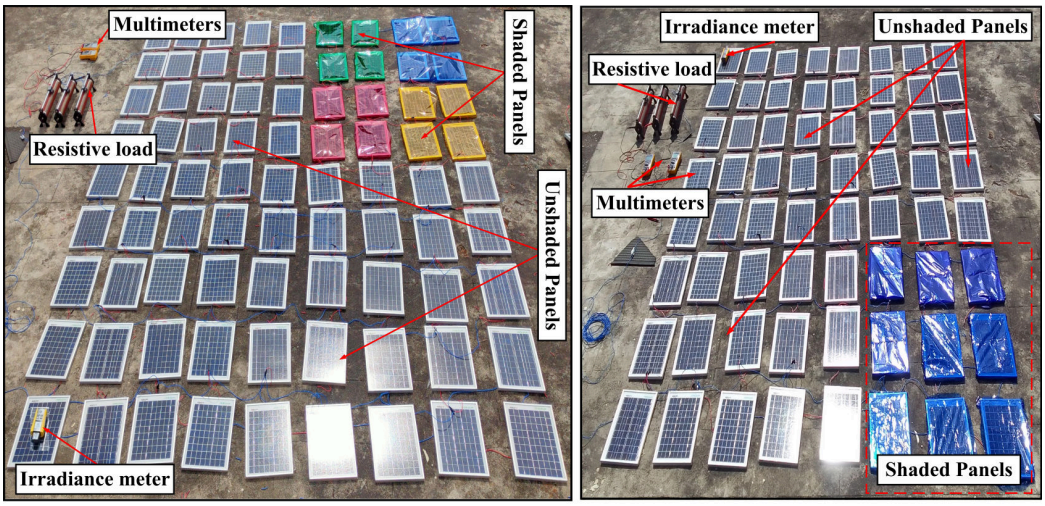

Figure 5.19: Experimental arrangement (a) 9×9 Array (b) 8×8 Array

The rating of PV module (LOOM SOLAR) considered is P_{mp} = 10W, open circuit voltage V_{oc} = 26.8 V, short circuit current I_{sc} = 0.55 A, MPP voltage, V_{mp} = 20

V, MPP current I_{mp} = 0.5A. The amount of insolation falling on the PV module ia measured by using solar irradiance meter. Various levels of solar insolation such as 700 W/m^2, 600 W/m^2, 500 W/m^2, 400 W/m^2, 300 W/m^2, 200 W/m^2 are achieved by using transparent sheets of different thickness. The output current from the PV array is measured by using multimeter connected in series to the load. The PV array output voltage is measured by using multimeter connected in parallel across the load. The output power form the PV array is obtained by multiplying the output voltage and current.The accuracy of multimeters used is ±0.5% for DC voltage and ±1.5% for DC current. The overall accuracy in measuring of PV array output power is ±2%. The experiment is conducted at 950 W/m^2 and 35^0C.

5.4.1 9×9 PV Array

To validate the proposed MOEP an experimental set up of 9×9 PV array is considered as shown in Fig. 5.19(a). The experimental results of 9×9 Array under shading patterns-I to V is given in Table. 5.8. In case of shading pattern-I, the GMPP attained by TCT, OE, OEP and MOEP methods are 554.12W, 562.54W, 613.14W and 630.36W respectively. Proposed MOEP method is able to increase the GMPP by 13.76%, 12.06% and 3.14% compared to TCT, OE and OEP methods. In case of shading pattern-II, the GMPP attained by TCT, OE, OEP and MOEP methods are 518.24W, 522.31W, 562.92W and 601.53W respectively. Proposed MOEP method is able to increase the GMPP by 16.07%, 15.17% and 6.86% compared to TCT, OE and OEP methods. In case of shading pattern-III, the GMPP attained by TCT, OE, OEP and MOEP methods are 524.12W, 552.76W, 568.84W and 602.31W respectively. Proposed MOEP method is able to increase the GMPP by 14.92%, 9.09% and 5.88% compared to TCT, OE and OEP methods. In case of shading pattern-IV, the GMPP attained by TCT, OE, OEP and MOEP methods are 519.12W, 523.37W, 561.15W and 603.36W respectively. Proposed MOEP method is able to increase the GMPP by 16.23%, 15.33% and 7.52% compared to TCT, OE and OEP methods. In case of shading pattern-V, the GMPP attained by TCT, OE, OEP and MOEP methods are 518.31W, 565.56W, 561.18W and 608.84W respectively. Proposed MOEP method is able to increase the GMPP by 17.47%, 7.65% and 8.49% compared to TCT, OE and OEP methods.

Table 5.8: Experimental results of 9×9 array and % Power Enhancement of MOEP method

Shade	GMPP (W)				Power Enhancement of MOEP over		
	TCT	OE	OEP	MOEP	TCT (%)	OE (%)	OEP (%)
SP-I	554.12	562.54	611.14	630.36	13.76	12.06	3.14
SP-II	518.24	522.31	562.92	601.53	16.07	15.17	6.86
SP-III	524.12	552.76	568.84	602.31	14.92	9.09	5.88
SP-IV	519.12	523.37	561.15	603.36	16.23	15.33	7.52
SP-V	518.31	565.56	561.18	608.84	17.47	7.65	8.49

5.4.2 8×8 PV Array

To validate the proposed MOEP an experimental set up of 8×8 PV array is considered as shown in Fig. 5.19(b). The experimental results of 8×8 Array under the above mentioned shading patterns is given in Table. 5.9. For S&N shading pattern, the GMPP attained by TCT, OE, OEP and MOEP methods are 510.52W, 510.52W, 536.36W and 546.64W respectively. Proposed MOEP method is able to increase the GMPP by 7.08%, 7.08% and 1.92% compared to TCT, OE and OEP methods. For S&W shading pattern, the GMPP attained by TCT, OE, OEP and MOEP methods are 427.28W, 508.96W, 492.74W and 517.14W respectively. Proposed MOEP method is able to increase the GMPP by 19.72%, 2.60% and 3.82% compared to TCT, OE and OEP methods. For L&N shading pattern, the GMPP attained by TCT, OE, OEP and MOEP methods are 494.58W, 424.84W, 471.24W and 508.18W respectively. Proposed MOEP method is able to increase the GMPP by 2.75%, 19.62% and 7.84% compared to TCT, OE and OEP methods. For L&W shading pattern, the GMPP attained by TCT, OE, OEP and MOEP methods are 428.68W, 438.24W, 414.16W and 460.24W respectively. Proposed MOEP method is able to increase the GMPP by 7.36%, 5.02% and 11.13% compared to TCT, OE and OEP methods.

Table 5.9: Experimental results of 8×8 array and % Power Enhancement of MOEP method

Shade	GMPP (W)				% Power Enhancement of MOEP over		
	TCT	OE	OEP	MOEP	TCT	OE	OEP
SN	510.52	510.52	536.36	546.64	7.08	7.08	1.92
SW	427.28	508.96	492.74	517.14	19.72	2.60	3.82
LN	494.58	424.84	471.24	508.18	2.75	19.62	7.84
LW	428.68	438.24	414.16	460.24	7.36	5.02	11.13

5.5 Energy Savings and Revenue Generated

The main aim of the proposed MOEP method is to increase the GMPP form the PV array under partial shading conditions. The increase in power generated from the PV array leads to increase in the revenue generated. In this section, a brief analysis of units (kWhr) generated and earnings (Rs) made per hour, per day and per year for 9×9 PV array by implementing proposed MOEP, OE, OEP and TCT methods is presented. For analysis, the simulation and hardware results are taken into consideration. Here the shadow falling on the PV array is considered for a period of six hours i.e. from 10 a.m to 4 p.m. The solar power tariff of Rs.8 (INR) per unit is considered for the assessment. Five shading patterns (SP-I, SP-II, SP-III, SP-IV and SP-V) are considered to take place over the array from 10 a.m to 12 a.m, 12 a.m to 1 p.m, 1 p.m to 2 p.m, 2 p.m to 3 p.m and 3 p.m to 4 p.m respectively. The number of units (KWhr) and earnings (Rs) generated by TCT, OE, OEP and MOEP methods in simulation and experimental studies is listed in Table. 5.10 and 5.11. Under simulation studies, the units generated per year (KWhr) by TCT, OE, OEP and MOEP methods are 31846.25, 33218.65, 35751.75 and 38007.45 receptively. The earnings generated per year (Rs) by TCT, OE, OEP and MOEP methods are 2,54,770.00, 2,65,749.20, 2,86,014.00 and 3,04,059.60 receptively. Under hardware studies, the units generated per year (KWhr) by TCT, OE, OEP and MOEP methods are 1163.631, 1200.20, 1268.875 and 1342.017 receptively. The earnings generated per year (Rs) by TCT, OE, OEP and MOEP methods are 9309.496, 9601.6024, 10151.00 and 10736.139 receptively. From the simulation analysis, it is observed that MOEP method is able to generate earnings (Rs) greater than TCT, OE and OEP methods by 19.35%, 14.42% and 6.31% per year. From the hardware analysis, it is observed that MOEP method is able to generate earnings (Rs) greater than TCT, OE and OEP methods by 15.33%, 11.82% and 5.76% per year. Similar analysis is carried out for 8×8 PV array and the proposed MOEP method is able to generate earnings (Rs) greater than TCT, OE and OEP patterns. From the analysis, it is observed that the proposed MOEP method is superior to TCT, OE, and OEP methods in saving the energy and generating more revenue.

Table 5.10: Units, revenue generated by TCT, OE, OEP and MOEP patterns for 9×9 array considering simulation results

Configuration	Duration	Pattern	GMPP	Hourly analysis		Day analysis		Year based analysis	
				Units	Earnings	Units	Earnings	Units	Earnings
TCT	10 a.m - 12 a.m	SP-I	15400	30.88	247.04				
	12 a.m - 01 p.m	SP-II	13970	13.97	111.79				
	01 p.m - 02 p.m	SP-III	14330	14.33	114.64	87.25	698	31846.25	2,54,770.00
	02 p.m - 03 p.m	SP-IV	14000	14.00	112				
	03 p.m - 04 p.m	SP-V	14070	14.07	112.56				
OE	10 a.m - 12 a.m	SP-I	15630	31.26	250.08				
	12 a.m - 01 p.m	SP-II	14270	14.27	114.16				
	01 p.m - 02 p.m	SP-III	15390	15.39	123.12	91.01	728.08	33218.65	2,65,749.20
	02 p.m - 03 p.m	SP-IV	14200	14.20	113.6				
	03 p.m - 04 p.m	SP-V	15890	15.89	127.12				
OEP	10 a.m - 12 a.m	SP-I	17240	34.48	275.84				
	12 a.m - 01 p.m	SP-II	15790	15.79	126.32				
	01 p.m - 02 p.m	SP-III	16160	16.16	129.28	97.95	783.6	35751.75	2,86,014.00
	02 p.m - 03 p.m	SP-IV	15790	15.79	126.32				
	03 p.m - 04 p.m	SP-V	15730	15.73	125.84				
MOEP	10 a.m - 12 a.m	SP-I	17850	35.70	285.60				
	12 a.m - 01 p.m	SP-II	17010	17.01	136.08				
	01 p.m - 02 p.m	SP-III	17070	17.07	136.56	104.13	833.04	38007.45	3,04,059.60
	02 p.m - 03 p.m	SP-IV	17080	17.08	136.64				
	03 p.m - 04 p.m	SP-V	17270	17.27	138.16				

GMPP in Watts, No. of Units in Kilowatt-hour, Earnings in Indian Rupees.

Table 5.11: Units, revenue generated by TCT, OE, OEP and MOEP patterns for 9×9 array considering hardware results

Configuration	Duration	Pattern	GMPP	Hour based analysis		Day based analysis		Year based analysis	
				Units	Earnings	Units	Earnings	Units	Earnings
TCT	10 a.m - 12 a.m	SP-I	554.12	1.10824	8.86592				
	12 a.m - 01 p.m	SP-II	518.24	0.51824	4.14592				
	01 p.m - 02 p.m	SP-III	524.12	0.52412	4.19296	3.18803	25.5042	1163.631	9,309..496
	02 p.m - 03 p.m	SP-IV	519.12	0.51912	4.15296				
	03 p.m - 04 p.m	SP-V	518.31	0.51831	4.14648				
OE	10 a.m - 12 a.m	SP-I	562.54	1.12508	9.00064				
	12 a.m - 01 p.m	SP-II	522.31	0.52213	4.17848				
	01 p.m - 02 p.m	SP-III	552.12	0.52212	4.41696	3.28822	26.3058	1200.20	9,601.6024
	02 p.m - 03 p.m	SP-IV	523.15	0.52315	4.1852				
	03 p.m - 04 p.m	SP-V	565.56	0.56556	4.52448				
OEP	10 a.m - 12 a.m	SP-I	611.14	1.22228	9.77824				
	12 a.m - 01 p.m	SP-II	562.92	0.56292	4.50336				
	01 p.m - 02 p.m	SP-III	568.84	0.56884	4.55072	3.47637	27.811	1268.875	10,151.00
	02 p.m - 03 p.m	SP-IV	561.15	0.56115	4.4892				
	03 p.m - 04 p.m	SP-V	561.18	0.5618	4.48944				
MOEP	10 a.m - 12 a.m	SP-I	630.36	1.26072	10.08576				
	12 a.m - 01 p.m	SP-II	601.53	0.60153	4.81224				
	01 p.m - 02 p.m	SP-III	602.31	0.60231	4.81848	3.67676	29.4141	1342.017	10,736.139
	02 p.m - 03 p.m	SP-IV	603.36	0.60336	4.82688				
	03 p.m - 04 p.m	SP-V	608.84	0.60884	4.87072				

GMPP in Watts, No. of Units in Kilowatt-hour, Earnings in Indian Rupees.

Table 5.12: Qualitative Comparison of MOEP method over other methods (L - Low, M - Medium, H - High)

Parameters	[10]	[11]	[12]	[13]	[14]	[15]	[16]	[17]	[18]	MOEP
Maximum Power Generation (P1)	L	M	H	H	H	H	M	M	M	H
Shade dispersion capability (P2)	L	M	H	H	H	H	M	L	M	H
Wiring complexity (P3)	L	M	L	L	L	M	M	H	H	L
Wiring loss (P4)	L	M	M	M	M	M	M	H	H	L
Applicability for any array size (P5)	H	L	L	L	M	L	M	H	H	H
Mismatch Power Loss reduction (P6)	L	M	H	H	H	H	M	M	M	H

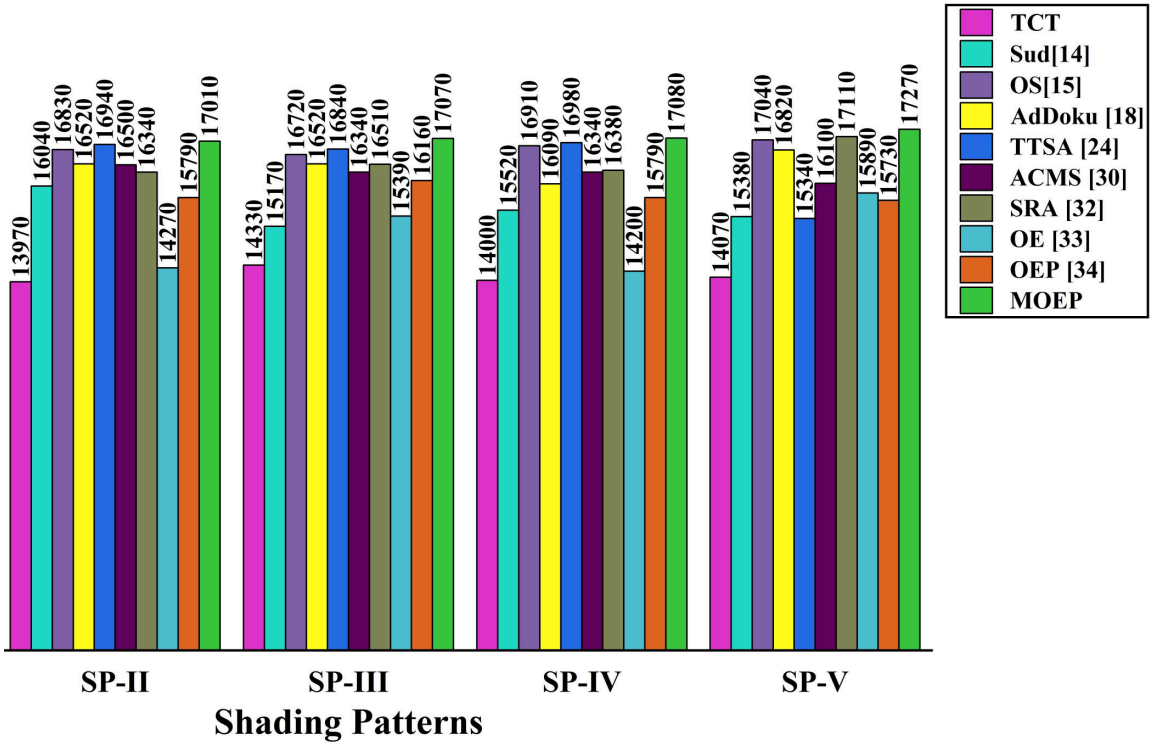

Figure 5.20: Simulation results of 9×9 array under various existing techniques

5.6 Comparative Analysis

The efficacy of the proposed MOEP method is proved by performing qualitative analysis between TCT, Sudoku, Optimal Sudoku, AdDoku, Twisted Two-step approach, Ancient Chinese Magic Square, Successive Rotation approach, Odd Even, Odd Even Prime, and the proposed MOEP method. The following parameters are considered for qualitative analysis.P1 - Ability to generate maximum power, P2 - Shade disper-

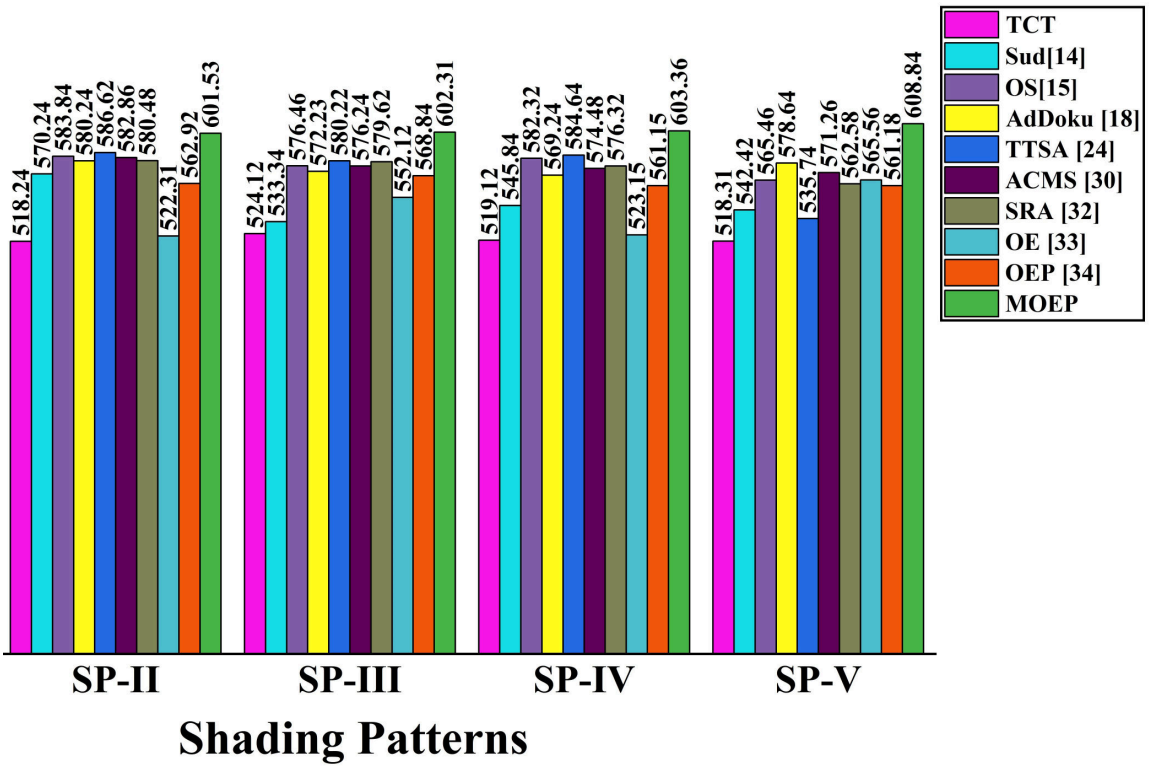

Figure 5.21: Hardware results of 9×9 array under various existing techniques

sion capability, P3 - Wiring complexity, P4 - Wiring loss, P5 - Applicability for any array size, P6 - Mismatch Power Loss reduction, which is shown in Table 5.12.

Further, the proposed MOEP is compared to the above-mentioned techniques in terms of GMPP generated under the five shading patterns considered in simulation and hardware environments. The GMPP generated by various existing techniques in the literature for a 9×9 PV array under the above shading patterns is shown in Fig.5.20 and Fig.5.21. The proposed MOEP method can generate more GMPP compared to existing techniques. From the analysis, it is observed that the MOEP method outperforms the existing techniques under the shading patterns considered for analysis.

5.7 MOEP method applied to RCT configuration

The efficacy of proposed MOEP method is proved by performing comparative analysis between MOEP method and different static reconfiguration techniques available in

the literature such as Sudoku, Optimal Sudoku, AdDoku, Twisted Two step, Ancient Chinese Magic Square, Successive rotation approach, Odd Even, and Odd Even Prime methods applied to RCT configured 9×9 PV array. The GMPP generated by above mentioned reconfiguration techniques under five different shading patterns for 9×9 PV array in both software (20.25kW system) and hardware (0.81kW system) are listed in Table.5.13 and Table.5.14. It is evident form the results, that the proposed MOEP method generates highest GMPP compared to other techniques.

Table 5.13: Simulation results of various reconfiguration techniques and proposed MOEP method applied on RCT configuration

Shade	Sud	OS	AdDoku	TTSA	ACMS	SRA	OE	OEP]	RCT-MOEP
SP-I	17530	17480	17120	16890	17110	17230	15110	16850	17480
SP-II	15960	16430	16230	16640	16320	16220	13210	14660	16540
SP-III	15040	16250	16220	16580	16110	16180	14960	15680	16680
SP-IV	15430	16540	15980	16760	16080	16160	13110	15240	16760
SP-V	15240	17260	16450	15120	15980	16560	15240	15410	16840

Table 5.14: Experimental results of various reconfiguration techniques and proposed MOEP method applied on RCT configuration

Shade	Sud	OS	AdDoku	TTSA	ACMS	SRA	OE	OEP]	RCT-MOEP
SP-I	570.48	568.42	566.36	544.26	546.64	562.12	501.26	554.24	580.64
SP-II	520.16	524.78	522.34	518.36	516.38	511.24	476.56	492.56	548.36
SP-III	484.86	518.48	526.24	520.36	511.24	514.36	486.84	501.24	552.68
SP-IV	496.58	522.46	520.48	514.78	520.56	490.34	472.56	494.64	556.46
SP-V	498.36	524.78	526.34	536.48	525.68	484.56	490.62	496.64	560.24

5.8 Summary

In this chapter, a Modified Odd Even Prime (MOEP) static reconfiguration scheme is proposed to enhance the power output from PV array. The proposed MOEP method along with TCT, OE and OEP is implemented on 9×9 and 8×8 PV arrays under different shading patterns. The key advantage of the proposed MOEP method is the shaded modules in particular column are displaced across the same column. Therefore, length of wire required for connecting the modules is less thereby wiring resistance and wiring loss decreases. MOEP method is simple and applicable for any

array size. For 9×9 PV array, the simulation and hardware results shown maximum power enhancement of 22.74%, 20.28%, 9.79% and 17.47%, 15.33%, 8.49% compared to TCT,OE and OEP methods. For 8×8 PV array, the simulation and hardware results shown maximum power enhancement of 21.07%, 21.21%, 13.82% and 19.72%, 19.62%, 11.13% compared to TCT,OE and OEP methods. MOEP method is able to generate earnings (Rs) greater than TCT, OE and OEP patterns. Further, there is reduction in mismatch power loss, shade dispersion ratio and increase in fill factor, efficiency compared to TCT, OE and OEP methods. The proposed MOEP method and the above mentioned techniques are further implemented on RCT configured 9×9 PV array. From the results obtained, it is clear that proposed MOEP method is able to improve GMPP of the array under PSCs by a significant margin compared to TCT, OE and OEP methods. Hence, MOEP method can be an efficient static reconfiguration technique to reduce the effects caused by PSCs.

Chapter 6

CONCLUSION AND FUTURE SCOPE

6.1 Contribution

Chapter 1 presented a brief overview solar photo voltaic systems and state-of-the-art fault finding techniques and partial shading reduction techniques. Chapter 2 presented a novel Diagonal Sensor Arrangement scheme to detect and localize the faults (Line-Line(LL), Line-Ground(LG), Open circuit (OC), and Partial Shading) in the PV array. It is implemented on 4×4 PV array in simulation and Hardware environments. The results proven the accuracy in identification of detection and location of faults in the PV array. Chapter 3 proposed, a novel Reduced Cross Tied (RCT) PV array configuration is proposed to enhance the power output from PV array under PSCs. The proposed RCT configuration is implemented on 7×7, and 8×8 PV arrays and validated in both simulation and hardware environments. From the simulation and experimental results it is observed that, RCT configuration can be considered as an alternative to TCT configuration. To mitigate the effects caused by partial shading, a static reconfiguration technique Cyclic Back Shift (CBS) is proposed in Chapter 4. This technique is implemented in software (9×9 square array of 20.25kW system) and hardware (9×9 square array of 0.81kW system) environments. In case of 9×9 array, CBS method is able to achieve power increment of 18.52%, 9.73%, 22.46%, 14.92%, 15.47% in software environment and 18.14%, 11.83%, 18.78%, 12.06%, 13% in hardware platform under five shading patterns considered. Chapter 5 proposed

a Modified Odd Even Prime (MOEP) static reconfiguration scheme is proposed to enhance the power output from PV array. The proposed MOEP method along with TCT, OE and OEP is implemented on 9×9 and 8×8 PV arrays under different shading patterns. For 9×9 PV array, the simulation and hardware results shown maximum power enhancement of 22.74%, 20.28%, 9.79% and 17.47%, 15.33%, 8.49% compared to TCT,OE and OEP methods. For 8×8 PV array, the simulation and hardware results shown maximum power enhancement of 21.07%, 21.21%, 13.82% and 19.72%, 19.62%, 11.13% compared to TCT,OE and OEP methods. MOEP method is able to generate earnings (Rs) greater than TCT, OE and OEP patterns.

6.2 Conclusion

1. Diagonal Sensor Arrangement (DSA) is applicable for any size of array. DSA strategy utilizes minimal number of sensors to identify and locate the faults. It is more effective in localizing the faults occurring at the module level and string level.

2. Reduced Cross Tied (RCT) configuration is able to generate GMPP close to TCT configuration with reduced cross ties.It has atleast 25% reduction in cross ties compared to TCT configuration for any array size, possess reduced wiring loss.

3. Cyclic Back Shift (CBS) method is very simple, economical and applicable for square and non-square arrays of any desired size.

4. In comparison to the other existing reconfiguration schemes Sudoku, Optimal Sudoku, Futoshiki, PRMFEC, PRFCPMFEC, Chaos Map, Twisted Two step, Tom Tom and Advanced Sudoku, the proposed CBS method of arrangement clearly generates at least 1% more power output under the shading patterns.

5. In the proposed Modified Odd Even Prime (MOEP) method, the modules are displaced across the same column. Therefore, length of wire required for connecting the modules is less thereby wiring resistance and wiring loss decreases.

6. On the whole, RCT, CBS, and MOEP methods are efficient techniques in reducing the partial shading effects.

6.3 Future scope

Based on the research carried out in this thesis, the recommendations for future research are as follows:

- To further develop a new strategy to detect and localize the fault occurring in the PV array at the module level.
- To integrate the proposed RCT, CBS and MOEP techniques along with an efficient MPPT control technique to track the GMPP.

Bibliography

Alam, M. K., Khan, F., Johnson, J., and Flicker, J. (2015). A comprehensive review of catastrophic faults in pv arrays: types, detection, and mitigation techniques. *IEEE Journal of Photovoltaics*, 5(3):982–997.

Albers, M. J. and Ball, G. (2015). Comparative evaluation of dc fault-mitigation techniques in large pv systems. *IEEE Journal of Photovoltaics*, 5(4):1169–1174.

Aljafari, B., Devakirubakaran, S., Bharatiraja, C., Balachandran, P. K., and Babu, T. S. (2023). Power enhanced solar pv array configuration based on calcudoku puzzle pattern for partial shaded pv system. *Heliyon*, 9(5).

Amar Raj, R. D. and Anil Naik, K. (2023). A generalized henon map-based solar pv array reconfiguration technique for power augmentation and mismatch mitigation. *IETE Journal of Research*, 69(11):8404–8422.

Amar Raj, R. D. and Naik, K. A. (2022). A novel solar photovoltaic array reconfiguration technique using two-dimensional generalized arnold's cat map. *Journal of Solar Energy Engineering*, 144(6):061001.

Anjum, S., Mukherjee, V., and Mehta, G. (2021). Advanced sudoku-based reconfiguration strategies for maximum power extraction from partially shaded solar photovoltaic array. *Journal of Solar Energy Engineering*, 143(6):061003.

Anjum, S., Mukherjee, V., and Mehta, G. (2022a). Addition progression structure photovoltaic array reconfiguration technique to generate maximum power under static partial shading condition. *Arabian Journal for Science and Engineering*, 47(11):14105–14118.

Anjum, S., Mukherjee, V., and Mehta, G. (2022b). Hyper sudoku-based solar photovoltaic array reconfiguration for maximum power enhancement under partial shading conditions. *Journal of Energy Resources Technology*, 144(3):031302.

Anjum, S., Mukherjee, V., and Mehta, G. (2022c). Modelling and simulation of addoku based reconfiguration technique to harvest maximum power from photovoltaic array under partial shading conditions. *Simulation Modelling Practice and Theory*, 115:102447.

Babu, T. S., Ram, J. P., Dragičević, T., Miyatake, M., Blaabjerg, F., and Rajasekar, N. (2017). Particle swarm optimization based solar pv array reconfiguration of the maximum power extraction under partial shading conditions. *IEEE Transactions on Sustainable Energy*, 9(1):74–85.

Ball, G., Brooks, B., Flicker, J., Johnson, J., Rosenthal, A., Wiles, J., and Sherwood, L. (2013). Inverter ground-fault detection 'blind spot'and mitigation methods. *Solar American Board for Codes and Standards*, 674:1–42.

Bana, S. and Saini, R. (2017). Experimental investigation on power output of different photovoltaic array configurations under uniform and partial shading scenarios. *Energy*, 127:438–453.

Belhachat, F. and Larbes, C. (2021). Pv array reconfiguration techniques for maximum power optimization under partial shading conditions: A review. *Solar Energy*, 230:558–582.

Bonthagorla, P. K. and Mikkili, S. (2020a). A novel fixed pv array configuration for harvesting maximum power from shaded modules by reducing the number of cross-ties. *IEEE Journal of Emerging and Selected Topics in Power Electronics*, 9(2):2109–2121.

Bonthagorla, P. K. and Mikkili, S. (2020b). Optimal pv array configuration for extracting maximum power under partial shading conditions by mitigating mismatching power losses. *CSEE Journal of Power and Energy Systems*, 8(2):499–510.

Bonthagorla, P. K. and Mikkili, S. (2020c). Performance analysis of pv array configurations (sp, bl, hc and tt) to enhance maximum power under non-uniform shading conditions. *Engineering reports*, 2(8):e12214.

Bonthagorla, P. K. and Mikkili, S. (2020d). Performance investigation of hybrid and conventional pv array configurations for grid-connected/standalone pv systems. *CSEE Journal of Power and Energy Systems*, 8(3):682–695.

Bower, W. and Wiles, J. (2000). Investigation of ground-fault protection devices for photovoltaic power system applications. In *Conference Record of the Twenty-Eighth IEEE Photovoltaic Specialists Conference-2000 (Cat. No. 00CH37036)*, pages 1378–1383. IEEE.

Bower, W. I. and Wiles, J. C. (1994). Analysis of grounded and ungrounded photovoltaic systems. In *Proceedings of 1994 IEEE 1st world conference on photovoltaic energy conversion-WCPEC (A joint conference of PVSC, PVSEC and PSEC)*, volume 1, pages 809–812. IEEE.

Brenna, M., Falvo, M. C., Foiadelli, F., Martirano, L., and Poli, D. (2012). Sustainable energy microsystem (sem): preliminary energy analysis. In *2012 IEEE PES Innovative Smart Grid Technologies (ISGT)*, pages 1–6. IEEE.

Candela, R., Di Dio, V., Sanseverino, E. R., and Romano, P. (2007). Reconfiguration techniques of partial shaded pv systems for the maximization of electrical energy production. In *2007 International conference on clean electrical power*, pages 716–719. IEEE.

Capparella, S. and Falvo, M. C. (2014). Secure faults detection for preventing fire risk in pv systems. In *2014 International Carnahan Conference on Security Technology (ICCST)*, pages 1–5. IEEE.

Chandra Sekhar, A. and Ramesh, T. (2023a). Hybridization of solar pv configurations for maximum power extraction under partial shading conditions. *IETE Journal of Research*, pages 1–18.

Chandra Sekhar, A. and Ramesh, T. (2023b). Novel double tied cross link with reduced cross cables for maximum power extraction under uniform and non-uniform shading conditions. *IETE Technical Review*, 40(6):806–821.

Chen, Z., Han, F., Wu, L., Yu, J., Cheng, S., Lin, P., and Chen, H. (2018). Random forest based intelligent fault diagnosis for pv arrays using array voltage and string currents. *Energy conversion and management*, 178:250–264.

Cheng, Z., Pang, Z., Liu, Y., and Xue, P. (2010). An adaptive solar photovoltaic array reconfiguration method based on fuzzy control. In *2010 8th World Congress on Intelligent Control and Automation*, pages 176–181. IEEE.

Deshkar, S. N., Dhale, S. B., Mukherjee, J. S., Babu, T. S., and Rajasekar, N. (2015). Solar pv array reconfiguration under partial shading conditions for maximum power extraction using genetic algorithm. *Renewable and Sustainable Energy Reviews*, 43:102–110.

Dhanalakshmi, B. and Rajasekar, N. (2018a). Dominance square based array reconfiguration scheme for power loss reduction in solar photovoltaic (pv) systems. *Energy conversion and management*, 156:84–102.

Dhanalakshmi, B. and Rajasekar, N. (2018b). A novel competence square based pv array reconfiguration technique for solar pv maximum power extraction. *Energy conversion and management*, 174:897–912.

EDITION, T. A. (2016). 2017 national electrical safety code®(nesc)®.

El-Dein, M. S., Kazerani, M., and Salama, M. (2012). An optimal total cross tied interconnection for reducing mismatch losses in photovoltaic arrays. *IEEE transactions on sustainable energy*, 4(1):99–107.

Fathy, A. (2018). Recent meta-heuristic grasshopper optimization algorithm for optimal reconfiguration of partially shaded pv array. *Solar Energy*, 171:638–651.

Fathy, A., Yousri, D., Babu, T. S., and Rezk, H. (2023). Triple x sudoku reconfiguration for alleviating shading effect on total-cross-tied pv array. *Renewable Energy*, 204:593–604.

Flicker, J. and Johnson, J. (2013a). Analysis of fuses for blind spot ground fault detection in photovoltaic power systems. *Sandia National Laboratories Report*.

Flicker, J. D. and Johnson, J. (2013b). Photovoltaic ground fault and blind spot electrical simulations. Technical report, Sandia National Lab.(SNL-NM), Albuquerque, NM (United States).

Ganesan, S., David, P. W., Murugesan, P., and Balachandran, P. K. (2023). Solar photovoltaic system performance improvement using a new fault identification technique. *Electric Power Components and Systems*, pages 1–13.

Hare, J., Shi, X., Gupta, S., and Bazzi, A. (2016). Fault diagnostics in smart micro-grids: A survey. *Renewable and Sustainable Energy Reviews*, 60:1114–1124.

Hariharan, R., Chakkarapani, M., Ilango, G. S., and Nagamani, C. (2016). A method to detect photovoltaic array faults and partial shading in pv systems. *IEEE Journal of Photovoltaics*, 6(5):1278–1285.

Jalil, M. F., Khatoon, S., Nasiruddin, I., and Bansal, R. (2022). Review of pv array modelling, configuration and mppt techniques. *International Journal of Modelling and Simulation*, 42(4):533–550.

Jalil, M. F., Sharma, D., and Bansal, R. (2023). Cross kit reconfiguration algorithm for enhanced output power of pv array during shading mismatch conditions. *Optik*, 288:171218.

Jazayeri, M., Jazayeri, K., and Uysal, S. (2017). Adaptive photovoltaic array reconfiguration based on real cloud patterns to mitigate effects of non-uniform spatial irradiance profiles. *Solar Energy*, 155:506–516.

Karakose, M., Baygin, M., Murat, K., Baygin, N., and Akin, E. (2016). Fuzzy based reconfiguration method using intelligent partial shadow detection in pv arrays. *International Journal of Computational Intelligence Systems*, 9(2):202–212.

Karmakar, B. K. and Pradhan, A. K. (2020). Detection and classification of faults in solar pv array using thevenin equivalent resistance. *IEEE Journal of Photovoltaics*, 10(2):644–654.

Krishna, G. S. and Moger, T. (2019a). Improved sudoku reconfiguration technique for total-cross-tied pv array to enhance maximum power under partial shading conditions. *Renewable and Sustainable Energy Reviews*, 109:333–348.

Krishna, G. S. and Moger, T. (2019b). Reconfiguration strategies for reducing partial shading effects in photovoltaic arrays: State of the art. *Solar Energy*, 182:429–452.

Krishna, S. G. and Moger, T. (2019c). Optimal sudoku reconfiguration technique for total-cross-tied pv array to increase power output under non-uniform irradiance. *IEEE Transactions on Energy Conversion*, 34(4):1973–1984.

Krishnan, V. R., Blaabjerg, F., Sangwongwanich, A., and Natarajan, R. (2022). Twisted two-step arrangement for maximum power extraction from a partially shaded pv array. *IEEE Journal of Photovoltaics*, 12(3):871–879.

Kumar, B. P., Pillai, D. S., Rajasekar, N., Chakkarapani, M., and Ilango, G. S. (2020). Identification and localization of array faults with optimized placement of voltage sensors in a pv system. *IEEE Transactions on Industrial Electronics*, 68(7):5921–5931.

Kumar, D. and Raushan, R. (2023). An innovative competence square technique for pv array reconfiguration under partial shading conditions. *International Journal of Modelling and Simulation*, pages 1–16.

Kumar, M. (2020). Enhanced solar pv power generation under pscs using shade dispersion. *IEEE Transactions on Electron Devices*, 67(10):4313–4320.

La Manna, D., Vigni, V. L., Sanseverino, E. R., Di Dio, V., and Romano, P. (2014). Reconfigurable electrical interconnection strategies for photovoltaic arrays: A review. *Renewable and Sustainable Energy Reviews*, 33:412–426.

Lal SR, S., Herbert GM, J., Arjunan, P., and Suryan, A. (2022). Advancements in renewable energy transition in india: A review. *Energy Sources, Part A: Recovery, Utilization, and Environmental Effects*, pages 1–31.

Madeti, S. R. and Singh, S. (2017). Monitoring system for photovoltaic plants: A review. *Renewable and Sustainable Energy Reviews*, 67:1180–1207.

Madhusudanan, G., Senthilkumar, S., Anand, I., and Sanjeevikumar, P. (2018). A shade dispersion scheme using latin square arrangement to enhance power production in solar photovoltaic array under partial shading conditions. *Journal of Renewable and Sustainable Energy*, 10(5).

Mahmoud, Y. and El-Saadany, E. F. (2017). Enhanced reconfiguration method for reducing mismatch losses in pv systems. *IEEE Journal of Photovoltaics*, 7(6):1746–1754.

Malathy, S. and Ramaprabha, R. (2018a). Reconfiguration strategies to extract maximum power from photovoltaic array under partially shaded conditions. *Renewable and Sustainable Energy Reviews*, 81:2922–2934.

Malathy, S. and Ramaprabha, R. (2018b). Reconfiguration strategies to extract maximum power from photovoltaic array under partially shaded conditions. *Renewable and Sustainable Energy Reviews*, 81:2922–2934.

Manju, S. and Sagar, N. (2017). Progressing towards the development of sustainable energy: A critical review on the current status, applications, developmental barriers and prospects of solar photovoltaic systems in india. *Renewable and Sustainable Energy Reviews*, 70:298–313.

Markvart, T. and Castañer, L. (2003). *Practical handbook of photovoltaics: fundamentals and applications*. Elsevier.

Matam, M. and Barry, V. R. (2018). Improved performance of dynamic photovoltaic array under repeating shade conditions. *Energy conversion and management*, 168:639–650.

Mehmood, A., Sher, H. A., Murtaza, A. F., and Al-Haddad, K. (2021). Fault detection, classification and localization algorithm for photovoltaic array. *IEEE Transactions on Energy Conversion*, 36(4):2945–2955.

Miao, W., Lam, K., and Pong, P. W. (2020). A string-current behavior and current sensing-based technique for line–line fault detection in photovoltaic systems. *IEEE Transactions on Magnetics*, 57(2):1–6.

Miao, W., Luo, Y., Wang, F., and Jiang, C. (2023). Fault detection and location algorithm by voltage characteristics for pv system. *IEEE Journal of Photovoltaics*.

Mostafaee, G. and Ghandehari, R. (2020). Power enhancement of photovoltaic arrays under partial shading conditions by a new dynamic reconfiguration method. *Journal of energy management and technology*, 4(1):46–51.

Murtaza, A. F., Bilal, M., Ahmad, R., and Sher, H. A. (2019). A circuit analysis-based fault finding algorithm for photovoltaic array under l–l/l–g faults. *IEEE Journal of Emerging and Selected Topics in Power Electronics*, 8(3):3067–3076.

Nasiruddin, I., Khatoon, S., Jalil, M. F., and Bansal, R. (2019). Shade diffusion of partial shaded pv array by using odd-even structure. *Solar Energy*, 181:519–529.

Nayak, B., Mohapatra, A., and Das, P. (2017). Optimal hybrid array configuration scheme to reduce mismatch losses of photovoltaic system. In *2017 Second International Conference on Electrical, Computer and Communication Technologies (ICECCT)*, pages 1–7. IEEE.

Ngoc, T. N., Phung, Q. N., Tung, L. N., Sanseverino, E. R., Romano, P., and Viola, F. (2017). Increasing efficiency of photovoltaic systems under non-homogeneous solar irradiation using improved dynamic programming methods. *Solar Energy*, 150:325–334.

Nguyen, D. and Lehman, B. (2008). An adaptive solar photovoltaic array using model-based reconfiguration algorithm. *IEEE Transactions on industrial Electronics*, 55(7):2644–2654.

Nguyen, D. D., Lehman, B., and Kamarthi, S. (2009). Performance evaluation of solar photovoltaic arrays including shadow effects using neural network. In *2009 IEEE Energy Conversion Congress and Exposition*, pages 3357–3362. IEEE.

Nihanth, M. S. S., Ram, J. P., Pillai, D. S., Ghias, A. M., Garg, A., and Rajasekar, N. (2019). Enhanced power production in pv arrays using a new skyscraper puzzle based one-time reconfiguration procedure under partial shade conditions (pscs). *Solar Energy*, 194:209–224.

Pachauri, R. K. (2022). Imperative role of optimization techniques to reconfigure solar photovoltaic array systems to diminish shading effects. *International Journal of Circuit Theory and Applications*, 50(1):317–353.

Pachauri, R. K., Mahela, O. P., Sharma, A., Bai, J., Chauhan, Y. K., Khan, B., and Alhelou, H. H. (2020). Impact of partial shading on various pv array configurations and different modeling approaches: A comprehensive review. *IEEE Access*, 8:181375–181403.

Pachauri, R. K. and Singh, J. G. (2023). Successive rotation approach based novel game puzzles for higher shade dispersion of pv array systems under non-uniform irradiations. *Energy Conversion and Management*, 276:116505.

Pachauri, R. K., Thanikanti, S. B., Bai, J., Yadav, V. K., Aljafari, B., Ghosh, S., and Alhelou, H. H. (2022). Ancient chinese magic square-based pv array reconfiguration methodology to reduce power loss under partial shading conditions. *Energy Conversion and Management*, 253:115148.

Palpandian, M., Winston, D. P., Kumar, B. P., Kumar, C. S., Babu, T. S., and Alhelou, H. H. (2021). A new ken-ken puzzle pattern based reconfiguration technique for maximum power extraction in partial shaded solar pv array. *IEEE Access*, 9:65824–65837.

Parlak, K. Ş. (2014). Pv array reconfiguration method under partial shading conditions. *International Journal of Electrical Power & Energy Systems*, 63:713–721.

Pendem, S. R. and Mikkili, S. (2018). Modelling and performance assessment of pv array topologies under partial shading conditions to mitigate the mismatching power losses. *Solar Energy*, 160:303–321.

Pillai, D. S. and Rajasekar, N. (2018). An mppt-based sensorless line–line and line–ground fault detection technique for pv systems. *IEEE Transactions on Power Electronics*, 34(9):8646–8659.

Raj, R. D. A. and Naik, K. A. (2022). Optimal reconfiguration of pv array based on digital image encryption algorithm: A comprehensive simulation and experimental investigation. *Energy Conversion and Management*, 261:115666.

Raj, R. D. A. and Naik, K. A. (2023). Novel shade dispersion techniques for reconfiguration of partially shaded photovoltaic arrays. *Smart Grids and Sustainable Energy*, 8(1):5.

Rajan, N. A., Shrikant, K. D., Dhanalakshmi, B., and Rajasekar, N. (2017). Solar pv array reconfiguration using the concept of standard deviation and genetic algorithm. *Energy Procedia*, 117:1062–1069.

Rajani, K. and Ramesh, T. (2020). Maximum power enhancement under partial shadings using a modified sudoku reconfiguration. *CSEE Journal of Power and Energy Systems*, 7(6):1187–1201.

Ramaprabha, R. (2014). Selection of an optimum configuration of solar pv array under partial shaded condition using particle swarm optimization. *International Journal of Electrical and Computer Engineering*, 8(1):89–96.

Ramaprabha, R., Mathur, B., et al. (2011). A comprehensive review and analysis of solar photovoltaic array configurations under partial shaded conditions. *International Journal of Photoenergy*, 2012.

Ramasamy, S., Seenithangam, J., Dash, S. S., and Chaitanya, K. (2016). A dodging algorithm to reconfigure photovoltaic array to negate partial shading effect. *Progress in Photovoltaics: Research and Applications*, 24(2):200–210.

Ramesh, T., Rajani, K., and Panda, A. K. (2020). A novel triple-tied-cross-linked pv array configuration with reduced number of cross-ties to extract maximum power under partial shading conditions. *CSEE Journal of Power and Energy Systems*, 7(3):567–581.

Rani, B. I., Ilango, G. S., and Nagamani, C. (2013). Enhanced power generation from pv array under partial shading conditions by shade dispersion using su do ku configuration. *IEEE Transactions on sustainable energy*, 4(3):594–601.

Rao, P. S., Ilango, G. S., and Nagamani, C. (2014). Maximum power from pv arrays using a fixed configuration under different shading conditions. *IEEE journal of Photovoltaics*, 4(2):679–686.

Reddy, S. S. and Yammani, C. (2020a). A novel magic-square puzzle based one-time pv reconfiguration technique to mitigate mismatch power loss under various partial shading conditions. *Optik*, 222:165289.

Reddy, S. S. and Yammani, C. (2020b). Odd-even-prime pattern for pv array to increase power output under partial shading conditions. *Energy*, 213:118780.

Rezazadeh, S., Moradzadeh, A., Hashemzadeh, S. M., Pourhossein, K., Mohammadi-Ivatloo, B., and Hosseini, S. H. (2021). A novel prime numbers-based pv array reconfiguration solution to produce maximum energy under partial shade conditions. *Sustainable Energy Technologies and Assessments*, 47:101498.

Rezazadeh, S., Moradzadeh, A., Pourhossein, K., Akrami, M., Mohammadi-Ivatloo, B., and Anvari-Moghaddam, A. (2022). Photovoltaic array reconfiguration under

partial shading conditions for maximum power extraction: A state-of-the-art review and new solution method. *Energy Conversion and Management*, 258:115468.

Sabbaghpur Arani, M., Hejazi, M. A., et al. (2016). The comprehensive study of electrical faults in pv arrays. *Journal of Electrical and Computer Engineering*, 2016.

Sahoo, S. K. (2016). Renewable and sustainable energy reviews solar photovoltaic energy progress in india: A review. *Renewable and Sustainable Energy Reviews*, 59:927–939.

Sahu, H. S. and Nayak, S. K. (2016). Extraction of maximum power from a pv array under nonuniform irradiation conditions. *IEEE Transactions on electron devices*, 63(12):4825–4831.

Sahu, H. S., Nayak, S. K., and Mishra, S. (2015). Maximizing the power generation of a partially shaded pv array. *IEEE journal of emerging and selected topics in power electronics*, 4(2):626–637.

Sanseverino, E. R., Ngoc, T. N., Cardinale, M., Vigni, V. L., Musso, D., Romano, P., and Viola, F. (2015). Dynamic programming and munkres algorithm for optimal photovoltaic arrays reconfiguration. *Solar Energy*, 122:347–358.

Sarkar, D. and Sadhu, P. K. (2023). Critical comprehensive performance analysis of static bipv array configurations to reduce mismatch loss and enhance maximum power under partial shading. *IETE Technical Review*, 40(4):465–497.

Satpathy, P. R., Jena, S., Jena, B., and Sharma, R. (2017). Comparative study of interconnection schemes of modules in solar pv array network. In *2017 International Conference on Circuit, Power and Computing Technologies (ICCPCT)*, pages 1–6. IEEE.

Strobl, C. and Meckler, P. (2010). Arc faults in photovoltaic systems. In *2010 Proceedings of the 56th IEEE Holm Conference on Electrical Contacts*, pages 1–7. IEEE.

Tabanjat, A., Becherif, M., and Hissel, D. (2015). Reconfiguration solution for shaded pv panels using switching control. *Renewable Energy*, 82:4–13.

Tatabhatla, V. M. R., Agarwal, A., and Kanumuri, T. (2020). Performance improvement by mitigating the effects of moving cloud conditions. *IEEE Transactions on Power Electronics*, 36(4):4214–4223.

Tatabhatla, V. M. R., Agarwal, A., and Kanumuri, T. (2021). A chaos map based reconfiguration of solar array to mitigate the effects of partial shading. *IEEE Transactions on Energy Conversion*, 37(2):811–823.

Triki-Lahiani, A., Abdelghani, A. B.-B., and Slama-Belkhodja, I. (2018). Fault detection and monitoring systems for photovoltaic installations: A review. *Renewable and Sustainable Energy Reviews*, 82:2680–2692.

Velasco-Quesada, G., Guinjoan-Gispert, F., Piqué-López, R., Román-Lumbreras, M., and Conesa-Roca, A. (2009). Electrical pv array reconfiguration strategy for energy extraction improvement in grid-connected pv systems. *IEEE transactions on industrial electronics*, 56(11):4319–4331.

Venkateswari, R. and Rajasekar, N. (2020). Power enhancement of pv system via physical array reconfiguration based lo shu technique. *Energy Conversion and Management*, 215:112885.

Vijayalekshmy, S., Bindu, G., and Iyer, S. R. (2016). A novel zig-zag scheme for power enhancement of partially shaded solar arrays. *Solar Energy*, 135:92–102.

Wiles, J. and King, D. (1997). Blocking diodes and fuses in low-voltage pv systems. In *Conference Record of the Twenty Sixth IEEE Photovoltaic Specialists Conference-1997*, pages 1105–1108. IEEE.

Winston, D. P., Kumaravel, S., Kumar, B. P., and Devakirubakaran, S. (2020). Performance improvement of solar pv array topologies during various partial shading conditions. *Solar Energy*, 196:228–242.

Yadav, A. S., Pachauri, R. K., Chauhan, Y. K., Choudhury, S., and Singh, R. (2017). Performance enhancement of partially shaded pv array using novel shade dispersion effect on magic-square puzzle configuration. *Solar Energy*, 144:780–797.

Yadav, V. K., Behera, A. D., Singh, R., Maheshwari, A., Ghosh, S., and Prakash, A. (2023a). A novel pv array reconfiguration technique based on circular array data structure. *Energy*, 283:128505.

Yadav, V. K., Yadav, R., Singh, R., Mishra, I., Ganvir, I., et al. (2023b). Reconfiguration of pv array through recursive addition approach for optimal power extraction under psc. *Energy Conversion and Management*, 292:117412.

Yang, B., Ye, H., Wang, J., Li, J., Wu, S., Li, Y., Shu, H., Ren, Y., and Ye, H. (2021). Pv arrays reconfiguration for partial shading mitigation: Recent advances, challenges and perspectives. *Energy Conversion and Management*, 247:114738.

Ye, C.-E., Tai, C.-C., Huang, Y.-P., and Chen, J.-J. (2021). Dispersed partial shading effect and reduced power loss in a pv array using a complementary sudoku puzzle topology. *Energy conversion and management*, 246:114675.

Yi, Z. and Etemadi, A. H. (2016). Fault detection for photovoltaic systems based on multi-resolution signal decomposition and fuzzy inference systems. *IEEE Transactions on Smart Grid*, 8(3):1274–1283.

Yousri, D., Allam, D., and Eteiba, M. B. (2020). Optimal photovoltaic array reconfiguration for alleviating the partial shading influence based on a modified harris hawks optimizer. *Energy Conversion and Management*, 206:112470.

Yousri, D., Fathy, A., and El-Saadany, E. F. (2022). Four square sudoku approach for alleviating shading effect on total-cross-tied pv array. *Energy Conversion and Management*, 269:116105.

Zhao, Y. and Lyons Jr, R. (2011). Ground-fault analysis and protection in pv arrays. *Proc. Photovoltaic Protection*, pages 1–4.

Publications

International Journals

1. **Ramesh, Dongara**, and Karthikeyan Anbalagan. "Modified Odd–Even–Prime pattern for effective dispersion of shade over the PV array under partial shading conditions." ***Solar Energy (Elsevier)*** 269 (2024): 112303.
2. **Ramesh.Dongara**, Karthikeyan Anbalagan., & Gaonkar, D. N. (2023). "A novel reduced-cross-tied configuration for extracting maximum power output from a symmetrical PV array under partial shading conditions". ***Electrical Engineering (Springer)***, 1-21.
3. **Ramesh, Dongara**, and Karthikeyan Anbalagan, "Cyclic Back Shift (CBS) Method for Maximizing PV Array Power under Partial Shading" ***Electrical Engineering (Springer)*** - **Under Review**
4. **Ramesh, Dongara**, and Karthikeyan Anbalagan. "Circular Shift Arrangement of PV Array for Harvesting Maximum Power under Partial Shading Conditions." ***Chinese Journal of Electrical Engineering*** - **Under Review**

Biodata

Name : Dongara Ramesh
Date of birth: 02-02-1987
Marital status: Married
E-mail: ramesh.d1487@gmail.com
Mobile: +91 9989089344

Address
Research Scholar
Department of Electrical & Electronics Engineering
National Institute of Technology Karnataka
Surathkal, Mangaluru, India-575025, India.

Education

- M.Tech., Energy Systems , University College og Engineering, JNTUH, Hyderabad, Telangana, Percentage - 83, 2015.
- B.Tech., Electrical & Electronics Engineering, University College og Engineering, JNTUK, Kakinada, Andhra Pradesh, Percentage - 75.32, 2009.

Work Experience

- 05-09-2015 to 04-06-2019, Worked as Adhoc Faculty, Department of Electrical and Electronics Engineering, MLRIT, Hyderabad, Telangana.